1997

Feasibility Study on the Reduction of Hydrostatic Pressure in a Deep-Water Riser Using a Gas-Lift Method.

Clovis Antonio Lopes
Louisiana State University and Agricultural & Mechanical College

FEASIBILITY STUDY ON THE REDUCTION OF HYDROSTATIC PRESSURE IN A DEEP WATER RISER USING A GAS-LIFT METHOD

A Dissertation

Submitted to the Graduate Faculty of the
Louisiana State University and
Agricultural and Mechanical College
in partial fulfillment of the
requirements for the degree of
Doctor of Philosophy

in

The Department of Petroleum Engineering

by
Clovis Antonio Lopes
B.S., Universidade Federal do Rio Grande do Sul, Brazil, 1978
M.S., Universidade Estadual de Campinas, Brazil, 1990
May 1997

ACKNOWLEDGMENTS

The author is deeply indebted to Dr. Adam "Ted" Bourgoyne, Campanile Charities Professor of Offshore Mining and Petroleum Engineering, under whose valuable guidance, supervision, and encouragement this work was accomplished. Sincere appreciation is extended to Dr. Andrzej Wojtanowicz, Dr. Gary R. Byerly, Dr. Julius P. Langlinais, Dr. Zaki Bassiouni, and for serving on the dissertation committee.

The author extends his deepest thanks to Petroleo Brasileiro S.A. Petrobras for providing him the financial support to attend the doctoral program at LSU. Furthermore, this research was financed by Petrobras through funds from its Technological Development Program and Deepwater Production System - PROCAP 2000. Sincere appreciation is due to Dr. Edson Y. Nakagawa, Dr. Shiniti Ohara, Dr. Alvaro Negrao, Mr. Andre Barcelos, Mr. Osmond Coelho, and Mr. Djalma R. de Souza of Petrobras, for their firm support throughout this project.

Special thanks are also due to Mr. O. Allen Kelly, Mr. Richard Duncan, and Dr. William J. Bernard of PERTTL-LSU, for their attention, ideas, and support during the experimental work of this study. Acknowledgments are also extended to Mr. Jason Duhe, Mr. Bryant LaPoint, Mr. Eddy Walls, and Mr. Ben Bienvenu for their invaluable help during the experiments. Mrs. Jeannette Wooden and Mrs. Jan Easley are thanked for their kind words of encouragement.

Finally, the author dedicates this work to his father Clowis and mother Gisela for their unwavering encouragement, to his wife, Angela, and to his children, Bruna, Luiza, and Clowis for their cheerful support and love.

TABLE OF CONTENTS

LIST OF TABLES

LIST OF FIGURES

ABSTRACT

Recent successful exploration efforts in deep waters have heightened interest in developing oil and gas reservoirs on the continental slope. Leases have been obtained in water depths up to 10,000 ft with a requirement that they be drilled within the next decade. Use of current techniques to drill these leases will require extremely large floating drilling units and large diameter marine riser systems.

This study presents the results of a feasibility study on the use of an automated gas-lift system for a marine riser that will maintain the hydrostatic pressure in the subsea well-head equal to that of the sea water at the sea floor. Hydrostatic control of abnormal formation pressure could still be maintained by a weighted mud system that is not gas-cut below the sea floor. Such a dual density mud system could reduce drilling costs by reducing the number of casing strings required to drill the well and so reducing the time required to drill a deep-water well. The system would have the advantages of riserless drilling without giving up the well control advantages of a closed, weighted mud system.

A steady-state numerical model was developed that can be used to determine the gas injection requirements needed to achieve a desired dual density configuration. The numerical model was verified through tests conducted in a 6,000 foot research well. Once verified, the model was used to define the gas requirements and practical limits of a marine gas-lift system based on estimated additional costs of gas compression and nitrogen membrane filters.

The practical limits are presented in terms of maximum mud density, water depth, and riser diameter combinations. The dissertation also discusses the operational changes

that would be required for various drilling procedures such as making a connection, running casing, kick detection, and well control operations.

CHAPTER I

THE RISER PROBLEM

This chapter presents the problem at hand, discussing the determining factors and their interrelationships. It also includes, as a background, the present industry situation concerning deep water rig availability and upgrade. Furthermore, a solution to the problem is proposed and described, showing its advantages over the traditional drilling method. The chapter finally states the objectives to be achieved by this dissertation.

1.1 - THE CONVENTIONAL RISER

The common riser string is designed to, primarily, raise the well to the rig floor. This allows for:

- Easy tool access to the hole;
- Conventional use of tools developed for land rigs;
- Convenient placement of mud treatment equipment (for easy maintenance);
- Traditional methods of kick detection, with an observable surface fluid level.

As a drawback, by achieving this objective, the conventional riser string introduces an extra hydrostatic pressure to the bottom of the well. This is due to the density difference between the mud inside the riser and the sea water outside it. This extra pressure was, historically, neglected while the industry's focus was on shallow to medium water depths (up to 2,000 ft). As the industry moves into deeper waters, this pressure increase becomes significant, leading to:

- More casing set points;
- Higher riser tensioner overpull;

- Lower riser safety margins;
- Bigger chances of formation fracture and formation damage.

1.2 - PROPOSED SOLUTION

The dual density riser idea consists in reducing the mud density in the riser by injecting air, or nitrogen, at the BOP level. This could be done using an external riser line, such as the kill or choke lines, as shown in Figure 1.1, but will probably require a dedicated gas injection line.

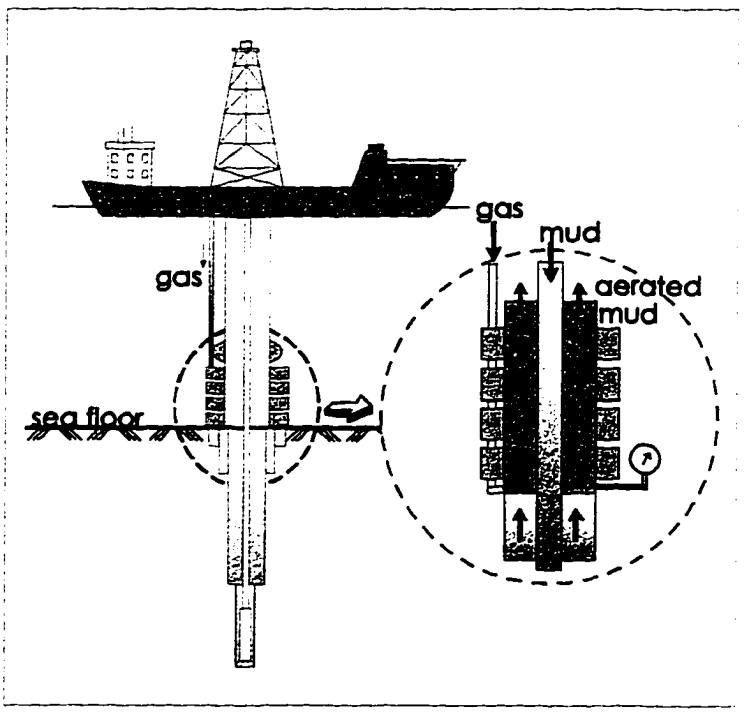

Figure 1.1 - The Dual Density Riser System

The objective is to maintain a mixture of air and mud in the riser annulus, having an average density equal to the sea water density, while injecting non-aerated mud through the drill string. The mud weight used should be greater than the expected pore pressure equivalent density plus a trip margin, to account for an emergency disconnection event.

Figure 1.2 shows the pressure profile for such a system. A 15.6 ppg mud replaces the original density of 13.7 ppg, when combined with the gas-mud mixture in the riser annulus. The nitrogen pressure distribution is also shown in the graph, along an external line with an internal diameter of 3 inches. It shows the pressure decrease, along the well, due to the dual density combined hydrostatic columns. It also includes a 100 psi drop across the injection valve for the gas curve.

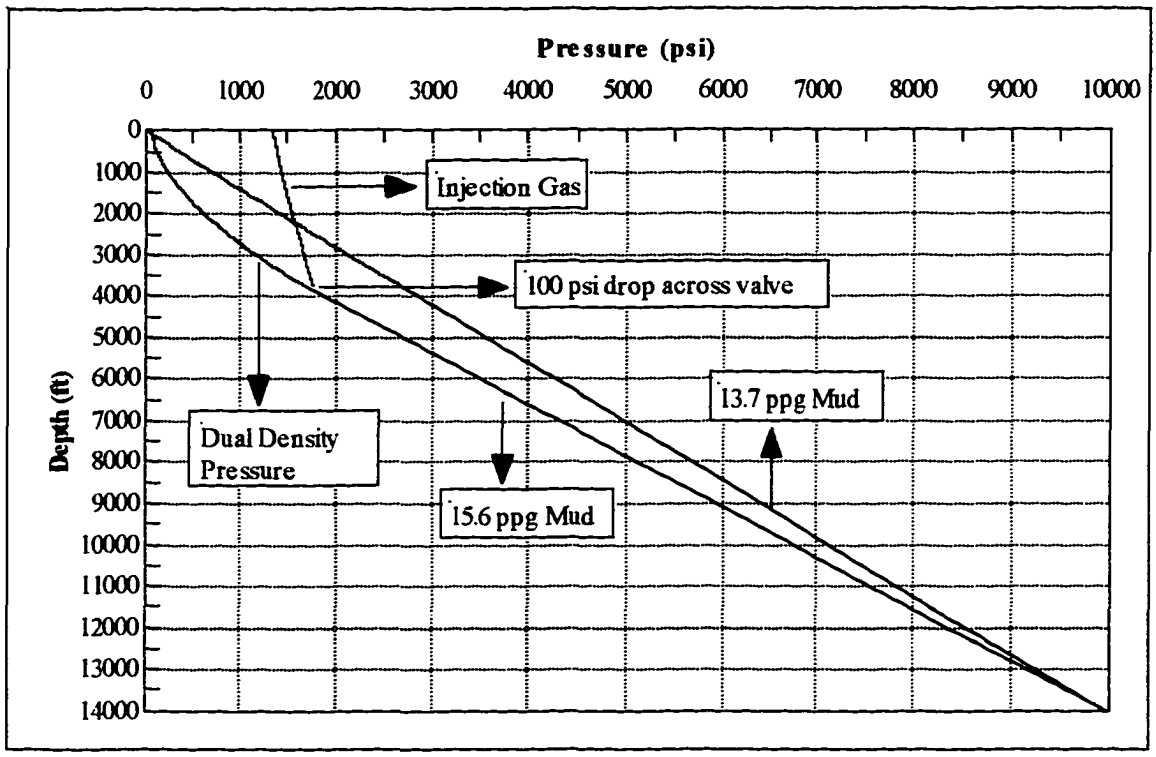

Figure 1.2 - The Dual Density System Pressure Profile

The system will probably require the use of Nitrogen Producing Units (NPUs), that will generate gas in a continuous basis, at low pressures. Later, the gas will be compressed before injecting it into the riser bottom. Prior to achieving steady-state conditions, the same gas lift techniques to unload a well could be used. A set of gas-lift valves could be used along the injection line, providing smaller kick-off pressures and reducing the compressors costs.

1.3 - CONVENTIONAL CASING DESIGN

Casing designers traditionally rely on the pore pressure and fracture gradient curves for a given location. These curves are normally referred to the sea surface, where the depth for the hydrostatic pressure calculations is counted from. The curves on Figure 1.3 are a typical example of a location in the Gulf of Mexico. The trip margin curve is obtained by adding 0.5 ppg to every point on the pore pressure curve. The kill margin, on the other hand, is drawn by subtracting 0.5 ppg from every point on the fracture gradient curve. This example would require 7 strings of casing to be safely drilled. The

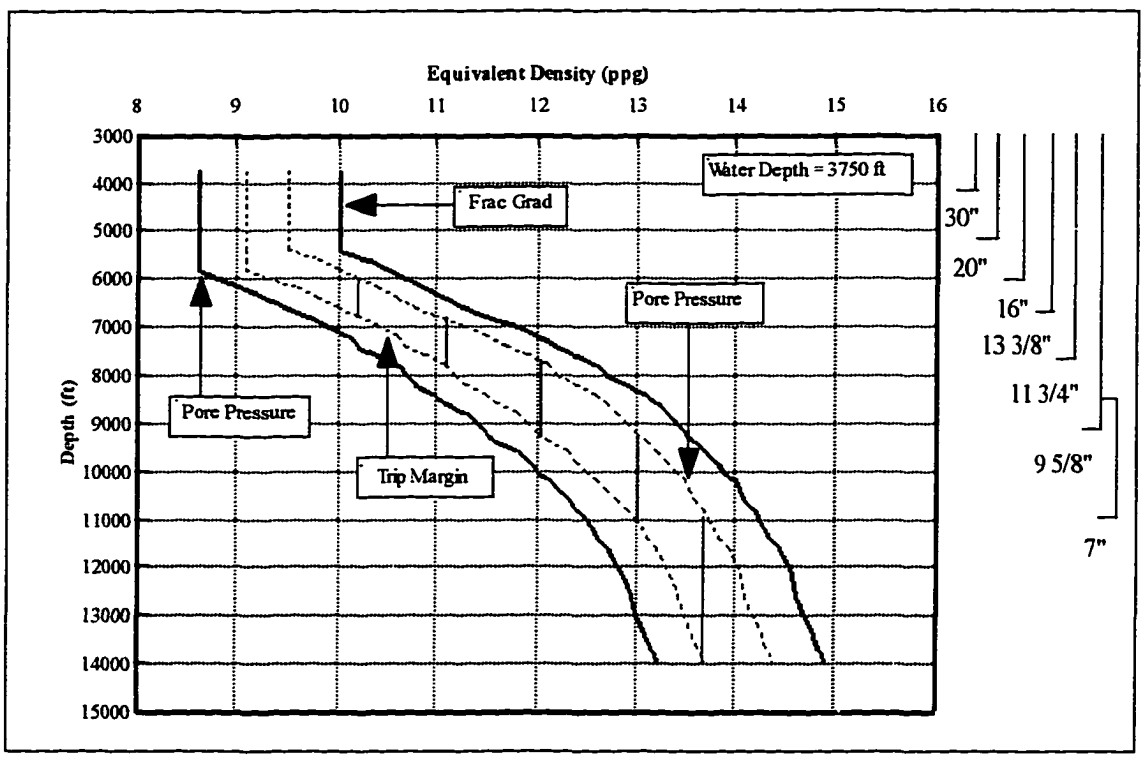

Figure 1.3 - Pore Pressure and Fracture Gradient Example for the Gulf of Mexico.

first two casing set points (1 and 2 in the figure) are usually chosen as the 30", and 20" pipes. After that, the expected diameters could be designed as: 16" (3), 13 $^{3}/_{8}$" (4), 11 $^{3}/_{4}$" (5), 9 $^{5}/_{8}$" (6), and 7" (7) casing. Another problem is that the bit diameters required

to drill many of these hole sections, are bigger than each of their preceding casing strings. This brings about under-reaming jobs prior to the casing runs. This is presented on Table 1.1.

Table 1.1 - Casing Depths and Bit Diameters for GOM Example

Depth (ft)	Casing OD (inches)	Bit Size (inches)	Under Reaming
3,750	Sea Bottom	-	-
4,100	30	36	No
5,350	20	26	No
6,000	16	20	Yes
6,800	13 3/8	17 ½	Yes
7,700	11 ¾	14 ¾	Yes
9,100	9 5/8	12 ¼	Yes
10,900	7	8 ½	No
14,000	4 ½	6	No

The great number of casing strings introduces the need for slim-hole drilling and the problems associated with it. If such a well was to be completed, further cost increase would come from the reduced production casing diameter.

1.4 - DUAL DENSITY CASING DESIGN

Figure 1.4 shows the dual density system applied to the same example well. The combination of mud and the aerated fluid in the riser annulus would not produce a straight vertical line. Instead, the equivalent density would vary with the reciprocal of the depth (see Appendix A). This fact allows the use of only four casing strings. The recommended diameters being: 30" (1), 20" (2), 13 $^{3}/_{8}$" (3), and 9 $^{5}/_{8}$" (4). The well could be drilled to the final depth with an 8 ½" bit and completed with a 7" production casing.

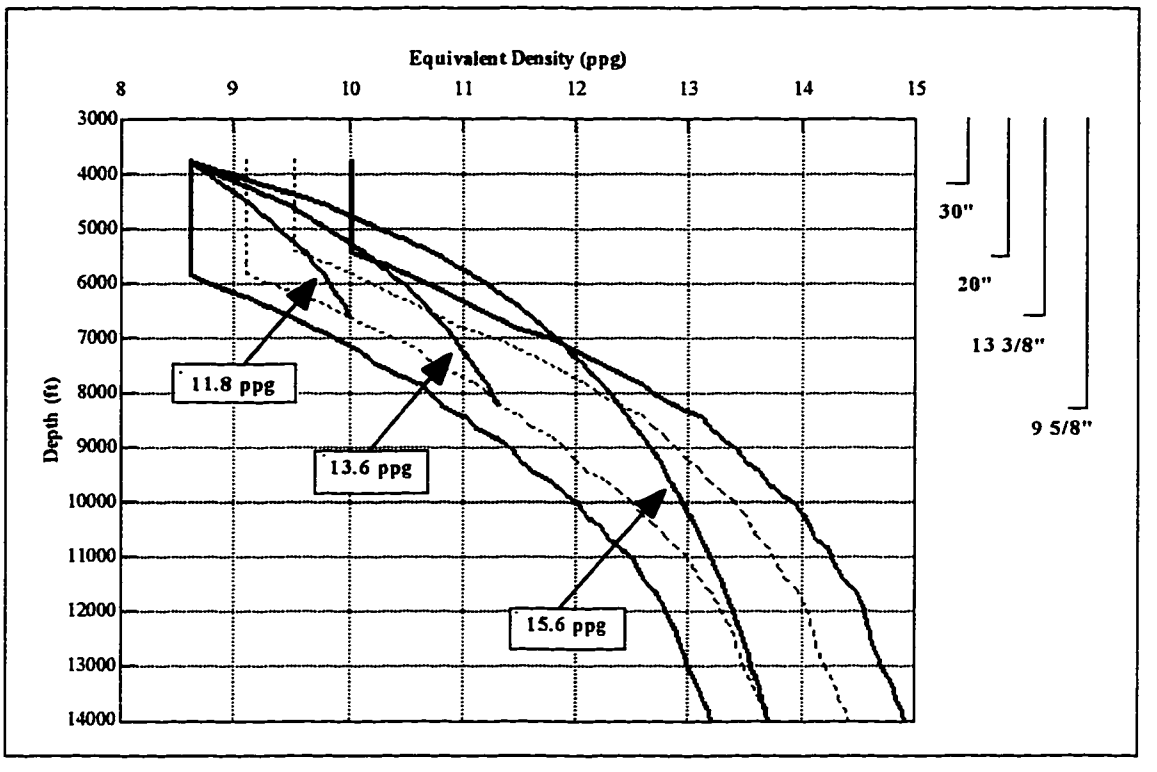

Figure 1.4 - Dual Density Casing Design for the Gulf of Mexico Example

1.5 - EMERGENCY DISCONNECTIONS

A riser emergency disconnection do cause a sudden decrease in bottom hole pressure. It is interesting to examine the factors that might lead to one of these events, in order to gauge their chances of occurrence and their consequences.

DP vessels always present the possibility for an emergency disconnection, which is defined as a Lower Marine Riser Package (LMRP) disconnection from the BOP, caused by an on going vessel position loss, or drift.

A DP vessel can either experience a drift-off or a drive-off. The former happens when the DP system ceases to command the thrusters, or when the environmental load exceeds the vessel's power to maintain position. A drive-off is a more serious situation,

where the DP controller becomes unstable and "drives" the ship to a new location, usually using all the thruster power available.

A classical drive-off chain-of-events starts when, for some reason, the position sensor provides a wrong location to the controller. The algorithm is designed to command the propellers to zero on a given set of coordinates. Thus, the greater the difference between the sensor's position and the desired location is, the greater is the thrust to eliminate that difference. A drive-off always means less time for an emergency disconnection than during a drift-off.

Drift-offs are much more common than drive-offs, and drift-offs caused by system failures are much more common than the ones caused by excessive weather conditions. As the system ages, unexpected equipment faults happen, even with careful preventive maintenance. We can cite a few examples:

- On the drillship Sedco-472, also in Brazil, in 1987, a corroded load-ring in the riser slip-joint started to torque up the riser string every time the ship changed heading. This action eventually broke the top 20" casing joint and allowed the wellhead to turn. When this happened, the ship was turning while maintaining position on data from the riser angle inclinometer, which was now turning along with the BOP. This changing data rendered the controller unstable and a drive-off occurred.
- On the drillship Pacnorse I, operating in Brazil, in 1989, a diode in one main generator exciter developed a crack, probably due to vibration. This crack only sometimes would prevent the generator from starting. On three occasions, when the DP system tried to bring that generator on line and failed, the whole power

system shut down, to prevent overloading the remaining generators. This fault caused black-outs and subsequent emergency disconnections.

- On the drillship Discoverer Seven Seas, in North Brazil, in 1993, during a routine maintenance inspection of the riser anti-recoil sensors, the crew put the auxiliary control computer off-line, before the inspection. But it came back on line and automatically performed an emergency disconnection. Although the technicians were able to reproduce the event, the fault was never found. The ship was scheduled for an upgrade that would replace that particular system. So, after trying, in vain, to find the problem, it was decided to disconnect the system entirely, until it was replaced.

A typical emergency disconnection sequence is automatic, although it can be done manually. The reason for this is that a micro-processor can do it in the least amount of time. The sequence usually is:

- Closure of a selected set of BOP pipe-rams, to prevent the drill string from falling in the well;
- Closure of the BOP shear rams, to cut the drill-string;
- Retraction of the Lower Marine Riser Package pods from the BOP;
- LMRP disconnection.

The whole sequence is normally clocked in around 23-25 seconds. It is normally commanded by the Subsea Operator or the Tool-pusher, but can be computer initiated, depending on the system. On the Discoverer Seven Seas, the system was design to automatically disconnect if the motion sensors detected an excessive heave, which would damage the riser motion compensation pistons.

The total time span of an emergency disconnection event varies according to the problem, the weather conditions and the operator judgment of when to press the AMF (Automatic Multiple Function) button. Experience tells us not to expect more than 5-10 minutes, with a range of 3-5 minutes being a safer estimate. In short, there is barely enough time to prepare the drill string for a proper hang-off operation.

The occurrence of emergency disconnections is not restricted to dynamic positioned drilling rigs. There are cases of anchor moored rigs being blown off location, or losing position due to mooring line breakage, anchor slipping, or both. Moreover, as the water depth increases, so does the possibility for anchor or mooring line failure.

1.6 - THE RISER SAFETY MARGIN

Riser Safety Margin can be defined as the difference between the equivalent density of the combined hydrostatic column (provided by mud and sea water) and the pore pressure equivalent density, plus a safety margin.

In equation form (see Appendix B), it can be expressed as:

$$RM = \frac{\rho_m(D-H)}{D} + \frac{\rho_w \cdot H}{D} - (P_p + SM) \qquad (1.1)$$

The fluid column composition changes after a marine riser disconnection. There is a decrease in hydrostatic pressure at the bottom of the well, due to the substitution of the drilling fluid, from the rig floor down to the seabed, by sea water. This decrement is almost instantaneous in case of an emergency disconnection.

Since the possibility of an emergency disconnection is an ever present one, in determining the mud density to be used we have to account for this. The total mud hydrostatic pressure, from the bottom of the well up to the seabed, plus the sea water

column, from the seabed up to the surface, must be greater than the pore pressure of any of the formations exposed.

But there is a mud density upper limit, determined by the minimum fracturing pressure of the exposed formations. In this case, we have to consider the hydrostatic pressure generated by the drilling fluid column, from the rig floor down to the weakest formation.

Furthermore, as the water depth increases, the formations tend to show lower fracturing resistance values, and this tends to narrow the operational mud range. With the current technology, there are cases where the operator can not afford to use a riser safety margin.

Figure 1.5 shows the previous Gulf of Mexico example, where the curve on the

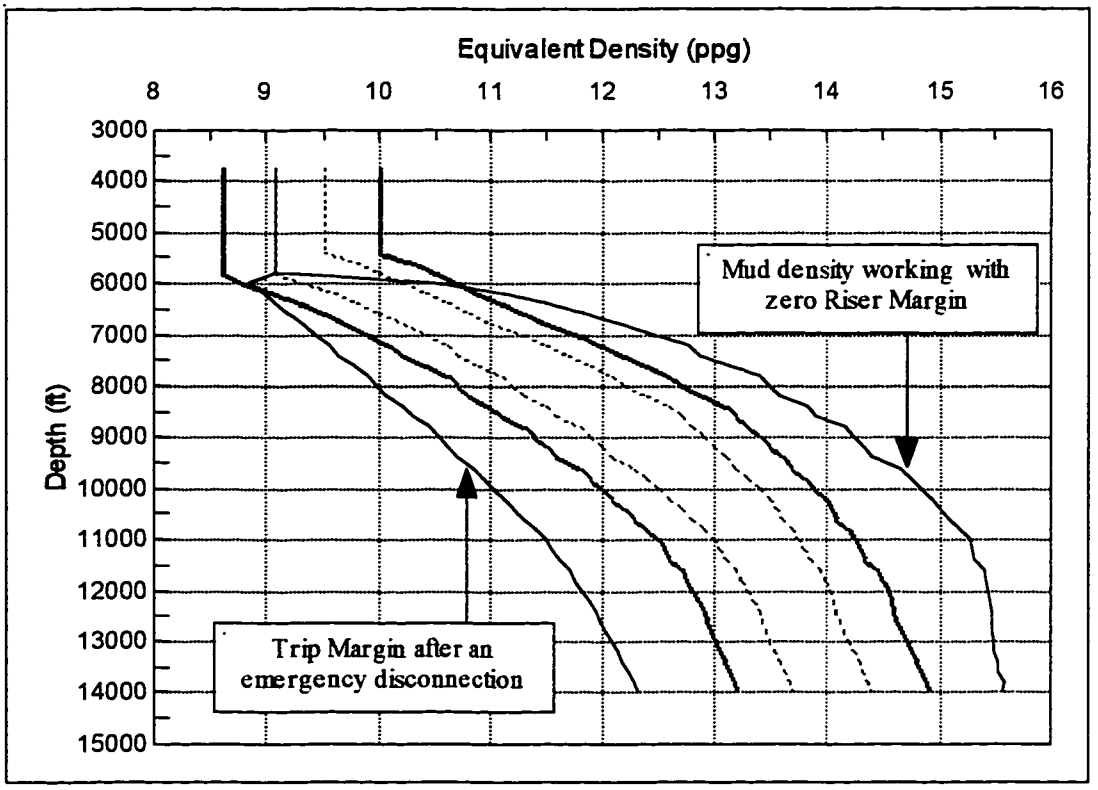

Figure 1.5 - Conventional Method Before and After an Emergency Disconnection

right is the forecast of the necessary mud weight to maintain a zero riser margin. This means that if, along the well the mud weight was to be kept equal to the pore pressure plus a trip margin of 0.5 ppg, the total hydrostatic pressure provided by the mud in the riser would fracture the formations below 6,000 ft.

On the other hand, if an emergency disconnection takes place, the zero riser safety margin would result in the curve on the left. This curve represents the combined effect of sea water and the equivalent mud weight in the wellbore with a 0.5 ppg trip margin. This means that, below 5,800 ft the well is prone to kick after an emergency disconnection.

In cases like this, the only way of drilling is to operate with negative riser safety margins, and hope that an emergency riser disconnection will not occur. In other words, the operator has to chance the consequences if the well is to be drilled at all. More complications arise in cases where abnormally pressured formations are encountered. As another example, while drilling the 1-PAS-25, in June/1993, the drillship Discoverer Seven Seas, working somewhat near the Amazon delta, faced this situation. The data is summarized in Table 1.2.

The mud logging unit reported a sharp increase in pore pressure at 8,530 ft (2600 m), while drilling shale. The last leak-off test had unexpectedly and abruptly fractured the well with a pressure equivalent to 11.7 ppg, showing a brittle shale formation. A squeeze job was required to seal the fracture. Using equation 1.1, the riser margin at 8,530 ft was a negative 1.0 ppg, while the maximum possible riser margin was - 0.8 ppg.

But this was a calculated risk, since even after setting the intermediate casing string, at 7,497 ft, the riser margin was already slightly negative (-0.08 ppg). Once the

Table 1.2 - Well 1-PAS-25 Data

Depth (ft)	Diameter (in)	Mud Weight (ppg)	Pore Pressure (ppg)	Fracture Gradient (ppg)
4,049	Sea Floor	-	-	-
7,497	13 3/8	10.5	9	11.7
8,530	12 ¼	10.8	10.2	11.7

Source: Petrobras

decision to take the risk was made, the rig had to wait for extra mud supplies to arrive and all the kick detection equipment to be verified. Also, by being in a remote location, extra measures were taken concerning emergency rescue crafts, which added up to the overall rig costs.

1.7 - DEEP WATER VESSELS AVAILABLE

Another consideration, when accessing the risk of emergency riser disconnections is rig utilization. When the utilization is high, it tends to make major maintenance jobs to be done far apart from each other, increasing the risks.

At the end of 1995, the world's fleet of semi-submersibles with drilling capabilities numbered 133, and the drillships 22. Although the minimum water depth for deep water operations is debatable, the number of semi-submersibles that can operate in waters deeper than 610 m (2,000 ft) is 39, and the drillships amount to only 10. And, if we restrict our search to vessels equipped with DP systems, we find only 8 semi-submersibles and 7 drillships [Source: World Oil Magazine, Dec/1995].

It is interesting to point out that the average age of the available deep water rigs is 14.5 years, and that DP vessels in Brazil are quickly approaching an average of 20 years of age.

Some of these rigs have received upgrades that replaced parts of their aging subsystems. Even so, there are so many parts in the overall system that can fail, and generate an emergency disconnection that, with an aging fleet this problem is bound to recur.

1.8 - RISER TENSIONERS CONSIDERATIONS

In the conventional riser technology the riser tensioners, needed to maintain the string under tension and avoid buckling, are strained by the weight of the mud inside the riser annulus (Fischer & Ludwig, 1965). Moreover, the water depth capability of a drilling rig can be defined as the maximum water depth it can run a riser, under the following criteria:

- Maximum mud weight of 16 ppg (119.68 lbs/ft^3);
- Buoyant weight equal to 10% of the riser string weight in air;
- Overpull of 50,000 lbf.

The force applied by the tensioners depends heavily on the density of the fluid within, since the pipe weight in water is greatly decreased by surrounding it with floatation devices. With the dual density riser system, the top tension could be greatly reduced. As an example, the drillship Pacnorse I is rated for a 4910 ft (1500 m) water depth for its riser tensioning capacity and riser size. The tensioning capacity is 960,000 lbf, and the riser size is 18 5/8" x 17 1/2" [RSV Gusto Engineering, 1979].

According to Heuze et al. (1975), the tension required at the top of the riser is:

$$F_T = R_w + W_{mud} - B + O \qquad (1.2)$$

Since, by design, (R_w - B) = 0.1 R_w, and that the riser length is related to R_w by:

$$R_w = h[\frac{490\pi}{(4 \times 144)}(OD_r^2 - ID_r^2)] = 108.614h \quad (1.3)$$

If we solve for the riser length:

$$h = \frac{F_T - O}{(7.48\rho_m \cdot C_r) + 10.861} \quad (1.4)$$

After calculating the riser capacity per foot, we find C_r = 1.458 ft^3/ft. For the design mud weight of 16 ppg, h = 4,908 ft (1,496 m), while for sea water (8.5 ppg), h = 8,785 ft (2677 m). A 79% increase in water depth capability, in this case.

This is a theoretical increase in water depth capability, though. The riser storage space available on board is usually at a premium, and in a semi-submersible rig deck load is always optimized at its maximum. Thus, the addition of dozens of extra riser joints to the permanent rig load would present a problem. The alternative would be the storage of the excess riser joints aboard supply vessels, kept waiting nearby.

1.9 - HIGH SEA CURRENTS ENVIRONMENT

The dual density riser would not only extend the water depth capabilities of any given rig, but would decrease the risk of riser recoil, during emergency disconnections. This would allow for tensions greater than normal, that could straighten the riser string in high current environments.

The ability of working in high currents is critical in areas like the Campos Basin, where mid-depth currents can be as strong as 1.5-2.0 knots, dangerously bowing the riser string. As an example, the Pacnorse I, in 1991, had two top riser joints bent after disconnecting in high currents. The reason for the disconnection was that the riser string had bowed so much, due to the current, that the angle at the ball-joint was varying between 9.0° and 9.5°. Since the Lower Marine Riser Package will not disconnect with

an angle greater than 10°, the rig had to disconnect for safety reasons. At the same time, the Sedco-709 kept on working, while operating in the same area, but being able to apply a much greater top tension to its riser (Source: Petrobras).

1.10 - COMPARISON WITH A FULL AERATED MUD SYSTEM

Proposing such a solution brings up the question of whether using a full blown aerated mud system instead, would not be more feasible, since this type of system already exists and has been tested.

The first consideration against the aerated mud system is that it requires that all the fluid is to be mixed with gas, at surface, increasing the gas volume needs. Moreover, the amount of gas would depend on the depth of the well, and not only on the water depth. This could lead to the adoption of equipment designed for wells that would be drilled only in rare occasions.

It would also add complexity to well control procedures, particularly in cases where the invading fluid is not a gas. Furthermore, with a system where all the mud is aerated with air, the possibility of downhole fires, especially in horizontal wells where drilling through the pay zone is a long process, can cause costly accidents.

1.11 - DISSERTATION OBJECTIVES

The basic objective of this dissertation is to determine the feasibility of the dual density riser solution. To do this, a few goals have to be established:

- A computer simulator: to be able to predict the size and power needed for the surface equipment. This simulator would have to provide the necessary gas rate to achieve the desired BOP level equivalent density. It should take into account all the variables involved, such as: pump rate, mud properties, riser and string

geometry and the temperatures, at surface and along the riser's length. This simulator should also allow the user to predict the gas injection pressure and the amount of time involved in achieving two-phase flow steady state.

- Experiments: to validate the computer simulator or to calibrate it. These experiments should be done in an actual well, using enough gas to achieve two-phase flow steady state. The well should be deep and the casing large enough to reasonably simulate a deep water riser string.
- Simulations: a few cases should be simulated to provide a picture of the system's possible performance. These cases should be chosen to replicate the Gulf of Mexico conditions, due to the large amount of work being done and scheduled for this area, and its high pore pressure gradients.
- Drilling operation procedures: different operations are performed during the drilling of an oil well. Many of these operations would be directly affected by the introduction of gas in the riser annulus. To determine if there would be any impossible hurdles in the implementation of such a system, there should be an analysis of the drilling procedures. Operations like the detection and circulation of a kick, simple drill-pipe connections, casing runs, logging jobs, pump failures and others should be discussed, case by case.
- Cost Estimates: enough information should be presented to provide a realistic cost comparison between the conventional riser system and the dual density solution. The cost of nitrogen generation and compression needed for the new system should be accessed, to establish its economical viability.

CHAPTER II

LITERATURE REVIEW

2.1 - AERATED DRILLING

Wilfred (1976) addressed the possibility of riserless drilling, considering two alternatives: non-concentric and concentric return line systems. Both systems would use a rotating head on top of the BOP stack. The return flow would come up by an external conduit (non-concentric system) or through a pipe placed inside the drill string (concentric system). He points out some potential problems for both systems:

- Rotating head reliability;
- Tangling of lines (in the non-concentric system);
- Reentry times;
- Especial heave compensation;
- High pressure losses in the return lines;
- Tension limits on the inner pipe (concentric system);
- Communication with the BOP when the drill string is out of the hole;
- Tripping times for a dual concentric string system;
- External line tensioning.

Both systems would require a riser safety margin to operate.

Wallace et al. (1979), provide data from 59 wells drilled with aerated mud in the Nevada Test Site, where big diameters are needed for nuclear testing. He compares four types of mixtures for the aerated fluid:

- Air-foam;

- Air-low water loss bentonite;
- Air-sepiolita;
- Air-thin bentonite.

The comparison is in terms of hole size and drilling costs. The results favored the air-low water loss bentonite mixture.

To determine the carrying capacity of the aerated mud, a minimum drag coefficient, D_c is used to calculate the particle slip velocity (v_{sl}). This drag coefficient is based on the work of Ikoku (1980), where values for sandstone, shales, and limestone are given.

Cobbet (1981) discusses the application of foam systems to vertical drilling in Oman, in loss circulation areas. The top hole section had diameters of 20" (0.51 m) and 17.5" (0.44 m) down to 2500 ft (762 m). It was possible to reduce air rates from 600 SCF/min to 150 SCF/min, and mud flow rates from 40 gpm to 15 gpm. The experience gained using different foaming agents provided adequate cuttings lifting capability. He reported that a velocity in the range of 15 ft/min (4.6 m/min) and 20 ft/min (6.1 m/min) provided adequate cleaning capacity to the mixture. In a 17.50" ID riser, with a typical 5.50" OD drill-pipe string, these velocities require a mixture flow rate between 169 gal/min and 225 gal/min. A computer simulator program was developed to determine the optimum back pressure, air-slurry ration and bottom hole pressure for foam coring, which provided good recoveries in very friable formations.

Rizo et al. (1984) describe the use of aerated drilling in geothermal wells in Luzon, Philippines, where lost circulation zones are found. They report severe pipe corrosion due to the exposure of the drill string to the oxygen contained in the drilling

fluid. Wells in that area are, normally, drilled with water and no return flow (blind drilling). The comparison between the two techniques showed that, in a 8,841 ft (2,694 m) well drilled with aerated mud, a total of 38 joints of drill-pipe was downgraded or junked due to corrosion. In another well in the same area, drilled blindly to 9,000 ft (2,743 m), the number was 10 joints.

Westermark (1986) described the use of a *parasite string* attached to the outside of a casing string, to inject air into the casing-drill pipe annulus. This was done by Phillips Petroleum Co. in a well drilled in Gallatin County, Montana. He reported that effective mud weights of 6 ppg (719.6 kg/m^3) were obtained for the mixture air-mud. To connect the 2 1/16" (52.4 mm) parasite string to a 13 3/8" (340 mm) casing string, a tie-in injection sub was built out of a 13 3/8" (340 mm) float-collar. The parasite string was attached to the casing by hinged clamps fastened to the casing collars.

Craytor et al. (1991) present the case study of a medium-radius horizontal well drilled with aerated mud for Marathon Oil Co. using the EMMWD tool. This tool operates by inducing an electric current into the surrounding rock formation, creating an electromagnetic wave that propagates in the formation and is channeled along the drill string. Information is transmitted by current modulation and is decoded at surface. The system allows bi-directional communication between the tool and the surface equipment, and the transmission of information while tripping. Since the tool transmits information through the drill string, it is capable of detecting a parted string, or if a fish has been successfully engaged. Craytor also concludes that the most critical mud properties were the yield point and gel strength. The optimal values were in the range of 6 and 12 lb/100 ft^2 for the yield point, and among 6 and 10 lb/100 ft^2 for the gel strength.

Guo et al. (1993) discuss the carrying capacity of aerated muds and the optimal air injection rate to ensure maximum penetration rates, using computer simulations. They state that bubbly flow dominates the aerated mud flow in drilling operations. Also that there exists an air injection rate that yields the lowest flowing annulus pressure for a given mud rate and well geometry. Moreover, their results show that there is an unfavorable range of mud flow rate that provides poor carrying capacity for the aerated mud for all air injection rates.

Their mathematical model for a three phase flow (air, mud, and cuttings) through a vertical pipe is based on the General Energy Equation, as described by Beggs (p58-60) and Bourgoyne et al. (128-129), neglecting the kinetic term:

$$H_{Tot} = \int_{P_d}^{P_u} \left(\frac{\frac{b \cdot T_{avg} \cdot z}{P} + Q_m + Q_c}{a\left[1 \pm d\left(\frac{b \cdot T_{avg} \cdot z}{P} + Q_m + Q_c\right)^2\right]} \right) dP \qquad (2.1)$$

with:

$$a = \frac{\gamma_g \cdot b}{53.34} + \rho_m \cdot Q_m + \rho_c \cdot Q_c \qquad (2.2)$$

$$b = \frac{Q_{gsc} \cdot P_{sc}}{z_{sc} \cdot T_{sc}} \qquad (2.3)$$

$$c = \frac{M}{A} \qquad (2.4)$$

$$d = \frac{2f \cdot c^2}{a^2 \cdot g_c \cdot D_e} \qquad (2.5)$$

Equation (2.1) is used iteratively to solve for P_u, the upstream pressure, in the computer simulator. The simulations were validated with data from 3 wells drilled with

aerated mud, with pipe sizes of 4.5" (11.43 cm) inside a 7 7/8" (20.00 cm), and show a consistent correlation.

The results also show that, for a fixed air flow rate, when the mud rate is increased, the mixture density increases, which reduces the particle slip velocity. This increase in mixture density also decreases the average fluid velocity at beginning, but after a certain value of mud rate is reached, this tendency is reversed. So, there is a range of values for mud rate and air flow rate in which the mixture carrying capacity decreases with mud rate. Cuttings accumulation in the riser is a problem even with non-aerated muds, especially in the bottom part of the riser, due to the sudden increase of conduit diameter.

Allan (1994) presents a nitrogen drilling system used by Meridian Oil on three horizontal wells in the San Juan Basin, in New Mexico. The nitrogen is generated on-site by removing the oxygen from atmospheric air, using an oxygen filter membrane. Since there is no need for cryogenic equipment, or transportation, the costs are significantly reduced. The objective was to eliminate the occurrence of downhole fires using an inert gas in the aerated drilling mud. The system's generation efficiency is defined by the ratio between the flow rate of output enriched air to the input flow rate. The higher the efficiency is, the higher is the oxygen content of the mixture. Oxygen content varied from 2% to 14%, with correspondent efficiencies of 35% to 75%. The theoretical maximum efficiency is 78%, corresponding to a zero oxygen content. He uses the following relationship to determine the minimum oxygen percentage necessary to maintain combustion:

$$O_{2_{min}} = 13.98 - 1.68 \log P \qquad (2.6)$$

where P is the downhole pressure (psia).

Kitsios et al. (1994) describe three field trials in Oman that use "stable foam" for underbalanced horizontal drilling. The referred stable foam is a mixture of air and a foaming solution, combined at surface, with liquid as the continuous phase. The consistency is that of a shaving cream, providing a lifting capacity superior to that of common drilling fluids. For directional measurements an electromagnetic propagation EMMWD system was employed. The transmission of data, in this system, is done by low frequency electromagnetic waves. Due to electromagnetic attenuation of the waves in the formations above the tool, there is a maximum working depth for transmission without a sequential relay system. This consists in a mini-MWD receiver-transmitter without sensors. A foam positive displacement downhole motor was developed to work with stable foam. Monitoring of sub-hydrostatic reservoir pressures was done with the use of an echo meter, together with surface annular pressure readings. To alleviate the problem of unloading the produced crude after connections, a jet sub was installed higher in the drill string. This was done to assist the lifting of the oil column and the cuttings to the surface, without inducing losses.

World Oil Magazine (August 1995) published an article about the same nitrogen generator used in the San Juan Basin of New Mexico and Colorado. The rate of downhole fires in this area is between 5% and 10% of the wells drilled. The generator is capable of delivering up to 3000 SCF/min, depending on product purity. The purity of nitrogen produced is dependent on compressed air flow rates, temperatures and pressures applied across the membrane modules, where the oxygen and water vapor are

stripped out. New equipment is being developed, using either hollow fiber membranes or pressure swing adsorption devices. It has recently being patented by Dow Chemical Co., with additional patents pending for nitrogen generation. Besides the horizontal and vertical wells in San Juan, successful underbalanced drilling using these units is also reported in Canada, Texas, Montana, and North Dakota.

2.2 - RISERS

Fisher and Ludwig (1965) solved the differential equation for riser deflection under static forces and presented generalized design curves to calculate the required minimum riser top tension. The determination of deflection, rotation and bending moment along the riser length is obtained through the solution of an ordinary linear fourth order differential equation for the deflection of a laterally loaded uniform vertical beam. They also explain why the effective axial tension at any point along the riser is equal to the supporting tension at the top less the combined weight in water of riser, mud and free-standing drill pipe or casing above the point under consideration.

Heuze et al. (1976) discuss the forces and strains in the riser system under dynamic and static conditions. They consider the bending moments introduced by high velocity currents and propose solutions for the generated stresses at riser top. They also analyze the force components that comprise the necessary top tension to avoid string buckling. They studied different buoyancy systems, such as external riser tanks where air can be injected to displace sea water and decrease the overall system density. Conventional synthetic foam buoyancy systems have also being tested and are described.

Erb et al. (1983) describe a riser collapse case history in 1,750 ft of water in the Gulf of Mexico. The three bottom riser joints collapsed after the rig took a kick with

only the 16" casing set. The BOP was not closed, out of fear of fracturing the formation and the diverter malfunctioned after three minutes of operation. The riser had 21 inches of outside diameter and 0.5 inches of wall thickness. They explain the mechanism of collapse and present curves to estimate the critical collapse water depths for different riser diameters and wall thicknesses.

Hall et al. (1986) describe the implementation of a riser diverter system, beneath the telescopic joint, to provide a safe handling of gas kicks inside the riser string.

Gault (1996) and McLeod (1976) discuss different alternatives for drilling without a conventional riser system. They point out the disadvantages of the present technology when applied for very deep waters. They emphasize the great inertia of long riser strings and its effects on the tensioner system, and the extra space and deck load capacity required for long risers. The alternatives presented do not include the aeration of the mud inside the riser string. They do not discuss the extra hydrostatic pressure added by the density difference between the sea water and the mud within the riser annulus.

2.3 - TWO-PHASE FLOW

Rader et al. (1975) studied the factors that affect the bubble rise velocity in an annulus. They conducted experiments in several laboratory scale models and in a 6,000 ft (1830 m) well. The scale models allow for visual observation of the phenomena. They concluded that bubble velocity and bubble fragmentation significantly affect the annular pressure losses. Moreover, that the annular geometry was the most important factor affecting bubble velocity, with the velocity increasing rapidly as the outer diameter increases, and increasing to a lesser extent when the inner diameter was increased.

Langlinais et al. (1983), conducted a study of frictional pressure losses for both single-phase (drilling fluid only) and two-phase flow (mud and methane gas), using two 6,000 ft (1830 m) wells, Baton Rouge, Louisiana. For the single-phase flow, they compared the experimental data with the pressure loss predictions given by different equivalent diameter criteria. These were the one defined by Crittendon (1958), the hydraulic radius concept, and the slot flow approximation. They used both the Bingham Plastic and Power Law Rheological Models. In two-phase flow, they compared the total pressure difference measured in the experiments, with the ones predicted by the Poettmann and Carpenter, Hagedorn and Brown (1964), Orkiszewski, and Beggs and Brill (1972) correlations. They concluded that, overall for the single phase flow, the Crittendon (1958) equivalent diameter in conjunction with the Bingham Plastic Model gave the best results for the muds tested. For the two-phase flow, they found that the best results were obtained with the Hagedorn and Brown (1964) correlation, using a Power Law Rheological Model and the hydraulic radius concept as the equivalent diameter.

Nickens (1985) developed a mathematical model for a kick simulator. He based his model in the continuity and momentum equations for a mixture of gas and liquid. The model also included equations of state for gas and liquid phases, and an empirical correlation for the gas slip velocity. He proposed a solution based on finite differences for the one dimension time-space problem. The annulus is divided in cells, equally spaced, and a set of six equations is solved, by iteration, from bottom upwards. The necessary variables are: gas and mud velocities, gas fraction, gas and mud densities, pressure, and temperature. Starting with the bottom cell, he assumes that the bottom

hole pressure (BHP) is kept constant (boundary condition), and makes a guess to solve the set of equations for the top of that cell. After iterating until the calculated value for BHP matches the initial value, he equates the calculated top variable values to the bottom of the next cell. In the next time step, there are two cells, and the process is repeated, advancing one cell at a time, until the top cell reaches surface. He points out that time steps of 1 second are desirable, but require too much processing time, for the hardware available by the time of his publication.

Casariego and Bourgoyne (1988), proposed a method to calculate gas rise velocity and gas concentration in vertical wells. Their model models the effect of gas concentration on gas velocity for both static and circulating conditions. A computer simulator was developed and the model showed good agreement with data from a 6,000 ft well.

Santos (1989) used the model proposed by Nickens to simulate the unloading of a well, to study well control operations with a diverter.

Nakagawa (1990), working in a well control project conducted by the Petroleum Engineering Department of Louisiana State University, studied the rise of gas in an eccentric flow loop, with different inclinations. The objective was to determine the gas fraction and gas velocity during the gas kick. He presented a model for the gas-rise velocity eliminating the bubble size and shape in the calculations.

Johnson and White (1990) studied the gas rise velocity, using air in water and in xanthan gum. The xanthan gum was used to emulated the rheology of a drilling fluid, while maintaining transparency, needed for visual observation through the plastic pipe used for the experiments. The comparison between the gas rise velocities in the two

media showed that the gas rises faster in the more viscous fluid than in water. This was explained with the observation that, for all the gas concentrations, the air rises up the pipe as large bubbles, as large as the pipe diameter. The gas flow rate determines the bubble frequency, instead of their size. Moreover, the gas velocity is independent of the gas fraction, for void fractions greater than 7.5%. The velocity value found was constant and equal to 0.55 m/s (1.8 ft/sec).

Ansari et al. (1990), proposed a comprehensive mechanistic model for the upward two-phase flow, where the flow pattern is predicted, before the calculations, by taking into account the flow pattern mechanism. After situating a given flow pattern between bubble, slug, churn and annular flow limits, the flow variables are calculated with a specific model for the identified flow pattern. The evaluation of the model was done with data from a data bank of 1,712 well cases, with its performance compared with six correlations and mechanistic models in use by the industry. It interesting to note that the Hagedorn and Brown (1964) correlation performance is excellent, with results comparable to the proposed model, showing the best results overall for deviated wells.

Cappuci and Serra (1991) studied the multiphase flow transient effect during the unloading of continuous gas lift systems. They used the Nickens mathematical model, modified to include the liquid and gas viscosities. The liquid viscosity was assumed to be only a function of temperature, while gas viscosity was assumed to depend on pressure and temperature, and was determined with an empirical correlation.

Hovland and Rommetveit (1992), experimented with oil and water-based muds in a full scale inclined well, in Stavanger, Norway. They found that the gas rise velocity is independent on gas void fraction, mud density, inclination, mud rheology, and surface

tension. Also that, for high concentration kicks the gas rise velocity is higher than in low and medium concentrations.

Aziz and Petals (1994) worked in a PC-based software for multiphase flow calculations. They assumed that, in order for bubble flow to exist, the pipe diameter has to be large enough, and the inclination steep enough to prevent bubbles from rising to the top of the pipe. Furthermore, they assume dispersed bubble flow when the gas in the liquid slug reaches, or exceeds, the maximum volumetric packing density. This happens when the liquid rate is high enough to break up the slug.

2.4 - KICK DETECTION

Drilling operations with aerated mud systems always present the problem of kick detection. The typical procedure of monitoring the mud system volume, to check for fluid influx into the well, depends heavily in the assumption of mud incompressibility. The dual density riser solution has the advantage of having just part of the system aerated: the mud in the hole can still be considered incompressible. But, since the return flow is aerated, new techniques for kick detection have to be developed, with the possible positioning of sensors at the BOP level.

Bryant et al. (1990) describe the technique of detecting gas influx in water-based muds using the signals generated by a standard MWD pulser. When the MWD pulser generates the positive-pressure signal needed for data transmission through the drill string fluid, another, pressure-negative pulse, is created under the pulser mechanism and propagates up through the annulus. The technique consists in receiving and analyzing this second signal, monitoring its phase and amplitude, to detect variations that will indicate the presence of gas in the annular space. Two sets of experiments were

conducted, in a 1,480 ft (451 m) vertical well and in a 63° directional well with a true vertical depth of 4,921 ft (1500 m). The detection times were around 1.5 minutes, and even less, on both cases, for gas concentrations greater than 8.3 scf/bbl. For smaller concentrations the detection times were in the 2.0 - 3.0 minutes span, although the signals were sample with a frequency of only one sample per minute. The system monitors the entire annular space, being able to detect gas influx entering at any depth. The detection is qualitative, although a quantitative model can be built, to automate the detection process.

Another way to detect the presence of gas in the mud was presented by Vestavik et al. (1990). This technique uses the measurements of an acoustic interferometer to differentiate the nature of a fluid. The sonic interferometer is a device where acoustic waves are generated between two parallel walls. At certain frequencies the system will resonate. The sound velocity and attenuation constant of the fluid between the plaques can be calculated from measurement of the center frequency and bandwidth of the resonance peak, so different liquids will have an acoustic "signature". When gas is introduced in the fluid, the system gets out of resonance and these peaks disappear. The system is able to detect gas in drilling fluids in concentrations as small as 1% in volume, and the authors suggest that it can find application in MWD tools.

Bang et al. (1994) present the results of experiments done on a 1210 m (3970 ft) well, with water and mud, in Norway. In these experiments a water gun was used as an acoustic source to generate an echo received by sonar sensors. Both emitter and receiver were located at the surface wellhead. To simulate a kick, gas was injected and allowed to rise by its buoyancy to surface. Results showed an average rising velocity for the gas, in

water, of 40 cm/s (1.312 ft/sec). The average for the gas rising velocity in mud was 25-30 cm/s (0.82-0.98 ft/sec). They noticed that the end of the drill string in the hole had no apparent influence on the echoes, neither as a source of reflections, nor as a cause of signal distortion. The system was able to detect an influx of gas 2-3 minutes after injection, although the reflection from the gas in mud was less distinctive than in water. The system is theoretically capable of detecting gas in depths of at least 5,000 m (16,405 ft). The system's sensitivity is increased when the column of liquid above the sensors is also increased. For the experiments, the sensors were positioned approximately 3 m (9.8 ft) below the return line level.

McCoy et al. (1992) describe a digital system for automatic calculation of bottom hole pressure from annular fluid level echometric surveys in pumping wells. The system is configured for long term unattended operation and controlled by software. The system has being field tested in a variety of conditions without any problems. The system uses an acoustic source to send a sound signal down the annulus. A pressure transducer detects the reflecting signal and the software calculates the fluid level. The device also accounts for temperature and acoustic velocity variations as well as changes in the fluid composition.

Benadelkarim and Galiana (1991) present a non-radioactive densitometer for monitoring cement slurry. The device uses a vibration tube in which the slurry flows through. The temperature and the oscillation period are measured and the density is directly proportional to the square of tube's oscillation period. The Coriolis fluid forces, which are perpendicular to the fluid velocity cause the tube to twist. This movement is measured electronically. The device directly measures density and flow rate with a time

response of 0.2 seconds, which is suitable for control systems to operate on real time. The accuracy is within 0.1 ppg.

2.5 - GAS LIFT AUTOMATION

Schnatzmeyer et al. (1994) describe the implementation of an electric gas-lift valve, where the size of the downhole gas injection orifice can be remotely adjusted from a surface control unit. A prototype has being field tested. It consists of an electrically operated valve controlled from the surface, pressure transducer and a controller. The prototype remained operational after 18 months of tests.

Cooksey and Pool (1995) discuss the development of modular systems that can automate load shedding that can result from gas lift fluctuations. When these fluctuations occur, an intelligent controller can automatically adjust the injection rate so the optimum rate can be provided. The system is composed of two main components: a controller and an adjustable choke. A standard orifice meter with pressure and differential pressure transducer provides the information to the controller.

CHAPTER III

SIMULATOR MODEL

3.1 - INTRODUCTION

During operation the dual density riser will be in a dynamic state, in that sea water density is achieved in the riser annulus through the constant injection of compressed gas, through an external riser line. This state will be subject to variations caused by changes in the mud flow rate, in the gas flow rate or in both. There will be a need to know the gas injection rate that will provide the right equivalent density at the BOP for every change of the mud pumping rate. Conversely, if there is an increase in the mud properties, such as the density, an appropriate increase in the gas injection rate should follow.

To simulate the dynamic states of the fluid in the riser annulus, a mathematical model is presented here. The proposed model is subdivided into a steady and an unsteady state sub-models.

3.2 - STEADY-STATE MODEL

3.2.1 - Assumptions and Considerations

The following assumptions and considerations have been made before the development of the simulator steady-state routine:

1) The temperature is constant over the entire length of the riser and gas injection line and behaves linearly.
2) The pressure at the top of the riser is known. This pressure is normally controlled by a choke mechanism and a manifold system.

3) The geometries of the riser annulus and the gas injection line are constant and known.
4) The liquid injection rate is known and constant.
5) The liquid phase is incompressible.
6) The gas injection rate is known and constant. Although the simulator can determine the gas rate for a desired overall mixture density, it does this by trying different gas rates to converge to the solution.
7) The gas injected is nitrogen or air. It is homogenous and has known composition. Moreover, its solubility in the drilling fluid is negligible.
8) The fluid properties are known and constant over the entire system.
9) There are no restrictions that introduce pressure losses in the simulated system. All the friction losses are due to the interaction of the single phase gas or the two-phase mixture with the pipe walls.

3.2.2 - Algorithm Flow

To model the Dual Density steady-state the direct integration method was chosen. The riser annulus and the injection line are divided in "cells", with height depending on a user input: the more cells, the more precise the algorithm and the slower the simulation.

Figure 3.1 shows the overall algorithm flow, which starts at the top, progresses towards the riser bottom and goes upwards through the injection line.

After the assignment of the top pressure's value to a temporary variable, the algorithm calculates the initial guess for the pressure at the bottom of the first cell.

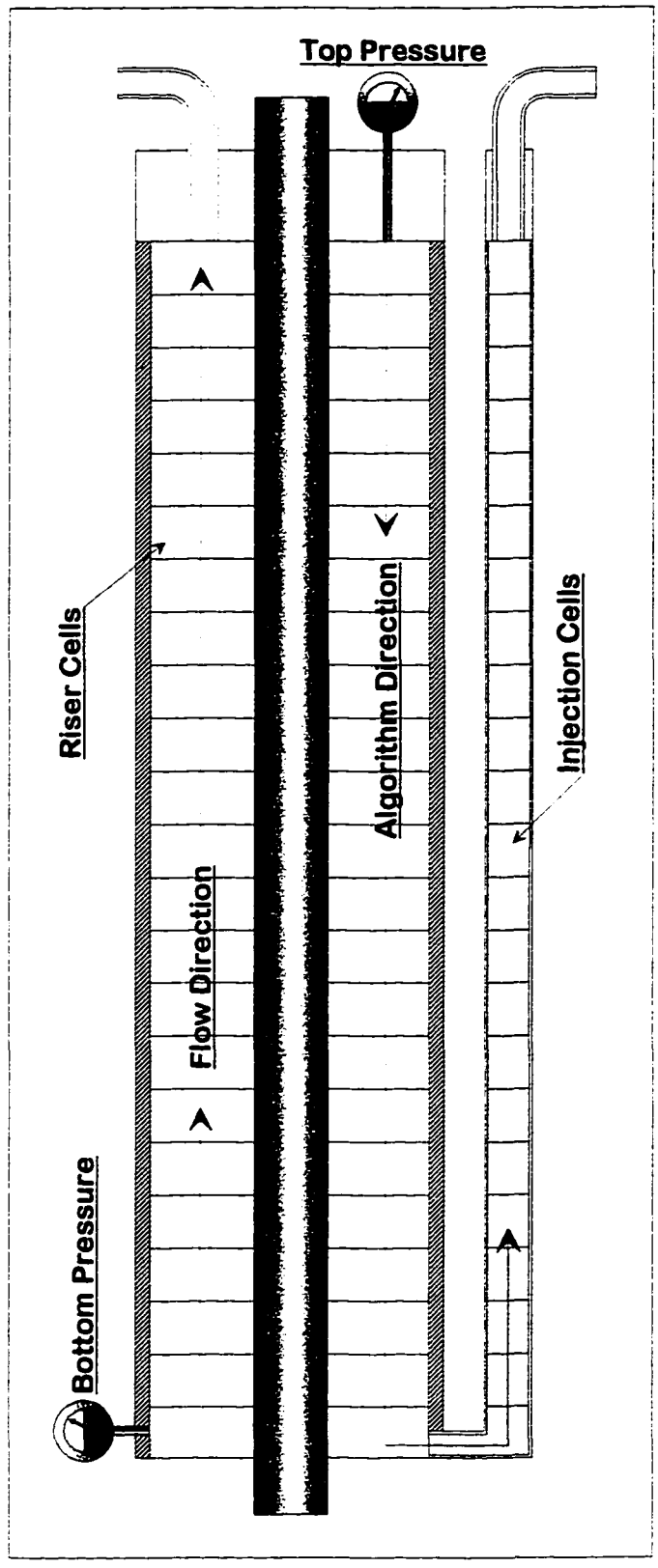

Figure 3.1 - Steady-State Algorithm and Flow Directions

Figure 3.2 shows the flow chart. The guess value is calculated by taken half of the hydrostatic pressure due to the liquid alone and summing it to the top pressure.

The algorithm then starts the outer loop that cycles through all the riser cells. The pressure for the top of the cell is recovered from the temporary variable and the cell's bottom pressure takes on the guessed value. The cell temperature is determined next, and assumed constant along the cell, before entering the inner loop. The inner loop is responsible for the convergence of the guessed pressure into the cell's bottom pressure. It calculates the variables in the following order:

- Gas Deviation Factor (Z). Input: Cell Temperature and Bottom Pressure. (dimensionless).
- Superficial Gas Velocity (Vsg). Input: Gas Rate, Temperature, Pressure and Z-factor. (ft/sec).
- Mixture Velocity (VmBot). Input: Superficial Liquid Velocity and Superficial Gas Velocity. (ft/sec).
- Gas Density (DgBot). Input: Z-factor, Temperature and Pressure. (lbm/ft3).
- Slip Velocity (Vslip). Input: Gas Density, Superficial Liquid Velocity and Superficial Gas Velocity. (ft/sec).
- Gas Velocity (VgBot). Input: Mixture Velocity and Slip Velocity. (ft/sec).
- Liquid Holdup (HlBot). Input: Superficial Gas Velocity and Gas Velocity. (dimensionless).
- Liquid Velocity (VlBot): Input: Liquid Holdup and Superficial Liquid Velocity. (ft/sec).

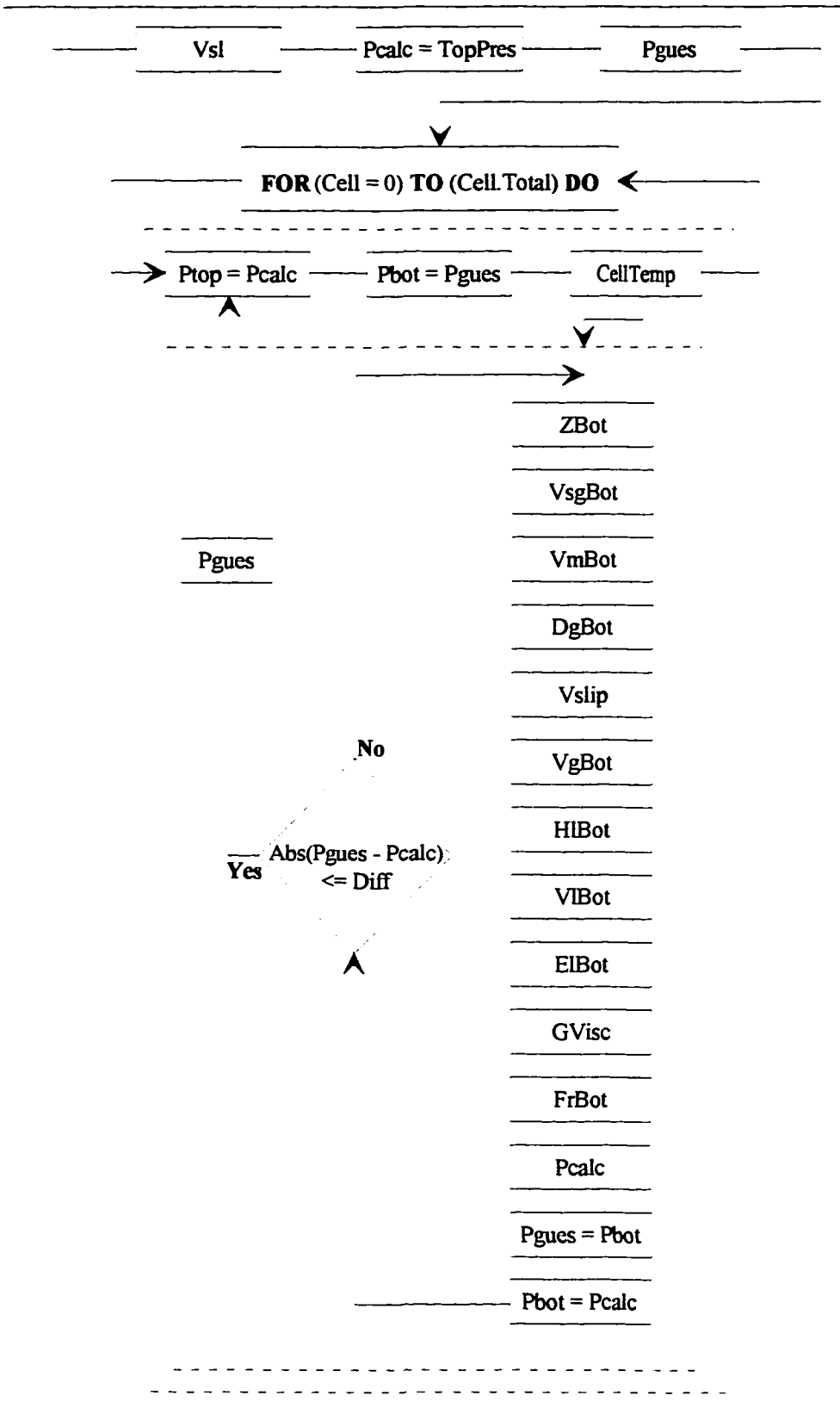

Figure 3.2 - Riser Steady-State Algorithm Flow Chart

- Mixture Density (ElBot). Input: Liquid Holdup and Gas Density. (lbm/ft3).
- Gas Viscosity (GVisc). Input: Temperature and Gas Density. (cp).
- Friction Loss (FrBot). Input: Liquid Holdup, Gas Viscosity, Gas Density, Gas Velocity and Superficial Liquid Velocity. (psi/ft).

With the Mixture Density and the Friction Loss the algorithm obtains the calculated pressure for the cell bottom (Pcalc). This value is compared to the guessed value, and if the absolute difference is smaller than a preset amount the algorithm goes on to the next cell, after guessing its corresponding bottom pressure. If the difference is greater, the inner loop cycles again, this time with the calculated value as the guessed cell's bottom pressure.

3.2.3 - Algorithm Steps for the Injection Line

Figure 3.3 presents the algorithm flow chart for the gas injection. The algorithm direction now is upwards, contrary to the gas flow. So the cell number in the outer loop begins where the riser loop left, at the last cell. After that, it goes back to the initial cell, calculating the top pressure of each cell, since the initial boundary condition is the bottom hole pressure found in the riser annulus. The variables are calculated in the following order:

- Gas Deviation Factor (Z). Input: Cell Temperature and Top Pressure. (dimensionless).
- Superficial Gas Velocity (Vsg). Input: Gas Rate, Temperature, Pressure and Z-factor. (ft/sec).
- Gas Density (DgTop). Input: Z-factor, Temperature and Pressure. (lbm/ft3).

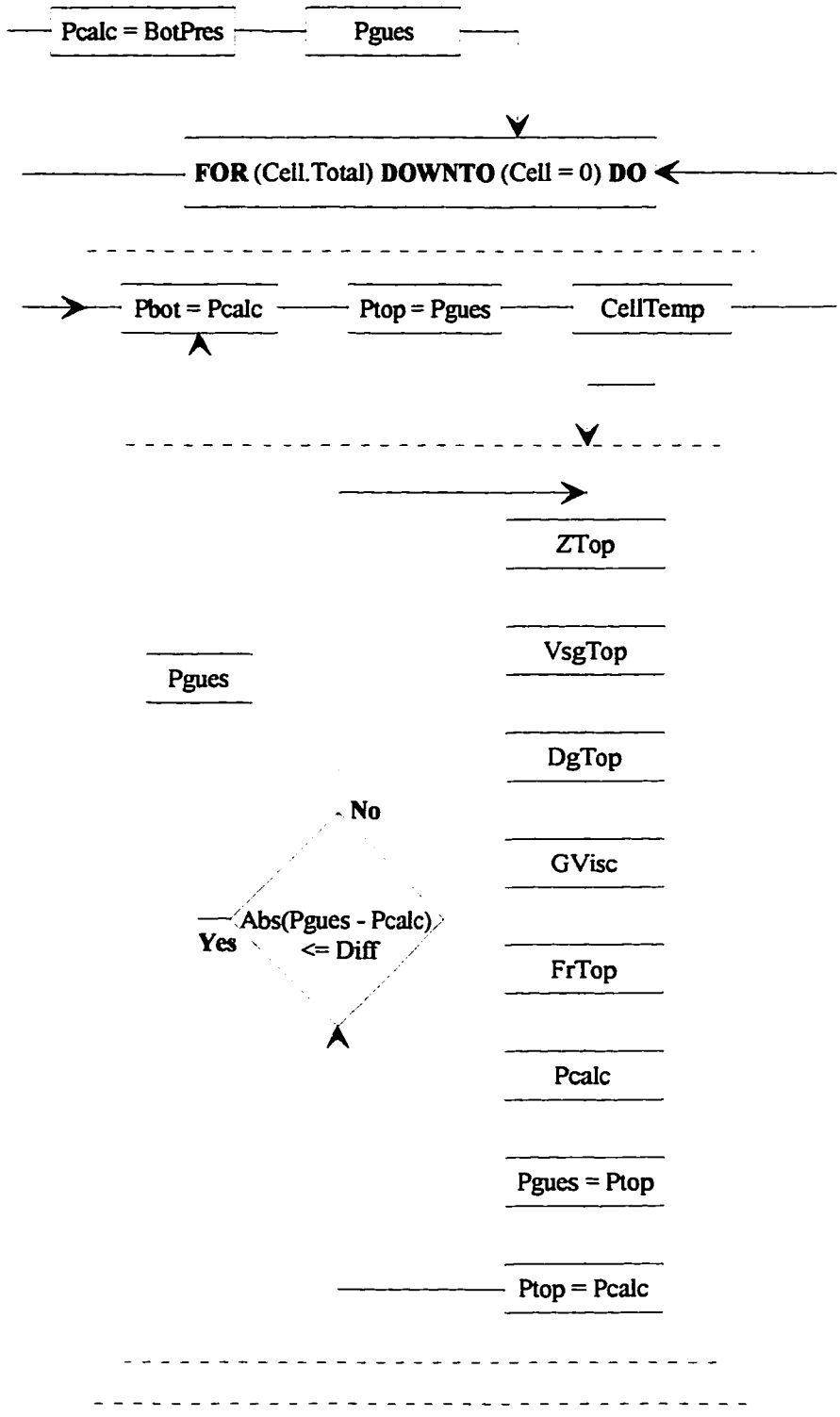

Figure 3.3 - Gas Injection Steady-State Algorithm Flow Chart

- Gas Viscosity (GVisc). Input: Temperature and Gas Density. (cp).
- Friction Loss (FrTop). Input: Superficial Gas Velocity, Gas Viscosity, Gas Density, and Injection Line ID. (psi/ft).

After convergence in the inner loop, the algorithm cycles to the next cell in the same manner as in the riser outer loop.

3.2.4 - Gas Compressibility Factor

The simulator has to calculate several two-phase flow variables in the steady-state algorithm and some of the procedures employed rely on empirical correlations to estimate the values needed. One of them is the determination of the gas compressibility factor.

Amongst the available routines in the literature, the Dranchuk and Abou-Kassem equation of state (Craft and Hawkins, p. 19, 1991) was chosen to estimate the Z-factor. The equation has the following form:

$$z = 1 + C_1(T_{pr})\rho_r + C_2(T_{pr})\rho_r^2 - C_3(T_{pr})\rho_r^5 + C_4(\rho_r, T_{pr}) \tag{3.1}$$

$$\rho_r = 0.27\frac{P_{pr}}{z \cdot T_{pr}} \tag{3.1a}$$

$$C_1(T_{pr}) = A_1 + \frac{A_2}{T_{pr}} + \frac{A_3}{T_{pr}^3} + \frac{A_4}{T_{pr}^4} + \frac{A_5}{T_{pr}^5} \tag{3.1b}$$

$$C_2(T_{pr}) = A_6 + \frac{A_7}{T_{pr}} + \frac{A_8}{T_{pr}^2} \tag{3.1c}$$

$$C_3(T_{pr}) = A_9\left(\frac{A_7}{T_{pr}} + \frac{A_8}{T_{pr}^2}\right) \tag{3.1d}$$

$$C_4(\rho_r, T_{pr}) = A_{10}(1 + A_{11}\rho_r^2)\left(\frac{\rho_r^2}{T_{pr}^3}\right)\text{Exp}(-A_{11}\rho_r^2) \qquad (3.1e)$$

where the constants are:

$A_1 = 0.3265$

$A_2 = -1.070$

$A_3 = -0.5339$

$A_4 = 0.01569$

$A_5 = -0.05165$

$A_6 = 0.5475$

$A_7 = -0.7361$

$A_8 = 0.1844$

$A_9 = 0.1056$

$A_{10} = 0.6134$

$A_{11} = 0.7210$

Since the Z-factor appears on both sides of the equation, the solution involves a trial-and-error algorithm. In this case the Newton-Raphson method is used, for its speed of convergence.

The Dranchuk and Abou-Kassen correlation presents an average absolute error of 0.486% over ranges of pseudo-reduced pressure and temperature of:

$$0.2 < P_{pr} < 30$$

$$1.0 < T_{pr} < 3.0$$

When using nitrogen the corresponding pressure and temperature ranges are

$$125 \text{ psia} < P < 18{,}802 \text{ psia}$$

$$438\ ^{\circ}\text{K} < T < 1314\ ^{\circ}\text{K}$$

The values for pressure and temperature applicable in the simulations are well within the specified range. The desired top pressure, although, should be as close as possible to the atmospheric pressure, since it generates a significant increase in the gas injection rate for a given riser bottom pressure.

The pseudo-critical pressure and temperature are calculated using the Sutton (Craft and Hawkins, p. 16, 1991) correlation for a given gas specific gravity.

3.2.5 - Slip Velocity

The correlation used was developed by Adam T. Bourgoyne (Ohara, 1995) and has the following form:

$$v_s = \frac{1}{0.3048}\left[0.18 + 0.07\text{Ln}(\mu_p)\sqrt{\frac{(7.48\rho_m - \rho_g)}{7.48\rho_m}}\right] \tag{3.2}$$

3.2.6 - Gas Velocity

The correlation used in the numerical simulator for the gas velocity is also attributable to Adam T. Bourgoyne (Ohara, 1995), and has the form:

$$v_g = v_m + \left[v_s + \left(0.18 + 0.07\text{Ln}\mu_p\sqrt{\frac{(7.48\rho_m - \rho_g)}{7.48\rho_m}}\right)v_m\right]\text{Exp}\left[-0.03\left(0.3048v_m\right)^2\right] \tag{3.3}$$

3.2.4 - Gas Viscosity

The correlation chosen for the gas viscosity is the semiempirical method developed by Lee, Gonzalez, and Eakin (Craft and Hawkins, 1991). It has the form:

$$\mu_g = \frac{K \cdot \text{Exp}(X \cdot \rho_g^Y)}{10000} \tag{3.4}$$

where:

$$\rho_g = \left(\frac{1}{10.73 \times 62.4}\right)\frac{P \cdot M_w}{Z \cdot T} \tag{3.4a}$$

$$K = \frac{(9.4 + 0.02M_w)T^{1.5}}{(209 + 19M_w + T)} \tag{3.4b}$$

$$X = 3.5 + \frac{986}{T} + 0.01M_w \tag{3.4c}$$

$$Y = 2.4 - 0.2X \tag{3.4d}$$

3.2.8 - Single-Phase Friction Loss

The friction factor was estimated using the Colebrook and White's equation (Beggs, 1991, p. 61):

$$\sqrt{\frac{1}{f_{Fan}}} = 1.74 - 2\text{Log}\left(\frac{2\varepsilon}{d} + \frac{18.7}{N_{Re}\sqrt{f_{Fan}}}\right) \tag{3.5}$$

Since this is an implicit function, where the unknown term appears on both sides of the equation, it has to be solved iteratively. The first guessed value is provided by the Drew, Koo and McAdams equation (Beggs, 1991, p. 60):

$$f_{Fan} = 0.0056 + 0.5N_{Re}^{-0.32} \tag{3.6}$$

3.2.9 - Two-Phase Friction Loss

The frictional pressure gradient is determined using the Beggs and Brill's (1973) friction factor correlation, modified to account for the non-Newtonian characteristic of the mixture. The friction loss gradient, in psi/ft, is calculated with:

$$\left(\frac{\delta P}{\delta L}\right)_{frc} = \frac{f_{tp} \cdot \rho_m \cdot v_m^2}{64.4D_e} \tag{3.7}$$

The two-phase flow friction factor f_{tp} is given by:

$$f_{tp} = f_F \cdot e^s \tag{3.7a}$$

where the no-slip friction factor f_F is single-phase friction factor described above. The non-slip friction factor used by Beggs and Brill was for a smooth pipe curve on a Moody diagram. The exponent for the ratio of the two-phase slip to non-slip friction e^s is:

$$s = \frac{\mathrm{Ln}\frac{\lambda}{H^2}}{-0.0523 + 3.182\mathrm{Ln}\left(\frac{\lambda}{H^2}\right) - 0.8725\left[\mathrm{Ln}\left(\frac{\lambda}{H^2}\right)\right]^2 + 0.01853\left[\mathrm{Ln}\left(\frac{\lambda}{H^2}\right)\right]^4} \tag{3.7b}$$

where the no-slip liquid holdup λ is defined as:

$$\lambda = \frac{q_l}{q_l + q_g} \tag{3.7c}$$

if (λ/H^2) is greater than 1.2 or less than 1.0, then the exponent is calculated with:

$$s = \mathrm{Ln}\left(2.2\frac{\lambda}{H^2} - 1.2\right) \tag{3.7d}$$

the frictional term is determined by:

$$\left(\frac{\partial p}{\partial z}\right)_{fric} = \frac{f_{tp}\rho_{ns}v_m^2}{2g_c d} \tag{3.7e}$$

where the mixture velocity v_m is defined as:

$$v_m = v_l H + v_g(1 - H) \tag{3.7f}$$

and the two-phase no-slip density ρ_{ns} is given by:

$$\rho_{ns} = \rho_l\lambda + \rho_g(1 - \lambda) \tag{3.7g}$$

3.2.10 - Temperature Gradient

Another problem to simulate is the determination of the temperature gradient for the riser string and the external line, which will be immersed in sea water and exposed to the deep water temperature gradient. Figure 3.4 shows the temperature profile for the Gulf of Mexico deep waters (Lai et al, 1989), with the minimum and maximum temperature variations. For depths greater than 3,500 ft (1,067 m), the temperature is constant and around 40 °F. The model take an average temperature of these two profiles, in order to calculate the gas pressures along the injection line, as can be seen in the Figure 3.5.

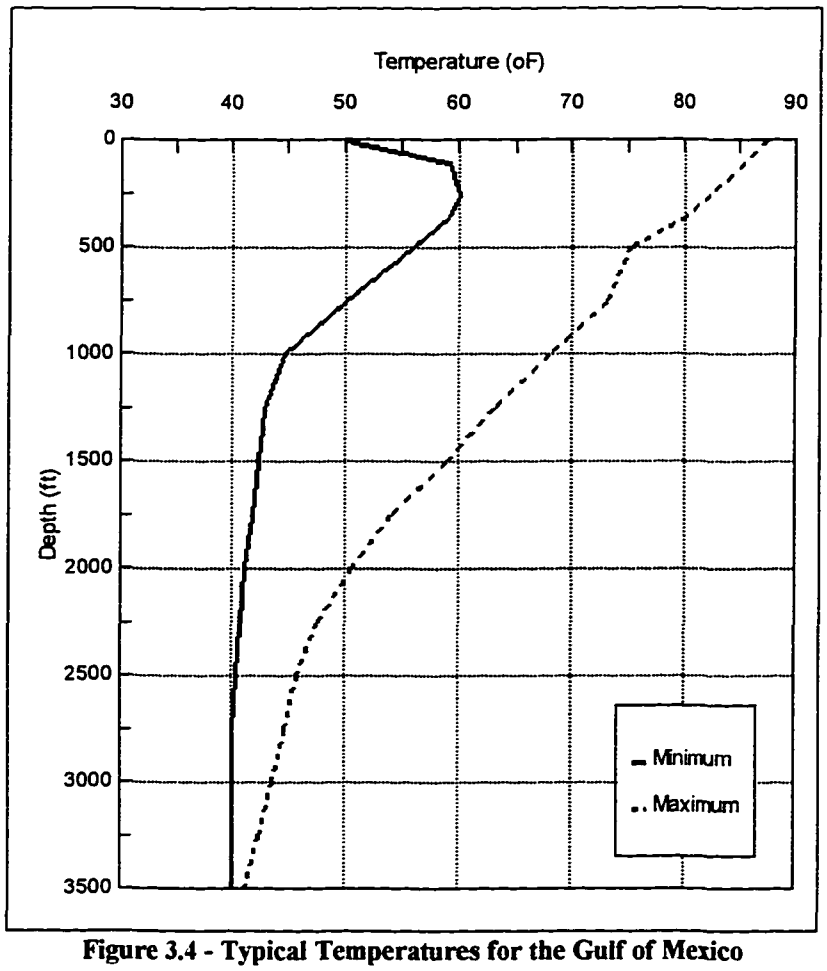

Figure 3.4 - Typical Temperatures for the Gulf of Mexico

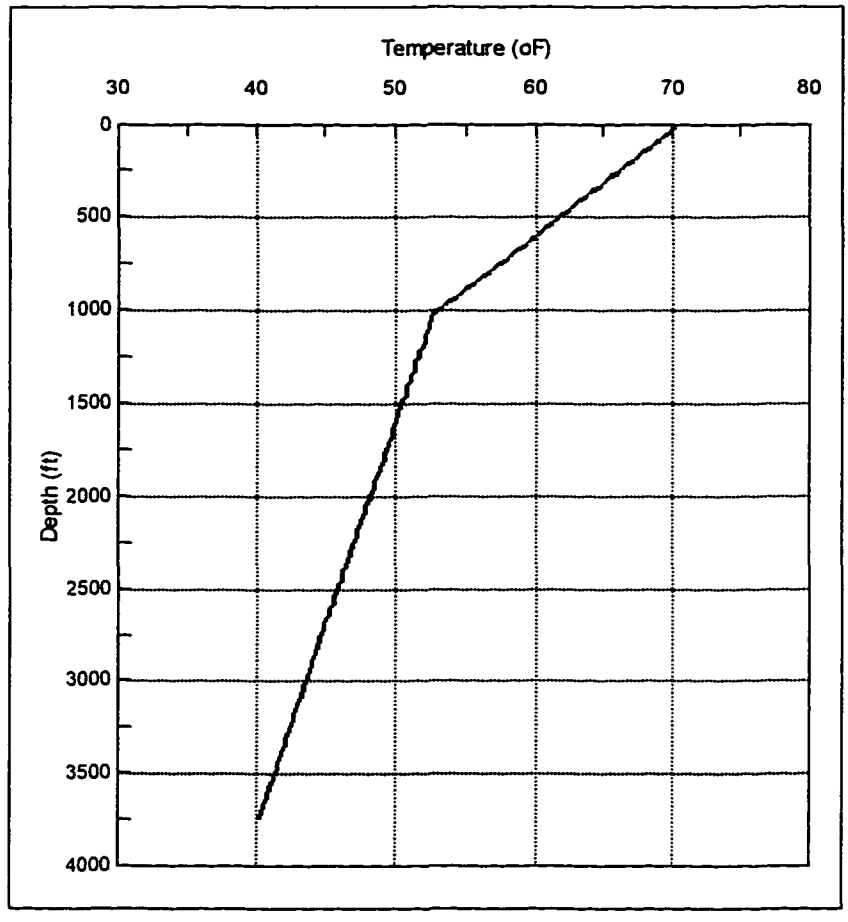

Figure 3.5 - Simulated Sea Temperature Profile

3.3 - UNSTEADY-STATE MODEL

The unsteady-state model was developed with the purpose of investigating the feasibility of a gas injection controller for the dual density riser system. This controller would use the model working under steady-state conditions. In case of a perturbation such a pump rate variation, it would adjust the gas injection rate to bring the bottom hole pressure to its previous stabilized value. One important parameter to be investigated with such a controller would be the response times required for any changes in the gas injection rate to affect the bottom hole pressure.

The two-phase flow inside the riser annulus is based on the model proposed by Nickens (1985). It was later developed by Santos (1989), to study the circulation of a

kick through a diverter, and modified by Ohara (1995), to develop a kick simulator for deep waters.

The mathematical model is based on six equations:

- The mass balance equation for liquid;
- The mass balance equation for gas;
- A momentum-balance equation for the two-phase flow of gas-mud;
- An equation of state for the liquid;
- An equation of state for the gas;
- A correlation relating the gas velocity to the average mixture velocity and the relative slip velocity between the two phases.

3.3.1 - Assumptions and Considerations

Before the development of the Unsteady-State Model the following assumptions and considerations were made:

1) The temperature is constant over the entire length of the riser and behaves linearly.
2) The pressure at the top of the riser is known.
3) The dimensions of the riser annulus and inner pipe are constant and known.
4) The liquid injection rate is known and constant.
5) The liquid phase is incompressible.
6) The gas injection rate is known and constant.
7) The gas injected is nitrogen or air. It is homogenous with a known composition and its solubility in the drilling fluid is negligible.

8) The fluid properties are known and constant over the entire system.

9) There are no restrictions that introduce pressure losses in the simulated system.

10) The gas is mixed in the liquid forming bubbles of same size and presents the same gas velocity profile throughout the riser annulus.

3.3.2 - Mass Balance Equations

The basis for these equations is the conservation principle. The liquid continuity equation, under unsteady two-phase flow conditions, is given by:

$$\frac{\partial Hl}{\partial t} + \frac{\partial (v_l \cdot Hl)}{\partial z} = 0 \qquad (3.8)$$

with the liquid holdup Hl defined as the ratio of liquid volume in an annular segment to the annular segment volume. The gas continuity equation is:

$$\frac{\partial \left[\rho_g (1 - Hl)\right]}{\partial t} + \frac{\partial \left[v_g \rho_g (1 - Hl)\right]}{\partial t} = 0 \qquad (3.9)$$

3.3.3 - Momentum Balance Equation

The momentum balance equation is based on Newton's second law of motion: the summation of all forces acting on a system is equal to the system's rate of change of momentum. Applying to two-phase flow the equation is:

$$\frac{\partial \left[v_l \rho_l Hl + \left(v_g \rho_g (1 - Hl)\right)\right]}{\partial t} + \frac{\partial \left[v_l^2 \rho_l Hl + \left(v_g^2 \rho_g (1 - Hl)\right)\right]}{\partial z}$$

$$+ \frac{\partial p}{\partial z} + \left(\frac{\partial p}{\partial z}\right)_{elev} + \left(\frac{\partial p}{\partial z}\right)_{fric} = 0 \qquad (3.10)$$

where $(\partial p/\partial z)$ is the pressure gradient, and the elevation, or hydrostatic pressure gradient is:

$$\left(\frac{\partial p}{\partial z}\right)_{elev} = \frac{g}{g_c}\left[\rho_l H l + \rho_g (1 - H l)\right] \tag{3.11}$$

3.3.4 - Equation of State

The equations of state for the liquid and gas are the corresponding equations for their densities. Since only water-based type of fluids are used offshore, due to the increasingly stringent environmental regulations, the liquid density can be considered incompressible. So the equation of state for the mud is:

$$\rho_L = \text{constant} \tag{3.12}$$

and the equation of state for real gases is used for the injected air:

$$\rho_g = \frac{pM}{zRT} \tag{3.13}$$

3.3.5 - Solution of the Differential Equations

A numerical method has to be used in the simulator to solve the differential equations in the previous section. The technique of finite differences used by Santos and Ohara, is called centered in distance and backward in time with a fixed space grid. The annular space is divided in a finite number of cells and the calculations begin in the bottom, continuing, cell by cell, to the top. Figure 3.6 shows a generic cell in two subsequent time steps.

The formulation of the continuity equation for the finite difference technique in the space derivative is given by:

$$\frac{\partial U}{\partial z} = \frac{U_4 - U_3}{\Delta z} \tag{3.14}$$

and the time derivative is given by:

$$\frac{\partial U}{\partial t} = \frac{U_6 - U_5}{\Delta t} = \frac{U_4 + U_3 - U_2 - U_1}{2\Delta t} \qquad (3.15)$$

where U is a function of z and t. By substituting these approximations into Equations (3.8) and (3.9), the finite difference formulation for liquid becomes:

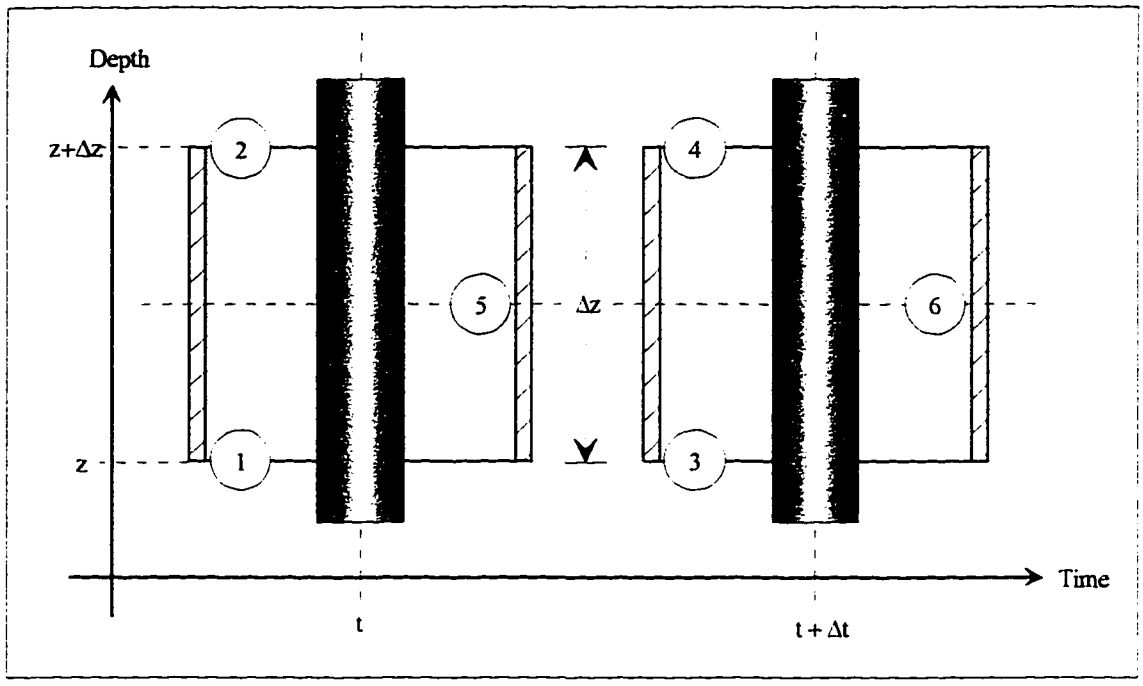

Figure 3.6 - Finite Difference Mesh

$$\frac{(v_l\rho_l Hl)_4 - (v_l\rho_l Hl)_3}{\Delta z} + \frac{(\rho_l Hl)_4 + (\rho_l Hl)_3 - (\rho_l Hl)_2 - (\rho_l Hl)_1}{2\Delta t} = 0 \qquad (3.16)$$

and for gas:

$$\frac{\left[v_g\rho_g(1-Hl)\right]_4 - \left[v_g\rho_g(1-Hl)\right]_3}{\Delta z}$$

$$+ \frac{\left[v_g\rho_g(1-Hl)\right]_4 + \left[v_g\rho_g(1-Hl)\right]_3 - \left[v_g\rho_g(1-Hl)\right]_2 - \left[v_g\rho_g(1-Hl)\right]_1}{2\Delta t} = 0 \ldots$$

..... (3.17)

The time derivative in the finite difference formulation for the momentum balance equation is the same as in Equation (3.15), but the space derivative is given by:

$$\frac{\partial U}{\partial z} = \frac{U_4 + U_2 - U_3 - U_1}{2\Delta z} \tag{3.18}$$

and by substituting Equation (3.18) into Equation (3.10), we obtain:

$$\frac{1}{2\Delta z}\left\{\left[v_g^2\rho_g(1-Hl)\right]_4 + \left[v_g^2\rho_g(1-Hl)\right]_2 - \left[v_g^2\rho_g(1-Hl)\right]_3 - \left[v_g^2\rho_g(1-Hl)\right]_1 + \right.$$

$$\left. + (v_l^2\rho_l Hl)_4 + (v_l^2\rho_l Hl)_2 - (v_l^2\rho_l Hl)_3 - (v_l^2\rho_l Hl)_1\right\} + \frac{1}{2\Delta t}\left\{\left[v_g\rho_g(1-Hl)\right]_4 + \right.$$

$$\left. + \left[v_g\rho_g(1-Hl)\right]_3 - \left[v_g\rho_g(1-Hl)\right]_2 - \left[v_g\rho_g(1-Hl)\right]_1 + (v_l\rho_l Hl)_4 + (v_l\rho_l Hl)_3 - \right.$$

$$\left. - (v_l\rho_l Hl)_2 - (v_l\rho_l Hl)_1\right\} - \frac{p_3 - p_4}{\Delta z} + \frac{1}{4}\left[\left(\frac{\Delta p}{\Delta z}\right)_1 + \left(\frac{\Delta p}{\Delta z}\right)_2 + \left(\frac{\Delta p}{\Delta z}\right)_3 + \left(\frac{\Delta p}{\Delta z}\right)_4\right]_{fric} -$$

$$-\left[\left(\frac{\Delta p}{\Delta z}\right)_1 + \left(\frac{\Delta p}{\Delta z}\right)_2 + \left(\frac{\Delta p}{\Delta z}\right)_3 + \left(\frac{\Delta p}{\Delta z}\right)_4\right]_{elev} = 0 \tag{3.19}$$

The flow properties for point 4 in Figure 3.3 are obtained from the values at points 1, 2, and 3, through an iterative process. The flow properties at points 1 and 2 are one time step behind the ones at points 3 and 4. The points 5 and 6 represent the average values between the top and bottom of the cell, for one time step and its successor, respectively.

3.3.6 - Algorithm Direction and Time Steps

Figure 3.7 shows the algorithm's direction of flow and its time steps. The only point where all the flow variables are known is the top of the riser. Thus, at the first step the algorithm calculates the pressure losses, and the elevation term, due to the liquid phase, all the way down to the bottom cell.

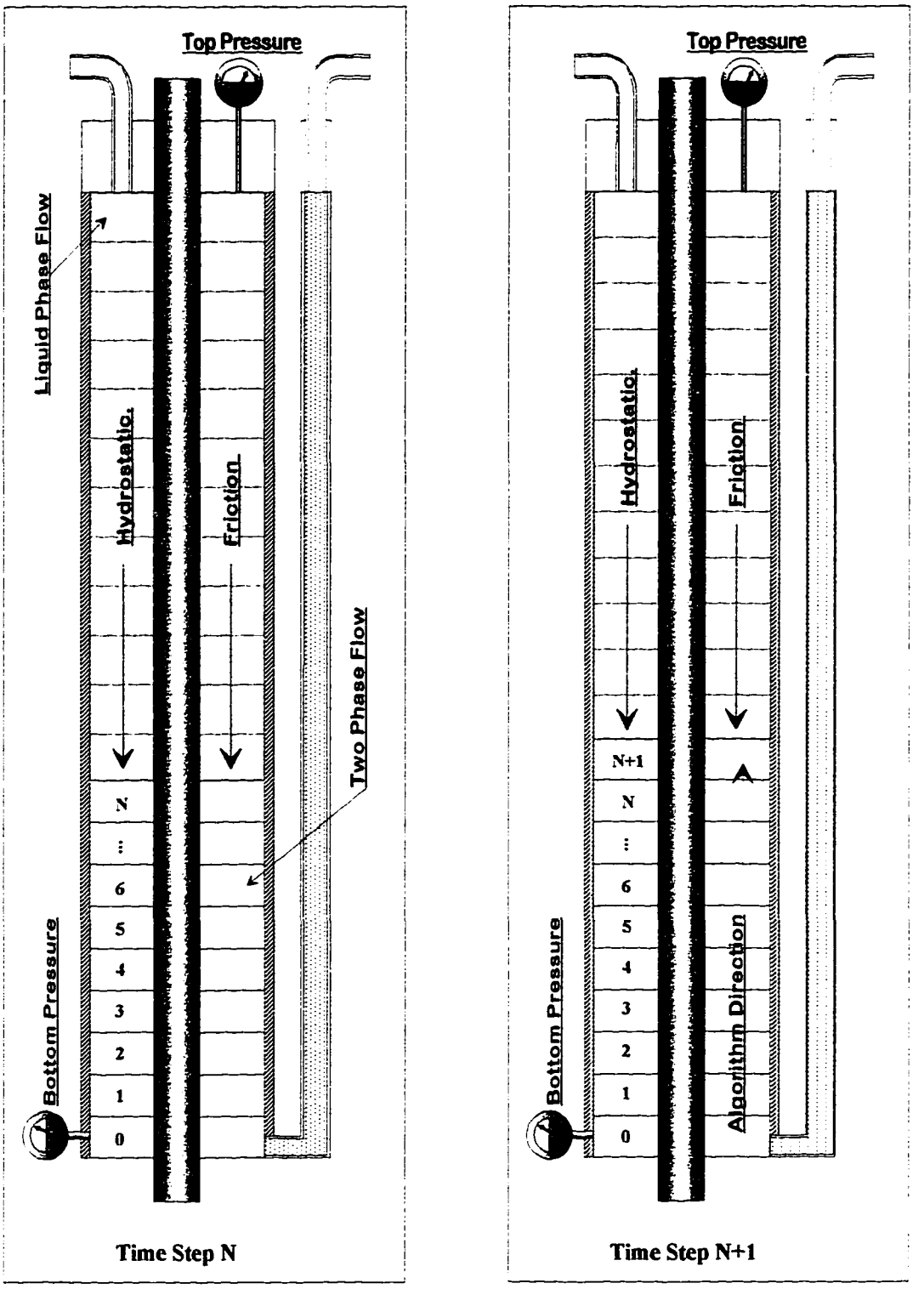

Figure 3.7 - Unsteady-State Time Steps and Algorithm Direction

Next, it determines the properties for this cell's bottom. After that, the algorithm needs to calculate the flow variables for the top of the first cell, that is already in two-phase flow.

The only known variables are the ones at the bottom of the first cell, in the previous time step, and the ones at the top of the last cell. The procedure restarts from the riser top and recalculates the pressures down to the top of the first cell. This pressure is the comparison pressure. Next, the algorithm iteratively computes the first cell's top pressure until it gets a value sufficiently close to the comparison pressure.

After this, the algorithm advances to the next cell, and to the next time step. It assigns all the flow variables to the previous instant and makes the properties of the bottom of the next cell equal to the ones calculated for the top of the last one.

3.3.7 - Algorithm Flow

Figure 3.8 shows the general unsteady-state algorithm flowchart. There is a Time Loop and a Cell Loop. Starting at time zero and cell zero, the first task is to calculate the comparison pressure at the two-phase leading edge. Since the boundary condition is the top riser pressure, the algorithm has to compute the hydrostatic pressure and the frictional loss for the liquid phase. These are inside the riser annulus, from the top riser cell down to the top cell of the two-phase flow.

Next, the procedure uses a root finding technique, the Van Wijngaarden-Dekker-Brent method (Numerical Recipes, p. 251, 1986), or Brent method. This algorithm is used to find a pressure value that closely matches the comparison pressure, by guessing the bottom riser pressure. This method uses a combination of root bracketing, bisection, and inverse quadratic interpolation to converge.

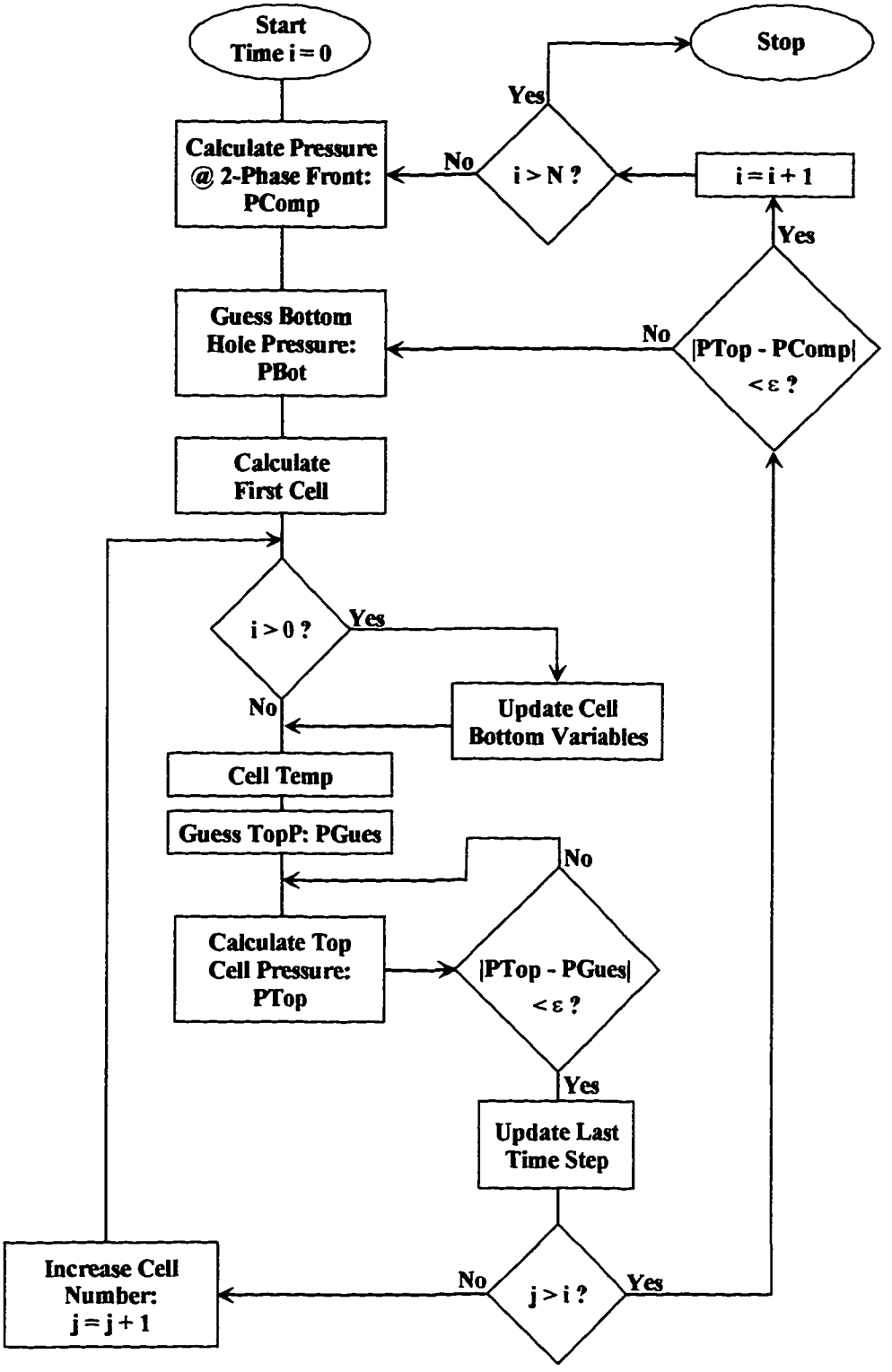

Figure 3.8 - Unsteady-State General Flowchart

The process involves a first guess for the bottom riser pressure, based on the last time step value. With this, it calculates the flow variables for the first cell, at the bottom.

Except for the first cell, the algorithm updates the cell bottom variables as soon as it computes the values for the bottom of the first cell. In this update, it assigns the values found for the top of the precedent cell to the following bottom cell variables, since they are in the same spatial position.

The cell's temperature is calculated next, before going on to the Top Cell Loop. There it has to guess the pressure at the top of the cell and iterate, to converge to its value.

Figure 3.9 shows in more detail the flowchart for the Top Cell Loop. Here, after guessing the top cell pressure, based on the last time step, the algorithm does the following:

1. Calculates the Gas Compressibility Factor at the cell top (ZTop), using the same correlation described for the Steady-State Model;
2. Computes the Gas Density at the top (DgTop), using equation (3.13);
3. Determine the Superficial Gas Velocity (VsgTop);
4. With the previously computed Superficial Liquid Velocity, the algorithm finds the Mixture Velocity (VmTop);
5. Next, the Slip Velocity (VsTop) is calculated using the same correlation employed in the Steady-State Model;
6. Computes the Gas Velocity at the cell top (VgTop), also using the previously described correlation from the Steady-State Model;

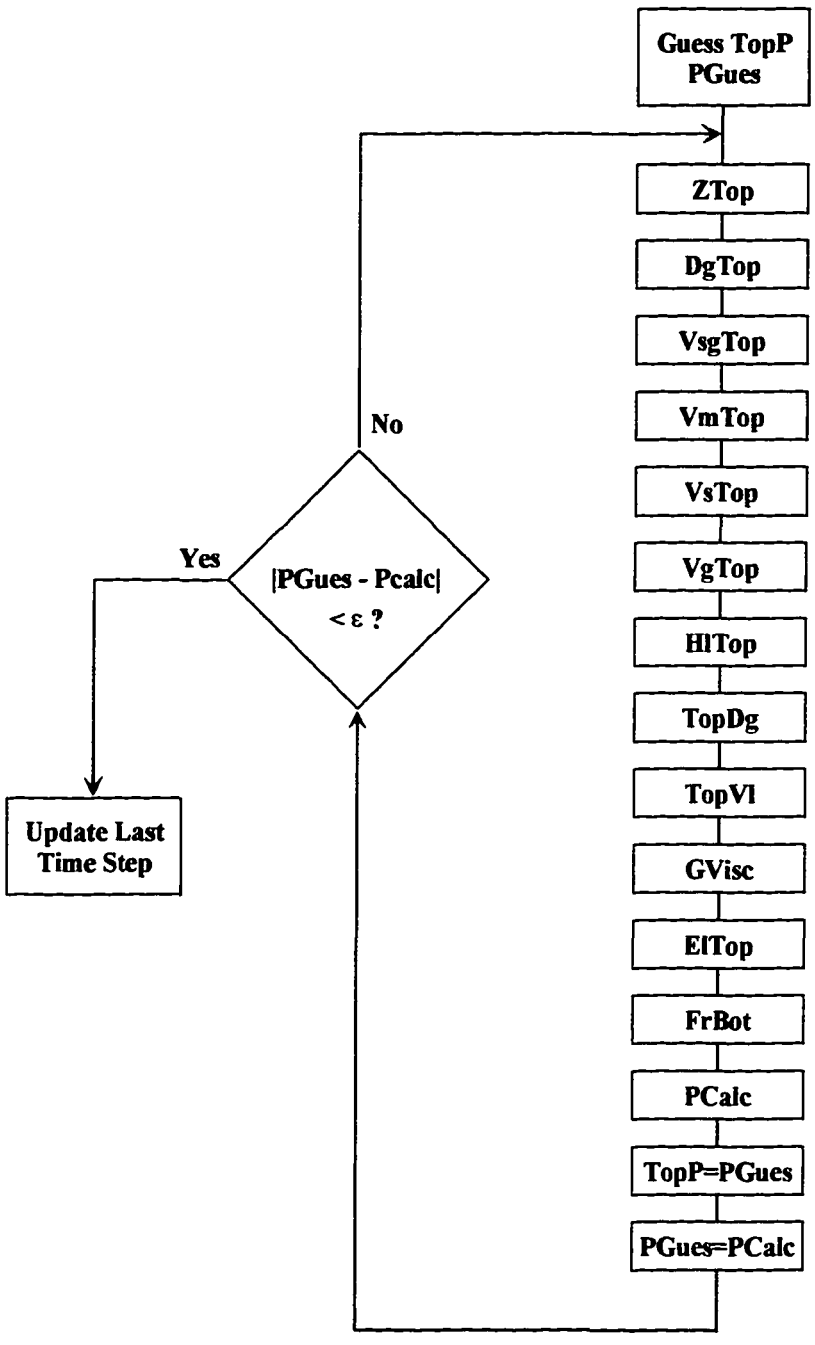

Figure 3.9 - Unsteady-State Top Cell Pressure Loop

7. Determines the Liquid Holdup (HlTop);
8. Calculates the Gas Density at the top of the cell (TopDg) using equation (3.17);
9. Computes the Liquid Velocity (TopVl) using equation (3.16);
10. After, the Gas Viscosity (GVisc) is obtained with the same correlation used in the Steady-State Model;
11. The Mixture Density (ElTop) is next determined using equation (3.11);
12. The Frictional Pressure Loss at the top of the cell (FrTop) is calculated using the same method described for the Steady-State Model;
13. The value for the previous guess is saved into a temporary variable (TopP), and the calculated value becomes the next guess;

The absolute values of the calculated and the guessed pressures are compared, and if they are bigger than a specified small difference, the loop cycles again. If not, the loop ends.

Once the convergence is attained, the algorithm updates the memory set holding the Last Time Step variables. It does this by assigning the values of the flow variables for the present time step to the previous one.

CHAPTER IV

EXPERIMENTAL PROGRAM

The experimental program had the primary objective of acquiring data to calibrate and validate the computer simulator program for the dual density riser system. The experimental procedure for obtaining the data is presented here. The experiments were done using a full scale well and nitrogen gas, from a cryogenic tank. Although the original plan foreseen 6 experiments, only 2 were carried out, due to funding delays. From these two, one was a partial failure, since the steady-state flow was not achieved.

4.1 - DESCRIPTION OF THE TEST WELL

Figure 4.1 shows the LSU well No. 2, which was used for the experiments planned. It is located at the Blowout Prevention Research Well Facility in Baton Rouge, Louisiana. This is a vertical well with 5,884 ft (1,793 m) of depth and 9 5/8". OD (244 mm) casing. Its completion includes a 1¼" (32 mm) gas injection line that runs inside a 3½" (89 mm) drilling fluid injection line. Apart from those, a 23/8" (60 mm) perforated tubing runs outside the mud injection line. This tubing can be used for lowering logging tools in the well, without the risk of getting the logging cable tangled around the 3½" string. Some care must be taken, though, in not running past the bottom, at 5816 ft, since there is no stopper.

Table 4.1 compiles the information on the tubulars used in the completion of the LSU number 2 well. It shows that the logging tubing has 94 holes, of 0.5" of diameter, per joint.

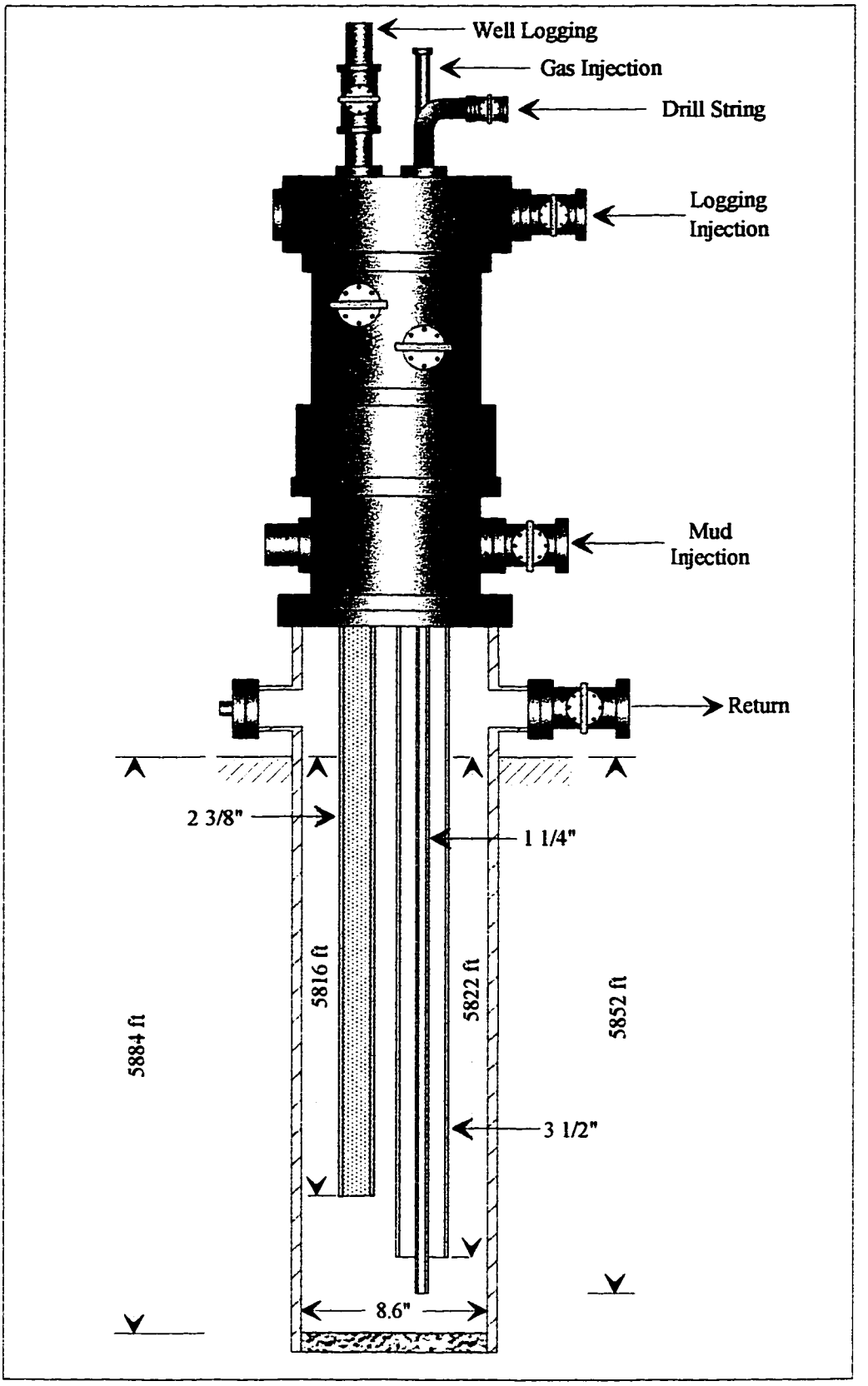

Figure 4.1 - LSU Number 2 Well

Table 4.1 - LSU No. 2 Well Tubulars

OD (inches)	ID (inches)	Depth (ft)	Weight (lb/ft)	Characteristics
9 5/8	8.535	0 - 3170	53.5	
9 5/8	8.681	3170 - 3908	47	
9 5/8	8.756	3908 - 5553	43.5	
9 5/8	8.535	5553 - 5876	53.5	
9 5/8	8.681	5876 - 5884	47	
3 ½	2.992	0 - 5822	9.3	J55, EUE
2 3/8	1.996	0 - 5822	4.7	94x0.5 holes/jt
1.66	1.279	0 - 5852	3.02	N80

4.2 - EXPERIMENTS METHODOLOGY

The drilling fluid used in the experiments was planned to be representative of the average type of mud used in Campos Basin, Brazil, in deep waters, with a fluid composition as shown in Table 4.2. But problems in the project's funding prevented it. Instead, the mud used was a simple mixture of water and bentonite, with the addition of caustic, to prevent equipment corrosion.

Nitrogen was injected from cryogenic tanks, with special triplex pumps mounted on trucks. The reasons for the use of nitrogen were:

- To avoid the corrosion associated with the use of compressed air;
- To avoid the high costs of renting high capacity compressors;
- The higher level of safety derived from working with an inert gas.

Working with a spreadsheet application, and applying the mass balance equations only, the first estimate for the maximum flow rates of mud and nitrogen will be 300 gpm and 2200 SCF/min, respectively. The mud flow rates are limited by the pumps capacity.

Table 4.2 - Typical Drilling Fluid Composition

Material	Unit	Amount
Activated Clay	lbm/bbl	4.0
Caustic	lbm/bbl	0.3
Polyacrilamide Partially Hydrolyzed	lbm/bbl	1.0
CMC AV-AS	lbm/bbl	0.3
CMC BV-AS	lbm/bbl	0.6
Potassium Chlorine	lbm/bbl	11.5
Barite	lbm/bbl	As Needed

The nitrogen was injected through the 1 ¼" (32 mm) tubing, while the drilling fluid was circulated through the annular space among the 3 ½" (89 mm) and 1 ¼" (32 mm) tubing strings. Returns were taken from the 9 5/8" (244 mm) casing.

Pressures on the drill pipe, casing and injection lines were monitored with instrumentation at surface. The down-hole pressure sensors were, in the first experiment, equally spaced along the well depth, to get data on the pressure losses in the annulus. In the other tests, it was deemed safer to run the pressure recorders in tandem, hanging from the bottom of the on-line pressure sensor. The safety considerations were:

- The essential information was the bottom pressure;
- The data quality from the pressure recorders was far superior than the data acquired by the on-line pressure sensor;
- There was a possibility of failure of one of the pressure recorders or the on-line tool itself.

The down-hole pressure sensors were run in a logging cable, with the top one collecting data on-line, while the others recorded their respective sets of data internally, to be retrieved at surface, after each run. The hydrostatic pressure values, registered

during the sensors descent and retrieval worked as a signature, that was used to synchronize all the sensors to a common time.

A data acquisition hardware from National Instruments was used to acquire and store all the information collected by the surface and down-hole sensors. This system is composed of:

- A channel multiplexer module, to sample and condition the volt sources for the control module;
- A control module for acquiring and digitizing the conditioned analog signals. It also relays the data to a receiving computer;
- A digital-to-analog converter module;
- A digital output module.

Along with it, a data acquisition and recording software, developed with the LabView for Windows application, provided an interface for monitoring the following data:

- Fluid pressure (psi);
- Gas injection pressure (psi);
- Bottom annular pressure (psi), from the down-hole pressure sensor;
- Pump speed (spm);
- Choke pressure (psi);
- Gas injection flow, (MSCF/hour).

Gas injection rates were registered using the Daniel model 2500 flow computer. This system acquires signals from different sensors and uses the information to calculate

a precise flow rate. The sensors collect data on differential pressure through an orifice, absolute pressure, and temperature.

Pressure and temperature recorders were also used to gather data. Three model EMR710 recorders were used from Geophysics Research Corporation (GRC). This model can acquire and store 21,000 pressure and temperature readings. It is programmable and stores the data in memory chips, for later recovery at surface. To maintain the stored information, it relies on batteries. An especial interface is used to transfer the data from the tools to a dedicated computer.

4.3 - TEST MATRIX

As can be seen on Table 4.3, there were six experiments scheduled, initially. The choices for the drilling fluid densities, 9.8 and 12.0 ppg, were based on the average mud weight used in Campos Basin, and in a theoretical maximum for the same basin, respectively. The first experiment was used as a knowledge base for the others, and the collected data was used to calibrate and reevaluate the parameters to be used in the following runs. A priori, the liquid flow rates were chosen as 0, 100 and 200 gal/min. The first choice was meant to give information about the gas rising velocity, and how

Table 4.3 - Test Matrix

Experiment Number	Mud Flow Rate (gal/min)			Mud Density (lbm/gal)	
	0	100	200	9.8	12
1	✔			✔	
2	✔				✔
3		✔		✔	
4		✔			✔
5			✔	✔	
6			✔		✔

well it would correlate with the mathematical model chosen for the computer simulator. It would also establish the feasibility of obtaining the desired mixture average density only with the nitrogen injection. The other mud flow rate choices were based on the pumps available capacity.

CHAPTER V

EXPERIMENTAL RESULTS

This chapter discusses the experimental work done and its results. It details the experiment procedures and presents the collected data in graphical form as functions of time. Simulation results are also included, comparing with the observed data.

5.1 - INTRODUCTION

Only two out of six planned experiments were carried out. Although the first test has being carefully prepared, a series of equipment failures and the lack of experience hampered it from the beginning. This prevented reaching the two-phase flow steady-state needed for a full comparison with the simulation results. The second experiment was a re-run of the first and was completed as scheduled, with its results giving insight on the data collected in the previous test.

5.2 - FIRST EXPERIMENT

5.2.1 - Operations and Incidents

Figure 5.1 shows the overall view of the first test. The boxed numbers on the graph point to operations and events that occurred during the experiment:

1) Running in the two bottom hole recorders by wire-line;
2) Running in the middle pressure and temperature recorder, after connecting it to the wire-line;
3) Connecting and running in the on-line pressure sensor using the logging cable;
4) Start of gas injection for the test;
5) Reducing the pump rate from 250 gpm to 225 gpm in order to reach a bigger decrease in bottom hole pressure;

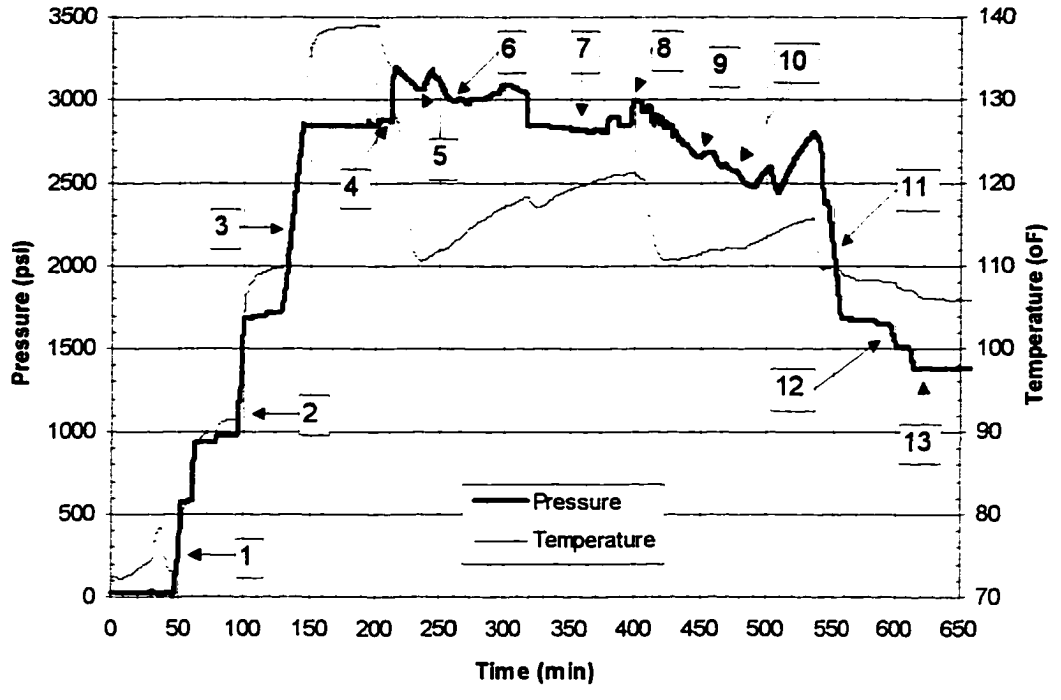

Figure 5.1 - Bottom Pressure and Temperature (at 5,800 ft) for Test 1

6) End of gas injection due to a severe leak in the stuffing box that sealed around the logging cable, circulating the gas out to work on the stuffing box;

7) Failed attempt to fix leaking stuffing box with no pumps;

8) Re-starting the gas injection;

9) Gas leading front reaching surface;

10) End of gas injection when the pumping unit ran out of nitrogen, starting to circulate gas out of the well;

11) Pulling the logging cable out of the hole;

12) Pulling the wire-line. The wire-line unit failed. Trying to pull the remaining wire with a tractor and giving it up;

13) Waiting for wire-line unit repairs.

5.2.2 - Bottom Hole Temperature

The maximum bottom hole temperature recorded was 139 °F, at 5800 ft, 51 minutes after reaching bottom. This agrees with the data collected in the second test. After gas and mud injection started, the temperature varied among 110-120 °F, staying around 112 °F during the second gas injection attempt.

5.2.3 - Mud Properties

The mud properties for the first experiment are summarized in Table 5.1. The mud weight was calculated based on the hydrostatic pressure measured when the bottom sensor reached its depth. The viscometer readings for 300 rpm and 600 rpm were taken before the run, from tank samples, showing very low viscosity values.

Table 5.1 - Mud Parameters for Test 1

Mud Properties				
Mud Weight	θ_{300}	θ_{600}	Plastic Viscosity	Yield Point
(ppg)	(d'less)	(d'less)	(cp)	(lbf/100 sqft)
9.37	10.5	16.5	6.5	4

5.2.4 - Bottom Hole Pressure

Figure 5.2 shows a detailed view of the second gas injection attempt in the first experiment. The mud pumps presented some speed fluctuations during the unload phase, without determined cause. The gas reached surface after approximately 49 minutes after the gas injection started.

The total increase in bottom hole pressure due to the choke was about 32 psi. Nitrogen injection lasted for about 73 minutes, and during this time the stuffing box kept leaking at surface.

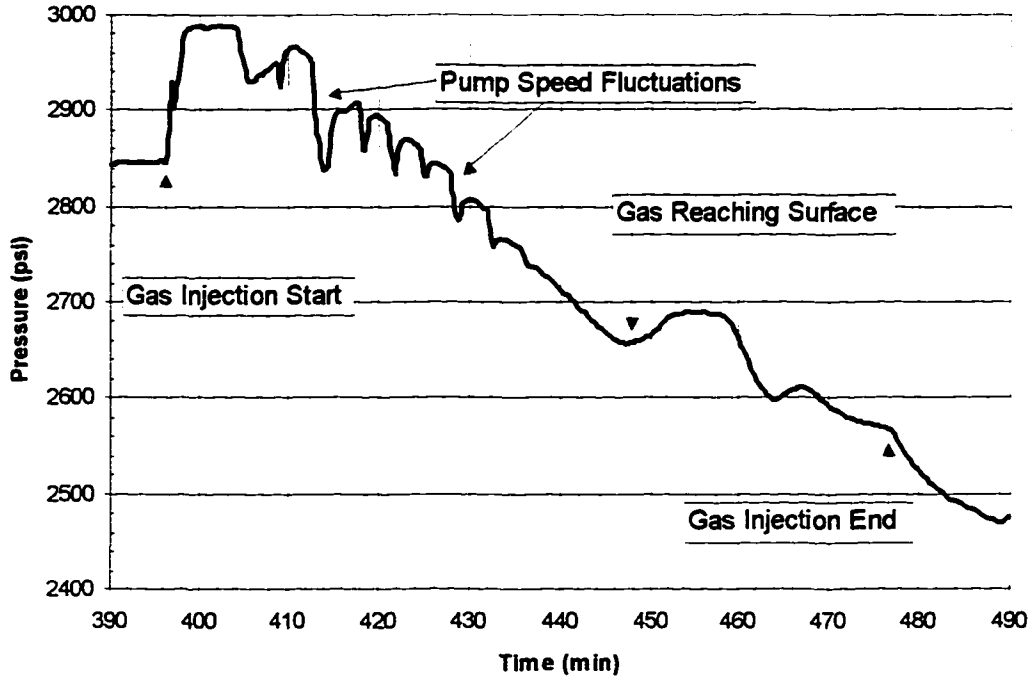

Figure 5.2 - Detailed View of Second Gas Injection of Test 1

5.2.5 - Nitrogen Injection Rate

Figure 5.3 shows the gas injection rates observed during the experiment. It was not possible to obtain a constant rate from the pumping unit and, during the attempt to fix the stuffing box, the operator kept the gas flowing to maintain the temperature in the burner. This resulted in a shortage of available nitrogen for the next attempt to perform the experiment. The observed gas injection rate during the last test attempt was around 1,120 SCF/min.

5.2.6 - Choke Pressure

The choke pressure readings for the entire experiment are presented in Figure 5.4. There is an initial peak, after the gas reached surface, when the two-phase mixture was flowing through one choke valve only at its fully open position. To lower down the top pressure, another choke valve was open.

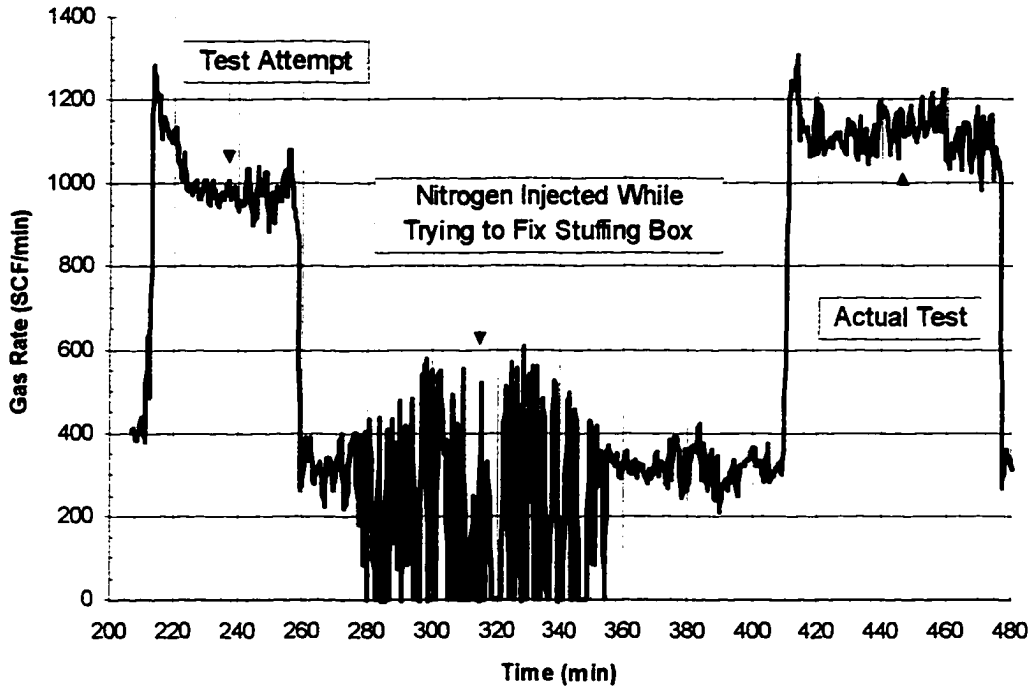

Figure 5.3 - Gas Injection Rates for Test 1

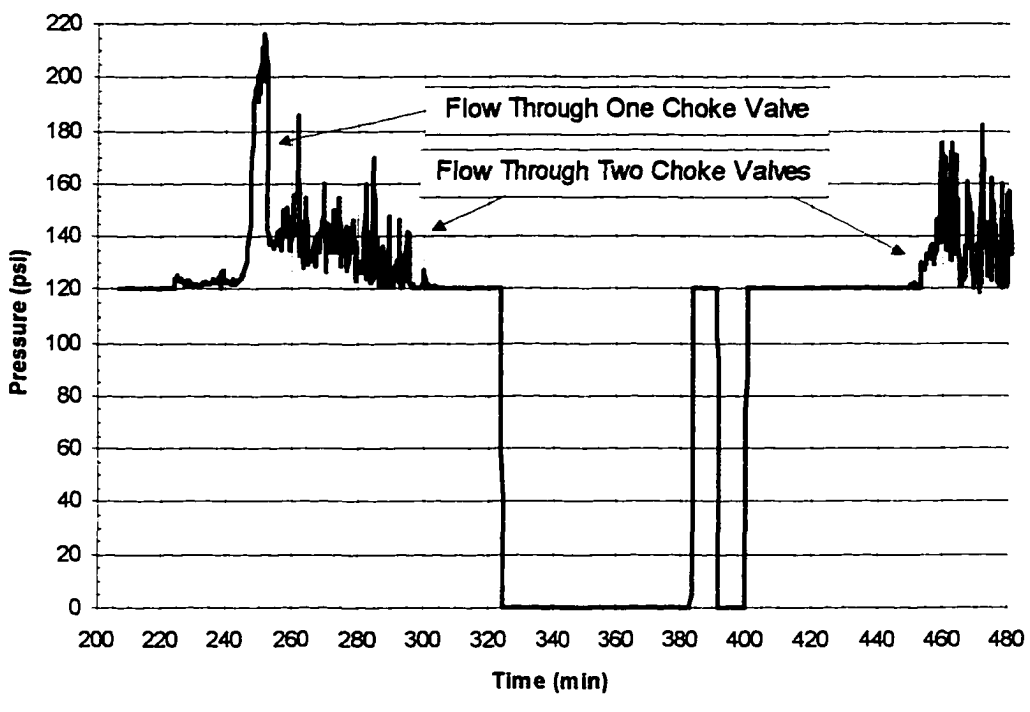

Figure 5.4 - Choke Pressure Readings During Test 1

These choke valves worked in their full open position during the entire test. The average value for the choke pressure after the gas reached surface in the last attempt was 141 psi.

5.2.7 - Mud Injection Rate

Figure 5.5 presents the observed liquid rates during the first experiment. The pump rate was initially set to 250 gpm. Later, since the maximum gas injection rate was around 1,200 SCF/min, the rate was reduced to 225 gpm, to provide a bigger decrease in the bottom-hole pressure. In the second test attempt, it was further reduced from 200 gpm to 150 gpm, before the starting the gas injection. During the attempt to fix the leaking stuffing box, the pumps were run at 100 gpm to test the seals, with no success.

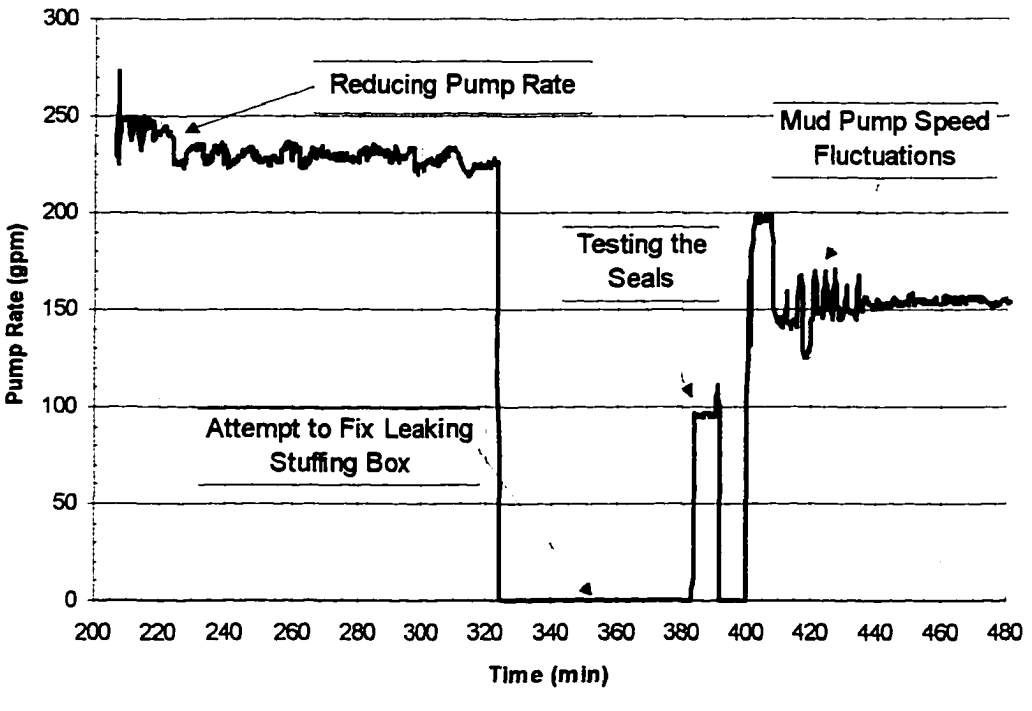

Figure 5.5 - Liquid Injection Rates Observed During Test 1

5.2.8 - Middle Tool Readings

The pressure behavior at the depth of 3,910 ft, where the third was set, can be seen in Figure 5.6. It is significant to point out that the temperature recorded for that depth was 112 °F. With the bottom hole temperature estimated in 138 °F, from the other recorders, the calculated gradient is 0.0137 °F/ft. Thus, starting with a surface temperature of 70 °F, the extrapolated bottom hole temperature should be around 149 °F, which agrees reasonably with the measurements.

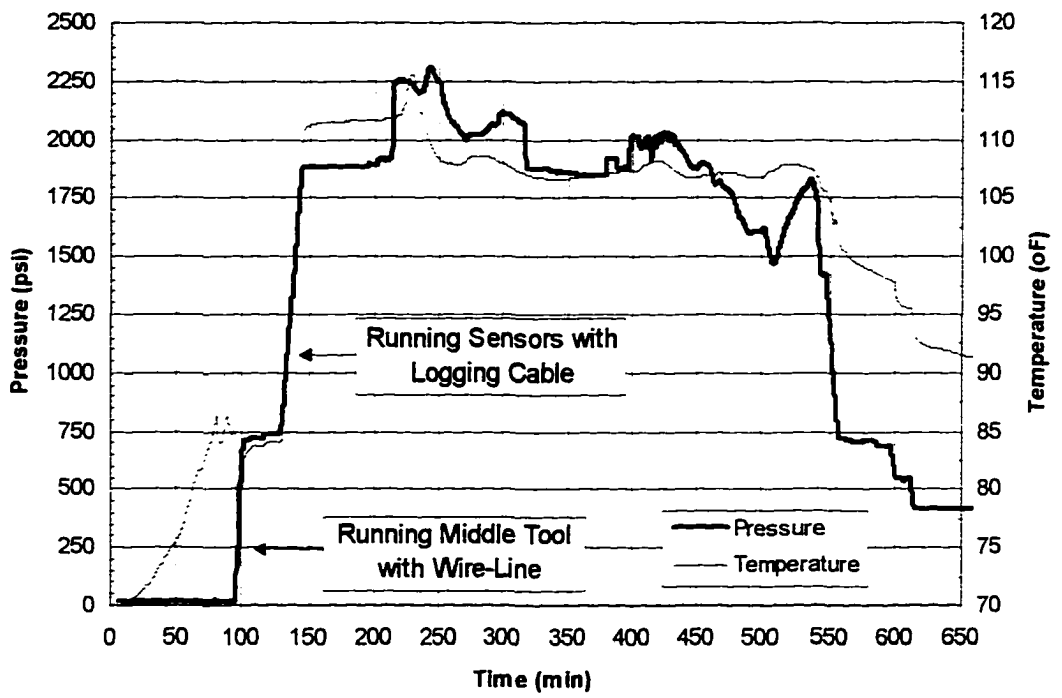

Figure 5.6- Pressure and Temperature Readings at 3,910 ft During Test 1

5.2.9 - Top Pressure Sensor

Figure 5.7 shows the data collected by the on-line pressure tool, at a depth of 2,380 ft. To get a better understanding of how fast the pressure drop propagates through the wellbore, the pressure data from sensors in three well depths were analyzed.

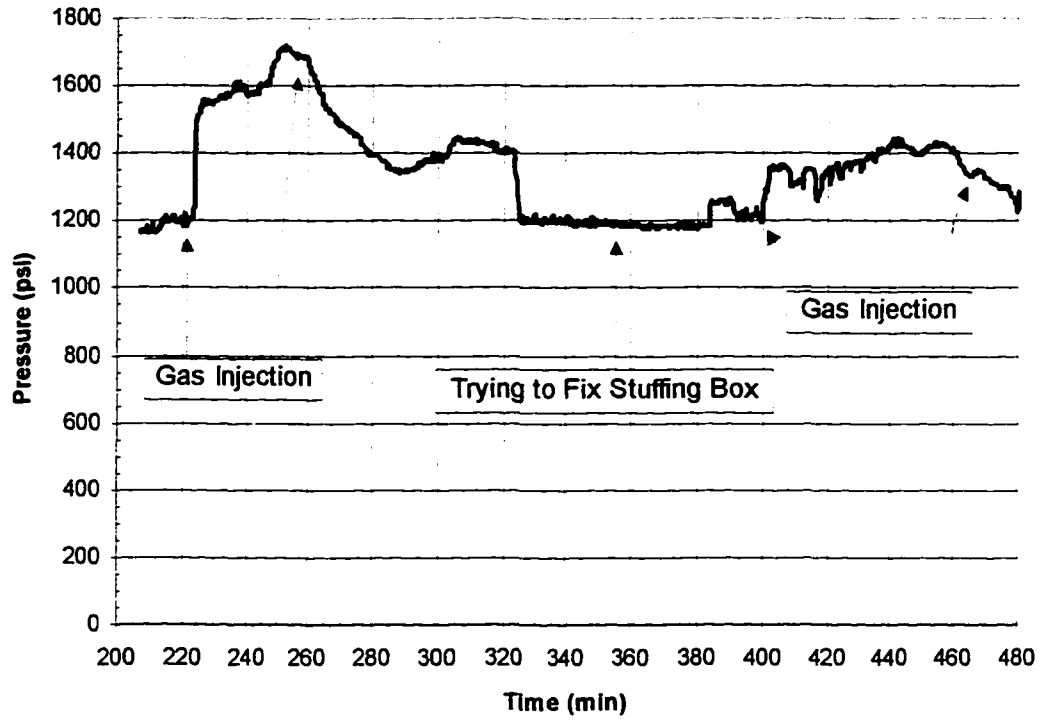

Figure 5.7 - Pressure Readings at 2,380 ft During Test 1

As the gas mass is rising, before the two-phase front reaches a sensor, the recorded pressure is due to the hydrostatic and the frictional losses, which are dependent on the mixture velocity. So, as the two-phase front approaches the sensor depth, the increased annular flow velocity generates a friction loss increase above the sensor and the recorded pressure should increase accordingly. But, when the front passes the sensor this pressure tends to decrease due to the smaller hydrostatic pressure above it.

Figure 5.8 shows the pressures recorded at 5,800 ft, 3890 ft, and at 2380 ft, in order from the top of the graph. The pressure starts to decrease at the 404 minutes mark for the bottom sensor, at 427.5 minutes for the middle sensor, and at 441.5 minutes for the top one. Thus, the average mixture velocity between the bottom-middle recorder pair is 1.35 ft/sec and it is 1.80 ft/sec for the middle-top pair of sensors. In comparison, the simulator run estimated 1.48 ft/sec for the mixture velocity at 3890 ft, and 1.86 ft/sec at

2380 ft. The average mixture velocity was 1.42 ft/sec for the 5,800-3,890 ft range, and of 1.71 ft/sec for the mixture velocity inside the 3890-2380 ft range.

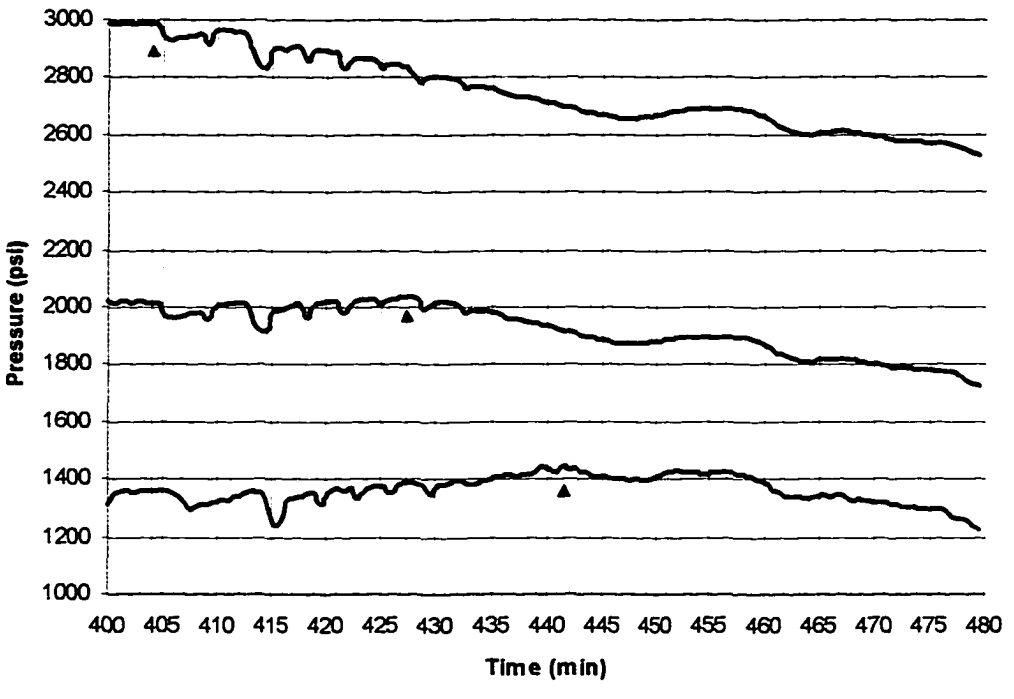

Figure 5.8 - Bottom, Middle, and Top Pressure Readings During Test 1

5.2.10 - Simulation Results

The first experiment did not reach the two-phase flow steady-state, and there is no data for a positive comparison with the steady-state simulation results, which were obtained using the input data compiled in Table 5.2.

Table 5.2 - Input Data for the Steady-State Simulation of Test 1

Simulator Input Data					
Casing ID	8.287	in	Choke Pressure	141	psi
Total Depth	5800	ft	Surface Temperature	75	Of
Injection Line ID	1.25	in	Bottom Temperature	112	oF
Pipe OD	3.5	in	Mud Density	9.37	ppg
Gas Rate	1,120	SCF/min	Plastic Viscosity	6	cp
Mud Rate	152	gpm	Yield Point	4	lbf/100sqft

The simulation pressure graph is presented in Figure 5.9. The final bottom hole pressure estimated by the simulator is 2,385 psia, or 2,400 psig, while the experiment ended while the pressure was still at 2,566 psig.

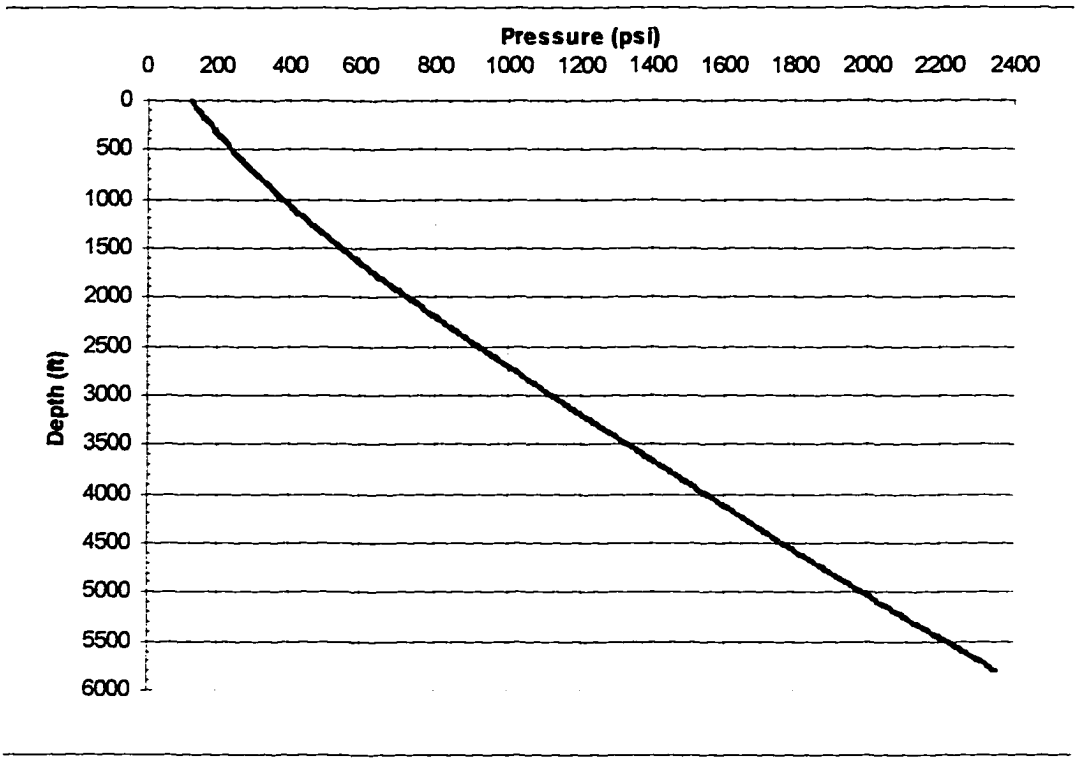

Figure 5.9 - Steady-State Flow Simulation for Test 1

An unsteady-state simulation run was performed, reading in the recorded values for choke pressures, nitrogen injection rates, and mud injection rates. The results can be seen in Figure 5.10, where the approximate time for the gas leading edge to reach surface is estimated in 35 minutes. The observed time for the leading gas front to surface was around 42 minutes, showing a reasonable agreement between simulation and test results. The simulated unsteady-state pressure behavior, however, did not significantly match the observed data from the first experiment. This is probably due to the assumption, in the simulator mathematical model, that the gas would rise with only one

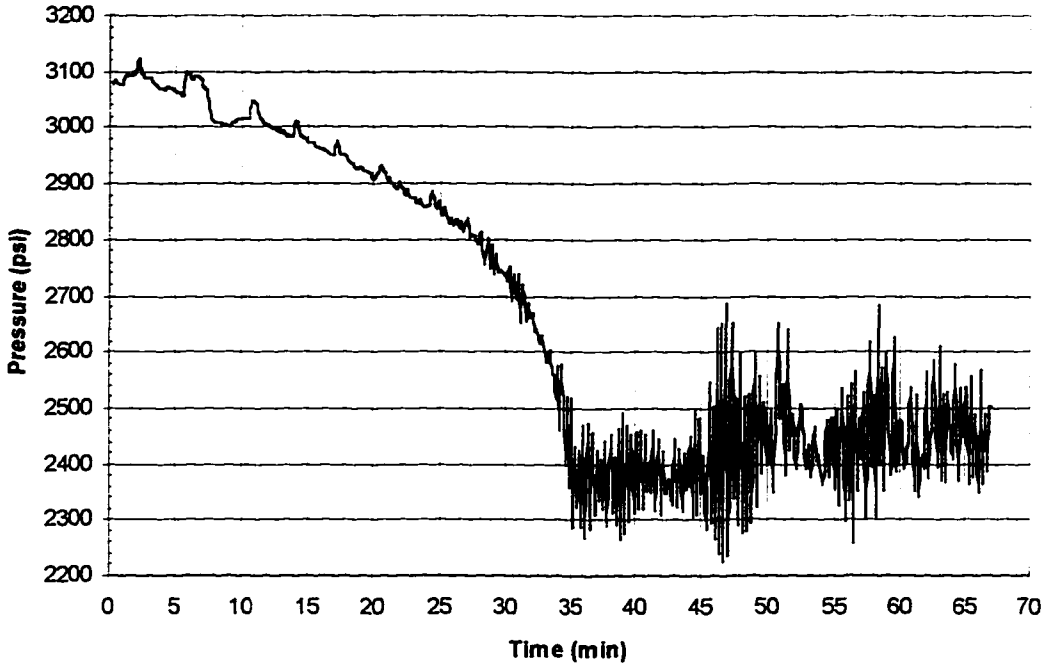

Figure 5.10 - Unsteady-State Flow Simulation for Test 1

mass rate. It was observed by Ohara (1995) that it separates in what was called the front, center, and gas tail, traveling at different velocities.

The simulation run did not reach a steady-state condition, since it was following the data from the experiment. The pressures estimated at the end of the run present values around 2,450 psia, or 2,465 psig, which are about 100 psi lower than the actual readings.

5.3- SECOND EXPERIMENT

5.3.1 - Operations and Incidents

In the second experiment the sensors were configured with the three recorders placed together at the bottom of the on-line pressure tool, so only the logging cable was used to run them in. This was done to ensure that the bottom hole data would be acquired (one of the bottom recorders failed during the test, producing garbled data).

Due to problems in the main data acquisition chassi, a backup one was used. But only 4 data channels were available, so the on-line tool was not made active. The bottom pressure and temperature data for the entire experiment are shown in Figure 5.11.

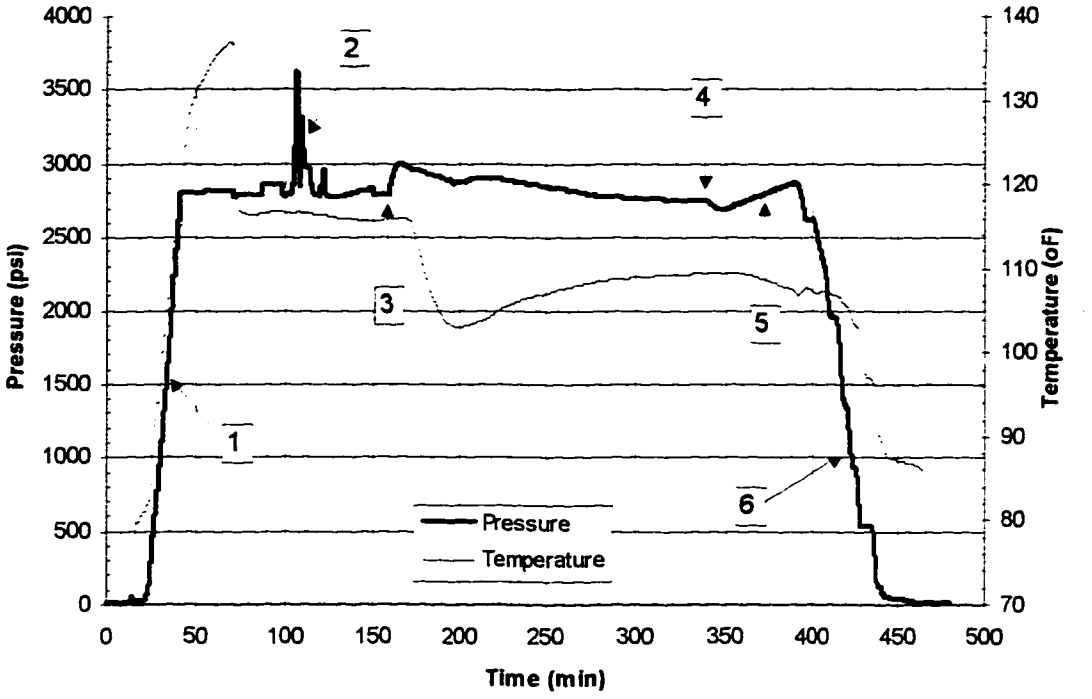

Figure 5.11 - Pressure and Temperature at 5,800 ft During Test 2

The numbers in the graph represent operations and incidents that occurred during the experiment:

1) Running the pressure and temperature recorders down the hole, using the logging cable;
2) Sensor tool became stuck in the hole. Changing pump pressure and working tool up and down to get it free and succeeding;
3) Begin of gas injection for the experiment;
4) End of gas injection;

5) Circulating the nitrogen out of the hole;

6) Retrieving the pressure and temperature recorders.

5.3.2 - Bottom Hole Temperature

The maximum bottom hole temperature recorded was 137 °F, at 5800 ft, 28 minutes after reaching bottom. It was still increasing when the circulation started, stabilizing at 117 °F. The stable bottom hole temperature after the gas injection was around 109 °F.

5.3.3 - Mud Properties

The mud was conditioned for the test with the addition of bentonite, which raised its density and viscosity. The mud properties are summarized in Table 5.3. The mud weight was again calculated based on the recorded hydrostatic values from the experiment.

Table 5.3 - Mud Parameters for Test 2

Mud Properties				
Mud Weight	θ_{300}	θ_{600}	Plastic Viscosity	Yield Point
(ppg)	(d'less)	(d'less)	(cp)	(lbf/100 sqft)
9.34	33	57	24	9

5.3.4 - Bottom Hole Pressure

A detailed view of the actual experiment is given in Figure 5.12. When the gas injection starts, the bottom hole pressure ramps up due to the increased friction loss caused by the surge in the mud speed.

The nitrogen starts filling the well some 6 minutes after the gas injection start, when the bottom hole pressure begins to decrease. The leading gas front reaches surface approximately 39 minutes after that, when the bottom pressure mounts up due to the increase in choke pressure.

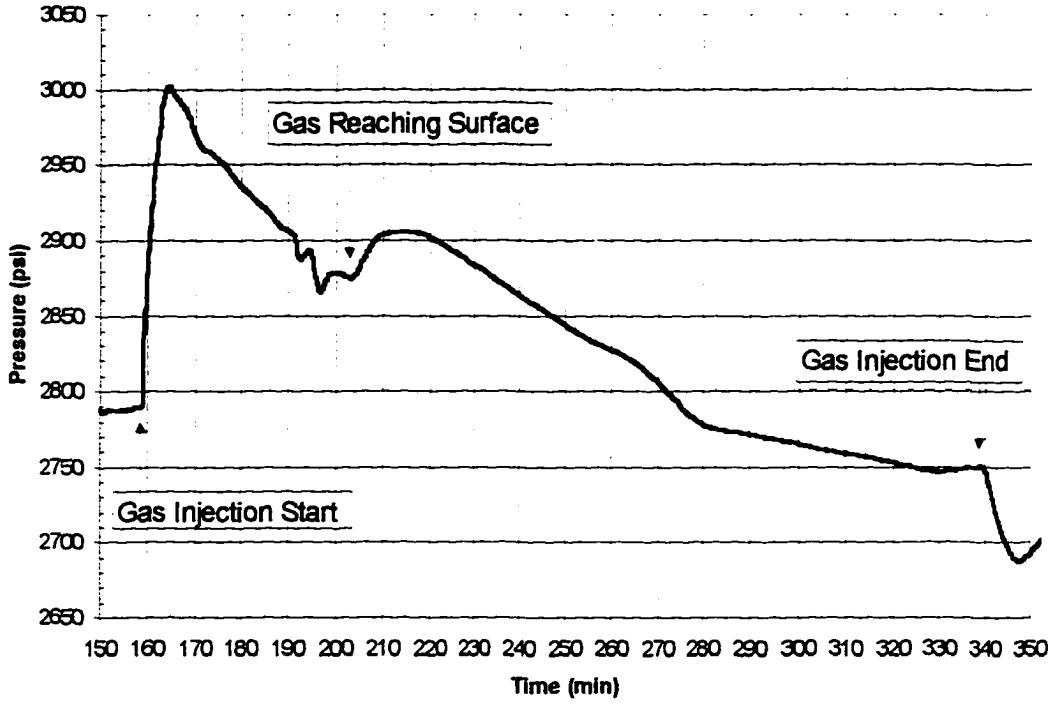

Figure 5.12 - Test 2 Bottom Pressure Sensor (Detailed View)

The total increase in pressure due to the added choke pressure is 27 psi. The nitrogen injection lasts for 181 minutes.

5.3.5 - Nitrogen Injection Rate

Although a constant gas injection rate was required from the bidding companies, the nitrogen unit used was not capable of such. The gas injection rate provided was dependent on the upstream pressure and varied accordingly.

Figure 5.13 shows the nitrogen injection rates observed throughout the experiment. It shows an initial peak of about 1,000 SCF/min, during about 4 minutes. This period should correspond to the time required to fill up the gas line and start to unload the well. After that, the rate decreases to around 450 SCF/min and steadily rises

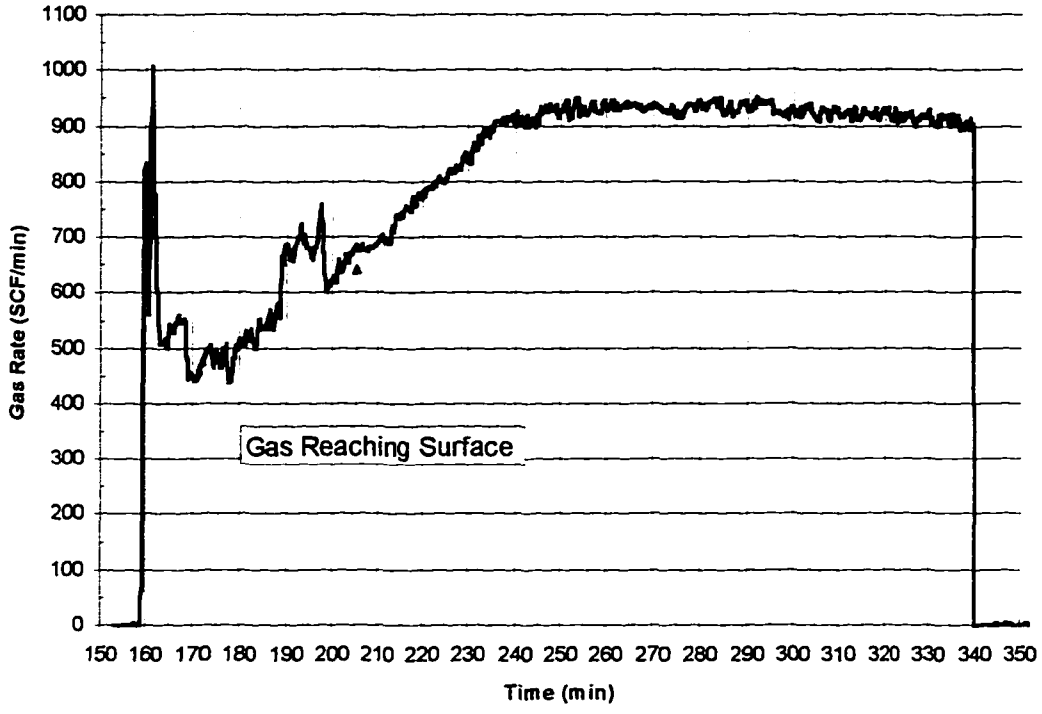

Figure 5.13 - Nitrogen Injection Rates for Test 2

as the bottom hole pressure decreases, until it reaches a stable average rate of 932 SCF/min. The time to reach stabilization was around 86 min.

5.3.6 - Choke Pressure

The behavior of the choke and manifold pressure is presented in Figure 5.14. While there was only liquid flow the top pressure remained stable around an average of 131 psi. When the two-phase flow reached surface the pressure steadily increased for about 65 minutes. After that, it reached a stable pressure around 230 psi that lasted up to the end of gas injection, or about 72 minutes more. It was observed a sequence of rapid choke pressure fluctuations after stopping the gas injection, but with the mud pumps still on. While the nitrogen was circulated out, the choke pressure started to decrease, and the circulation was concluded when the values showed a tendency to stabilize around 145 psig. The choke position was held fully open during the entire test.

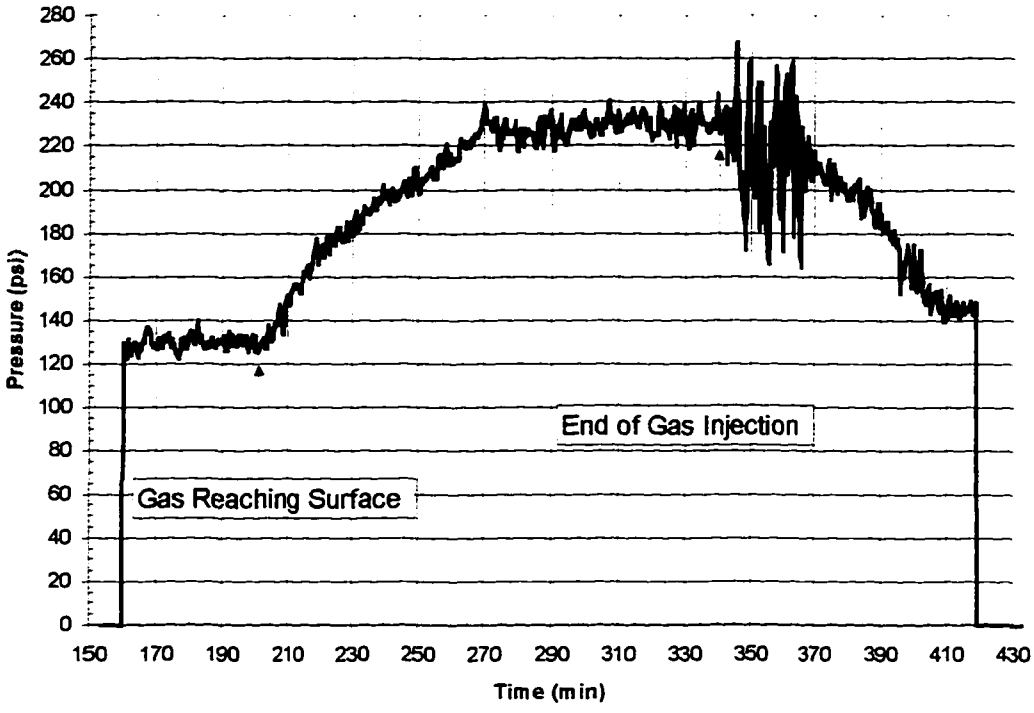

Figure 5.14 - Choke Pressure Readings for Test 2

5.3.7 - Mud Pump Rate

Figure 5.15 shows the behavior of the mud rate during the test. The mud pump throttle was initially set to provide 150 gpm and was kept without any changes throughout the experiment.

When the gas injection started, the liquid rate decreased to about 140 gpm and some fluctuation was observed until the gas front reached surface. This was probably caused by the U-tube effect while unloading the well. The liquid rate was stable during the rest of the test at around 140 gpm. It increased right after the gas injection ended to a maximum of 165 gpm and slowly decreasing as the gas was circulated out.

5.3.8 - Mud Injection Pressure

The behavior of the mud pump pressure is presented on Figure 5.16. The values remained fairly stable throughout the experiment, with a maximum value of

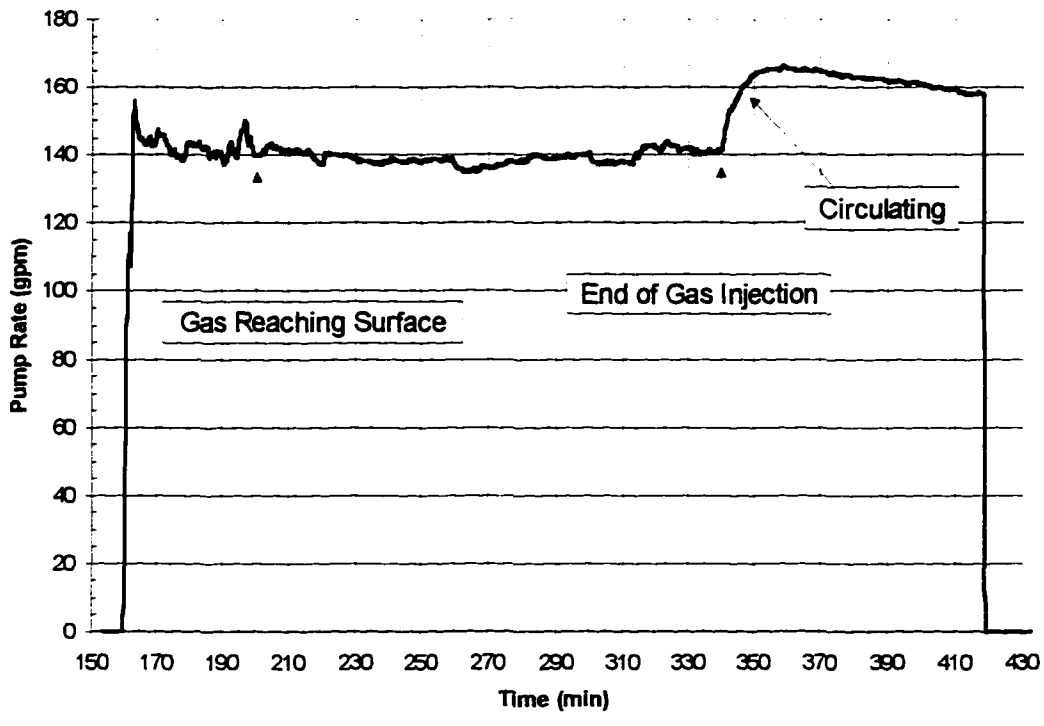

Figure 5.15 - Liquid Rate Readings for Test 2

approximately 1,500 psi. It can be observed a slight pressure increase during the well unloading and a small pressure decrease after the choke pressure stabilizes, due to the decreasing bottom hole pressure.

5.3.9 - Simulation Results

After compiling the test data, the average values for the stabilized flow were taken as input for the steady-state simulator. These values are presented in Table 5.4.

Table 5.4 - Input Data for the Steady-State Simulation of Test 2

Simulator Input Data					
Casing ID	8.287	in	Choke Pressure	230	psi
Total Depth	5800	ft	Surface Temperature	53	Of
Injection Line ID	1.25	in	Bottom Temperature	109	oF
Pipe OD	3.5	in	Mud Density	9.34	ppg
Gas Rate	923	SCF/min	Plastic Viscosity	24	cp
Mud Rate	140	gpm	Yield Point	9	lbf/100sqft

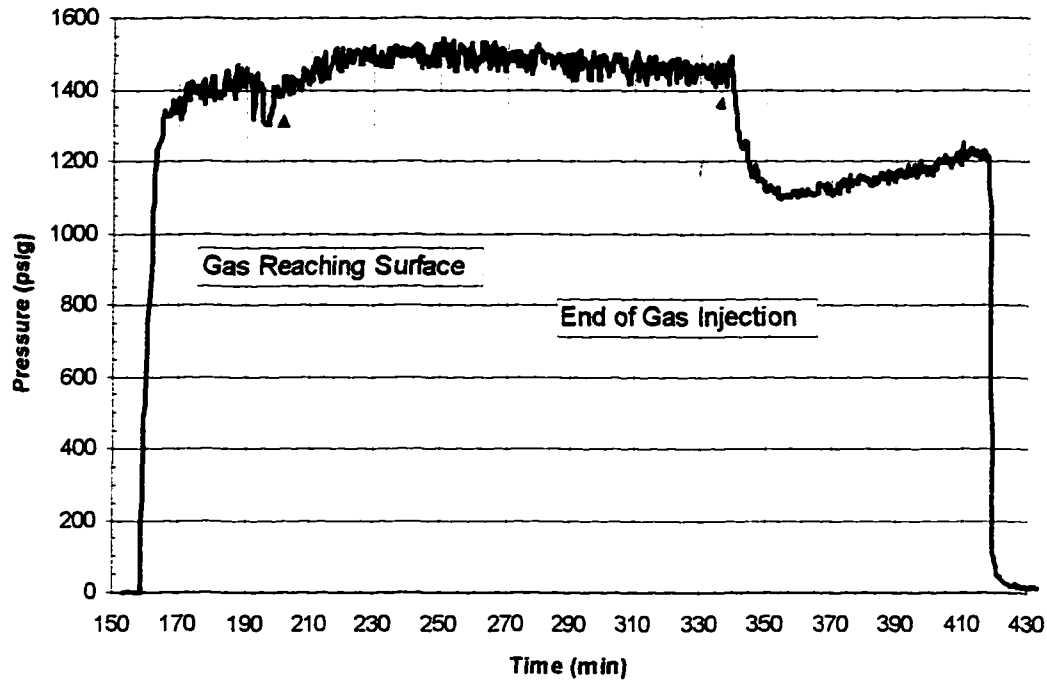

Figure 5.16 - Mud Pump Pressure During Test 2

The resulting simulation is presented in Figure 5.17, where the pressure along the well, at the steady-state conditions, is shown. The bottom pressure value was 2717 psia, or 2731 psig. This is in good agreement with the pressure of 2755 psig, observed in the experiment.

The unsteady-state simulation, shown in Figure 5.18, did not present a good match for the unsteady portion of the test, but also agreed on the steady-state value for the final pressure. The final bottom hole pressure in this case was 2,749 psia, or 2,764 psig. The lack of agreement in the unloading phase is probably due to the assumption of only one gas bubble size for all the cells in the algorithm. Further development of an unsteady-state simulator should account for multiple gas bubble sizes in the riser system. Such a simulator could, then, be used to build a gas injection controller to investigate the feasibility of such a device in the dual density riser system.

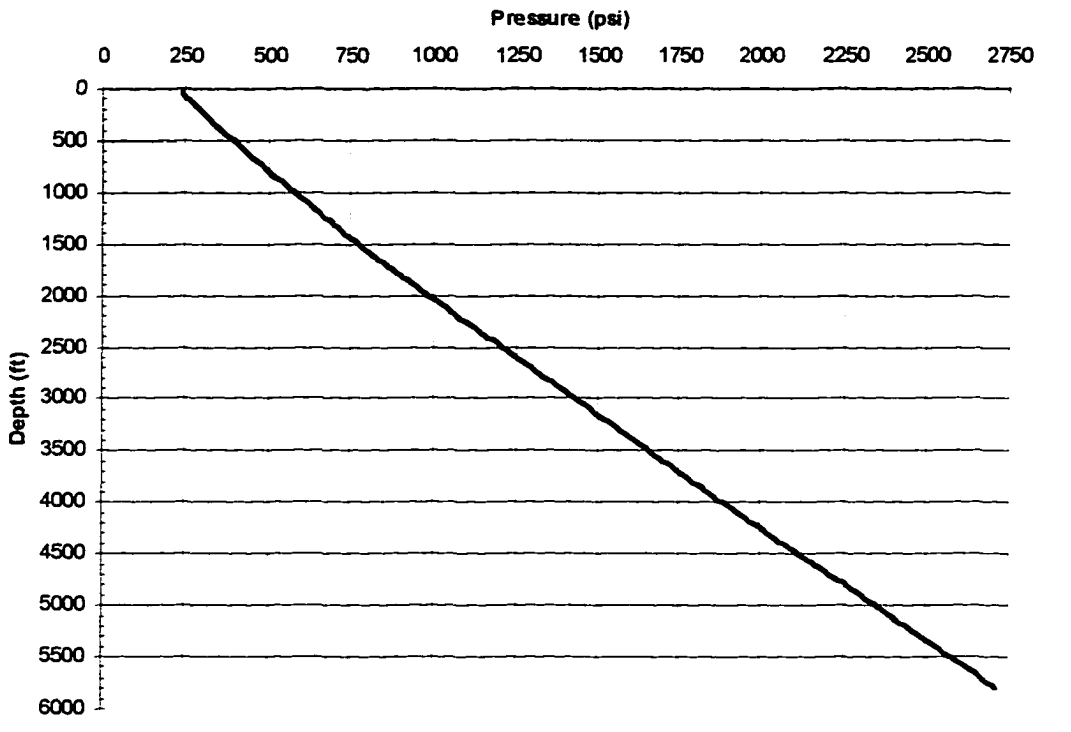

Figure 5.17 - Steady-State Simulation Pressure Profile for Test 2

The simulation input data included the observed values for choke pressure, gas injection rate, and liquid rate. These values were read in from a file, during the simulation.

During the experiment the observed time required for the gas leading front to surface was approximately 39 minutes. In the simulation this time is about 32 minutes, showing a reasonable match for the leading gas front velocity. But, with only one gas bubble size, the gas expands near the surface at the same rate it is injected.

This brings the overall mixture density to values much lower than the ones observed in the experiment. As the simulation progresses, the pressure values converge to the ones observed in the test. This effect is probably due to convergence of the observed gas velocities into one close to the predicted by the simulator.

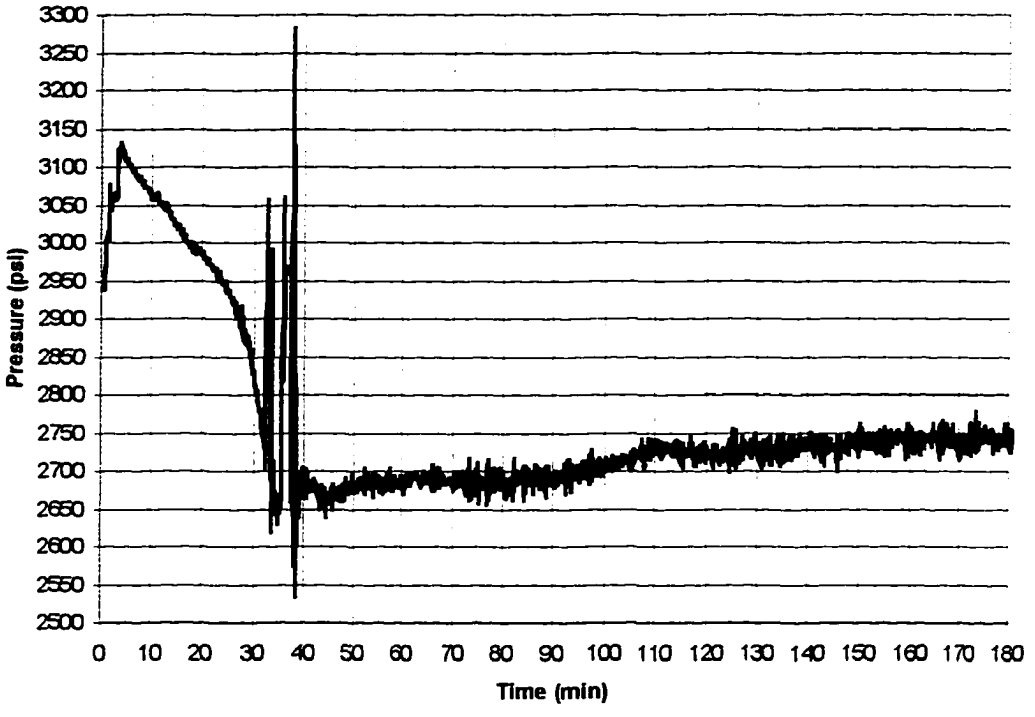

Figure 5.18 - Unsteady-State Flow Simulation Results for Test 2

As pointed out before, the nitrogen was injected 30 ft below the mud injection point, with little turbulence to mix the two fluids. New experiments should inject the mud below the gas, for further investigation.

CHAPTER VI

DRILLING OPERATIONS

Drilling in deep waters comprises many different operations for each step of the way. Almost all of them are performed through the riser column and many are affected, in some way, by the pressures within the riser string. We must investigate what differences the dual density system might introduce, to determine if these operations can be successfully completed under the new system.

6.1 - OPERATION SUMMARY

The riser string is run only after the Spud-in operations, which comprise all the actions needed to get the surface casing, with the wellhead, in position. Normally this means setting a conductor pipe first. In places like Brazil, where the ocean bottom is extremely soft, a foundation support pipe is jetted in before the conductor casing.

Once the riser and BOP are in place, there is a set of operations that are performed in a certain order. We will try to describe these tasks, and then discuss how they can possibly be carried out under the dual density system. The common task order is:

6.1.1 - Shoe Drill-Out and Mud Change

After connecting the Bottom Hole Assembly and the bit, the drill string is run down to the top of cement inside the surface casing, which usually has 20" of diameter. At this point, the riser is full of sea water and the casing contains spud mud. The spud mud is flocculated drilling fluid, with low density (usually around 9.0 ppg) and very high viscosity.

Since the fresh cement to be cut is chemically active, and tends to flocculate any new mud, sea water is usually used to drill the casing shoe, to avoid mud contamination. So, only after drilling out the cement and washing the rat hole, the drilling fluid scheduled to be used is pumped in.

6.1.2 - Leak-Off Test

A leak-off test sometimes is done after the 20" casing is set. This is a standard practice with Petrobras. Some companies prefer not to do it, out of fear of breaking a too weak formation. On all the other casing sizes this operation is normally performed.

6.1.3 - Drilling Ahead

During drilling operations the most common task is the drill-pipe connection. In each one the driller stops the pumps before pick the string off bottom. The time required to complete a connection varies, depending on the crew speed and the pipe handling equipment. It can take up to 15 minutes, but usually stays among 5 and 10 minutes. The procedure varies according to well conditions. When the driller is worried that the borehole might be swelling in, he will ream the hole at the end of each joint, before start a connection.

6.1.4 - Pipe Trips

When drilling the 17 ½" hole, which is the usual diameter after the surface casing, the bit size usually is 14 ¾", since the inside diameter of common BOPs is 16 ¾". The borehole is enlarged to its nominal size by means of under-reaming. This operation can be done while drilling, but it is usually done separately. The reason is that reaming while drilling often leads to high borehole angles. So, after drilling, there is usually the need for another run, thus a drill-pipe trip.

After the intermediate casing is set, bit trips become more common, since the smaller diameter holes and tougher formations require more bits to complete each part of the well.

6.1.5 - Borehole Conditioning

Once the well reaches the depth planned for another casing string to be set, it is time to make sure the wellbore does not have any tight spots. These spots could prevent the casing from being lowered all the way. A short trip up to the casing shoe, and a lengthy circulation when back on bottom, are the norm. The driller watches closely the amount of drag while tripping to avoid kicking the well and to determine if it needs reaming. This operation is usually skipped on the 17 ½" hole, since the under-reamer arms need pump pressure to be open, but with a top-drive system it might be enforced in these cases. In the smaller, long portions of the well, sometimes short trips are also performed, before the casing set point, to check the wellbore.

6.1.6 - Logging

Logging jobs can take a long time to complete. Depending on the amount of information to be extracted from the well it can demand several days of work. Sometimes it is even necessary to recondition the hole, to resume logging. In deep waters, where almost each hole is a wild-cat, every section of hole is logged. But, unless a reconditioning job is scheduled, no circulation is involved.

6.1.7 - Casing Runs

These operations require lengthy surface preparations, and take long time to be carried out, since the pipe handling equipment has to be rigged up and each pipe connected. Moreover, each pipe connection, after being carefully inspected, can take

some time to be made up, due to cross-threading caused by the rig movement. The bigger the threads are, and the worst the weather is, the more time it takes to get a connection properly made up.

6.1.8 - Cement Jobs

Although dual stage cement jobs are fairly common on shallow water drilling, they are not done in deep waters. The reason is that, in shallow waters it is possible to connect an extra length of casing all the way up to the rig floor, after landing the casing string on the wellhead. This allows for launching the second stage cement plug. In some cases in deep waters the total length of casing to be run does not even reach the wellhead, after it is all made up.

With the latest cement mixing units, nowadays a cement job can have a great degree of automation (Benabdelkarim and Galiana, 1991), with slurry densities that can be accurate to the 0.1 ppg density difference. Also, very light slurries are possible with the use of spherical glass beads as extenders. This way, it is possible to cement long sections of a well, even in areas with very weak formations.

6.1.9 - Wellhead Operations

Wellhead operations comprise all the work that has to be done to ensure sealing between the last and the previous casing strings. Usually the casing being lowered is locked into the wellhead, exceptions made when there is the possibility that the temperature stretch will build up too much tension into the wellhead.

The task of landing the pack-off seal assembly on its exact position is critical and great effort is made to make sure it is properly set. Energizing the pack-off seal assembly is another sensitive operation, since this is normally done by rotating the landing string

and building up enough torque to expand the sealing element. In deep waters, with very long landing strings, applying the required amount of torque can be difficult. There are systems where this operation is done by setting weight on the pack-off, but they bring other problems, too. Nevertheless, all the work is done without any circulation, unless the wellhead needs to be flushed, to get it clean before the pack-off is run.

6.1.10 - Kick Detection

Kicks are a fact of life. The only time, during drilling operations, that the rig is safe against kicks, is when the well is cased and the shoe has not yet being drilled out. This is assuming the casing string does not have any leaks. So, the lookout for a kick is a constant job for the rig personnel. The earlier a kick is detected, the more chances it has to be short lived. Unfortunately for the dual density riser system, the strongest indicator of a kick is the increase in pit level. Although other indicatives include pump acceleration, pressure decrease and drilling breaks, it is the flow check, performed with the pumps down, that really tells the tale.

6.1.11 - Kick Circulation

Once a kick is detected, the next thing to do is to close the BOP and let the pressures stabilize, so that the kick can be assessed. In a conventional system, the Shut-in Drill Pipe Pressure (SIDPP) is used to determine the kick's pressure, assuming the fluid inside the drill string is homogeneous.

Usually the kick is circulated out first, and the kill mud is pumped in afterwards. The bottom hole pressure is kept constant by adjusting the surface choke to maintain a given SIDPP constant.

6.1.12 - Well Testing

In deep waters well testing is conducted using a safety valve installed on the wellhead. In case of an emergency, this valve is closed, either from a command from the surface or automatically. Only cased holes are tested. All the flow is directed into the testing string by means of a bottom packer. This packer is unseated at the end of the test to let the annular hydrostatic pressure kill the well. The fluids inside the testing string are normally reverse circulated to surface.

6.2 - SHOE DRILL-OUT AND MUD CHANGE

In the dual density system the new drilling fluid is normally much heavier than sea water at the end of the 17 ½" hole. Its density is normally increased as the well gets deeper, depending on the expected formation pore pressures.

In the dual density system the fluid changeover, from sea water to new mud, should be done while injecting nitrogen at the BOP level. Sensors would be monitoring the riser bottom pressure, and a computer control system would be adjusting the gas injection rate. This would maintain the BOP equivalent density around the sea water value.

6.3 - LEAK-OFF TEST

In a leak-off test the BOP is closed and hydraulic pressure is applied to the borehole by injecting fluid through the drill-string. Since the BOP is sealing the well, the dual density system is disabled. The full hydrostatic pressure provided by the drill-string is acting on the exposed formation. Although the mud weight at the beginning of each drilling phase is usually equal to the previous one, the densities required for the dual density system can be greater than what the formation can take.

If this is the case, or if there is doubt about the formation's fracture gradient, the leak-off test should be done with a lighter fluid, or with a sea water cushion inside the drill-pipe. This should be calculated to place the mud-sea water interface around the ocean floor. There will be the need to circulate out this cushion. With an automatic controller system, the gas injection rate would be adjusted as needed when the fluid density changes.

6.4 - DRILLING AHEAD

With the dual density system, if the gas injection is also stopped, the process of gas migration will cause an increase in the riser bottom pressure, due to the gravitational separation of gas and fluid. Since the gas rise velocity is around 1 ft/sec, in 15 minutes it can rise up to 900 ft before the gas injection resumes. So, when this happens, there will be a 900 ft column of dense liquid ahead of the injection point that has to be pushed up, creating spikes in the riser bottom pressure. The foreseen solution to this problem is to keep the gas injection going, but at a much lower rate, determined by the automatic controller, equal to the rate with which the gas is migrating. This would keep the process transparent to the driller, that would not have to worry with yet another problem during the frantic pace that a drill-pipe connection demands.

6.5 - PIPE TRIPS

When is time to pull the drill-string, the dual density system should be deactivated. To maintain the same bottom hole pressure, sea water should be injected in the riser annulus, displacing the mud-gas mixture. Doing so would allow pulling the string with the annulus open, avoiding wear on the rotating head at surface. It would also save nitrogen.

Displacing the mud in the riser annulus with sea water is not uncommon. In situations where a riser disconnection is orderly planned, this is a required operation. The drawback is that it takes some time to complete. The longer the riser is, the longer it takes to changeover. The common riser size in a deep water rig has a diameter of 17 ½". That translates into a riser capacity is 0.30 bbl/ft. So, for a 5,000 ft water depth the changeover volume is 1,500 bbl. In a rig using the dual density system, a higher pump output should be considered, along with smaller diameter risers.

The need for substituting the mud-gas mixture in the riser for sea water would arise in many other operations, such as: running casing, logging, well testing, etc.

6.6 - BOREHOLE CONDITIONING

Short trips to the shoe can be uneventful. But, there is always the possibility of coming across tight spots that need reaming. In the dual density system, there would probably be the choice between changing over the riser fluid to sea water, prior the short trip, or doing it by stripping against the rotating head. With the latter option, if reaming becomes necessary, circulation should be possible by means of a Top-Drive circulation system, while maintaining gas injection going. The industry would have to develop new rotating-heads elements that would be rugged enough to take stripping jobs without problems. It is important to note that the required top pressure for the dual density system should not exceed 150 psig, well below the rated pressure for this kind of equipment.

6.7 - LOGGING

Since normally there is no circulation involved during logging jobs, the riser fluid should be substituted by sea water, before performing the job, to avoid any gas injection.

In case the well needs reconditioning, the procedure should be the same adopted for the short trip case.

6.8 - CASING RUNS

Casing runs in the dual density riser system will demand the same procedure advised for tripping pipe. Since it is a fairly long operation that does not normally require circulation, the fluid in the riser annulus should be switched over to sea water. As the casing is lowered into the well, a significant mud volume is displaced into the riser annulus. In the case of a large diameter pipe, such as the 13 3/8" casing, for a 3,000 ft string the mud volume would be around 3,000 ft^3. This would translate into a 1,785 ft height of heavy mud inside the riser annulus, after the run is completed.

To avoid injecting nitrogen while running the casing, special float valves could be used, as shown in Figure 6.1. These valves should allow the casing to be open while being lowered, and after reaching its setting point, a release mechanism should liberate flappers in the float valves. Similar float valves have being used by Petrobras in the past (source: Petrobras) in deep water drilling operations. These valves were required to provide a passage to an inside pipe TV camera, needed to assist the reentry operations.

There would still be the extra steel volume to consider. In the case above, the flooded casing string would still displace mud 325 ft up into the riser annulus. But, since the casing string is shorter than the riser, the total steel volume would displace sea water while the string is being lowered inside the riser.

Once the casing starts entering the well, sea water could be injected in the riser to keep it full. But, to compensate for the extra hydrostatic pressure provided by the displaced mud from the well, a small calculated portion of the riser could be kept empty.

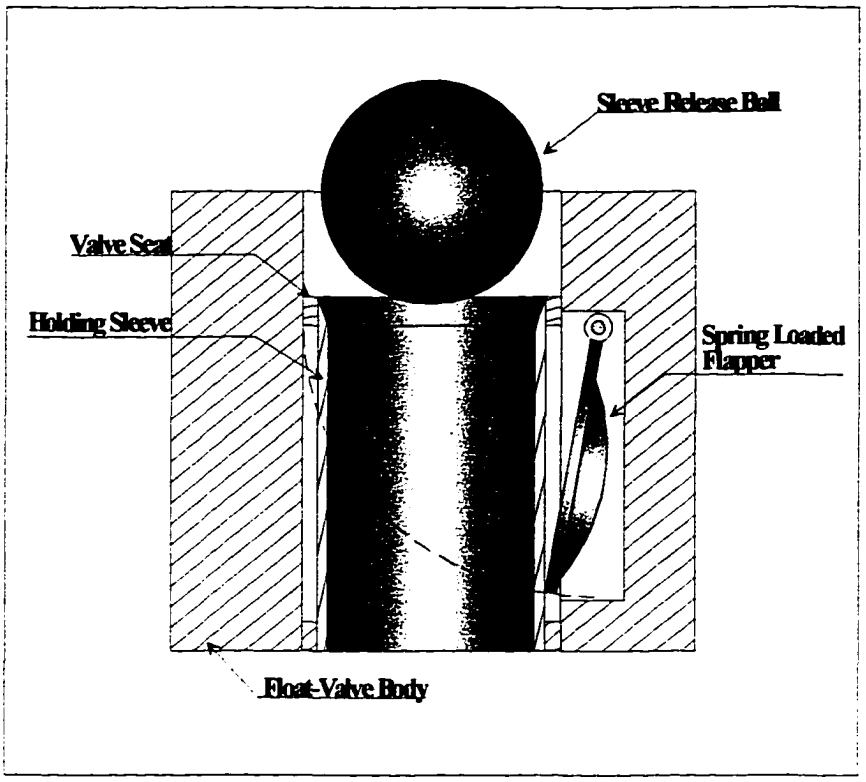

Figure 6.1 - Casing Float Valve for Dual Density System

If regular float valves should be used, the casing would have to be stripped in. This would require packing elements in the rotating head that could cope with large diameters. The small back pressure should not pose any collapse threat to the casing.

Another idea is the adoption of a valve in the BOP that could be open to the sea, from the surface. By closing the rotating head at top, the mud volume displaced by the casing string would be dumped out of the system, at the sea floor.

6.9 - CEMENTING OPERATIONS

The dual density riser system introduces a constant U-tube effect that will increase the so called cement "free-fall". This increase in slurry speed has being associated with formation fracture in some cases. Lighter slurry densities might solve this

problem if it occurs. Otherwise, cement displacement should be treated much like another circulation.

6.10 - WELLHEAD OPERATIONS

This task could be carried out filling the riser with sea water, before running in with the tools needed, to save the wear and tear on the rotating head. On the other hand, changing the riser fluid demands time. Either way, the dual density system should not pose any special problem to complete this set of operations.

6.11 - KICK DETECTION

Early kick detection presents a challenge for the implementation of a dual density riser system. Any technique eventually developed for this purpose will, probably, depend on sensors installed at the BOP, below the gas injection point.

For conventional kick detection based on pit volume increase, the mud volume in the marine riser would need to be "totalized" with the active pit volume. With the dual density system, this could be done by accurately measuring pressures at the bottom of the riser. For example, for a 17 1/8" riser ID, and a mud weight of 15.6 ppg, a 10 bbl gain in the riser mud volume would cause a 30 psi pressure increment at the BOP. In addition, if an influx of 1.5 bbl/min was occurring, there should be an increase of approximately 5 psi in the first minute, at the riser bottom. A micro-processor could be assigned to monitor these small changes and provide early warning.

There are, also, three systems cited in the literature, that look promising. One way is to use the negative pressure pulse generated by a MWD tool as a source signal. This signal travels up the annulus and can be monitored by a sensor at the BOP level.

The acoustic wave amplitude and phase angle present large variations, for small changes in the natural frequency or the damping ratio of the annular medium (Bryant et al., 1991).

Another technique is based on the use of a sonic interferometer installed in a MWD tool. Acoustic waves are generated between two parallel walls, and at certain frequencies the system is in resonance. Different fluids will show resonance at different frequencies, and the resonance is not disturbed by fluid flow. The resonance peaks are detected by varying the wave frequencies sent between the walls, and monitoring the signal through a spectrum analyzer. If gas flows through the two walls, the resonance disappears, since the medium has changed (Vestavik and Aas, 1990).

The above mentioned techniques have a strong drawback: they depend on having a tool in the hole, and normally will not send any information unless the fluid is being pumped. One way to monitor the well while tripping, or with the pumps off, is by a wellhead sonar (Bang et al., 1994). Acoustic waves are generated at the BOP level and directed down the well, while an acoustic sensor, also installed at the BOP, picks up the sonic reflections. If any gas is present in the mud, it will generate a reflection due to the difference in acoustic impedance between the mud and the gas-fluid mixture.

6.12 - KICK CIRCULATION

The possibility of a kick occurrence is always present while drilling any well, anywhere in the world. Once the invading fluid is inside the wellbore, the problem is how to circulate it out or to bullhead it back in.

In the dual density system, after a gas influx is detected, the mud pumps should be stopped. Once the mud stops, the nitrogen injection should be shut down also, and the

BOP should be closed with the choke line open. The choke line should be kept filled with sea water, as is the common practice. This is done to avoid clogging the sub-sea choke valve with solids settlement from the mud.

The density difference between the mud inside the drill string and the composite column in the wellbore and choke line should lead to a U-tube effect inside the drill pipe. This lowers the mud level until the hydrostatic pressure in the drill string equals the bottom hole pressure. It is probable that this mud level will be above the ocean floor due to the increase in pressure caused by the kick.

After the initial flow through the choke line is reduced, signaling the end of the U-tube flow, the choke line should be closed to get a reading of the bottom hole pressure. The first difficulty is how to determine the bottom hole pressure: since the liquid level inside the drill pipe is below surface, there should be no pressure reading in the drill string. This information might be obtained by means of a well sounder, to determine the fluid level inside the drill pipe. Acoustic measurements of downhole liquid levels are routine in operations like well testing and sucker rod pumping with reliable results. Such a device should be installed on the Top Drive system, to be readily available always.

Once the kick pressure is known, the gas injection rate could be adjusted, with computer assistance, to produce a gas-mud mixture. This would result in an effective hydrostatic pressure equal to the one that is needed to control the kick.

With the hydrostatic adjusted, the kick could be circulated out through the choke line. A sub-sea choke could be used, to reduce the pressure load on the gas injection line, or the surface choke, if the pressure range is within the installed compressor capabilities.

If cryogenic tanks are available, the surface choke could be used through out the entire circulation, since nitrogen pressure availability should not be an issue. Figure 6.2 shows the system with a gas kick rising in the annulus.

6.13 - WELL TESTING

Since the well remains isolated from the annular riser fluids, and the flow is upward, the dual density system should not interfere with a normal cased well test program. The reverse circulation, at the end of the test, will probably demand new equipment. One idea is to install a pressure regulator valve in an external riser line.

The hydrostatic pressure could be reduced by using this valve in much the same way the subsea choke would operate, but in the opposite direction. Another idea could be the use of a concentric test string, with an inner and an outer pipe. Mud could be pumped down the annulus between the two pipes, while the well fluids would be recovered through the inner pipe. A valve, operated from surface, would seal the bottom of the string, preventing the circulation pressure from being exerted on the bottom of the hole.

6.14 - RISER COLLAPSE

The riser string has a low collapse resistance due to its small wall thickness to diameter ratio. When considering a system designed to lower the annular riser pressure we need to verify if there would be a pressure differential that might tend to collapse the riser string.

The pressure profile in the riser annulus, under steady state conditions, is exemplified in the Figure 6.3. Here the mud weight considered was 15.6 ppg and the water depth was 10,000 ft.

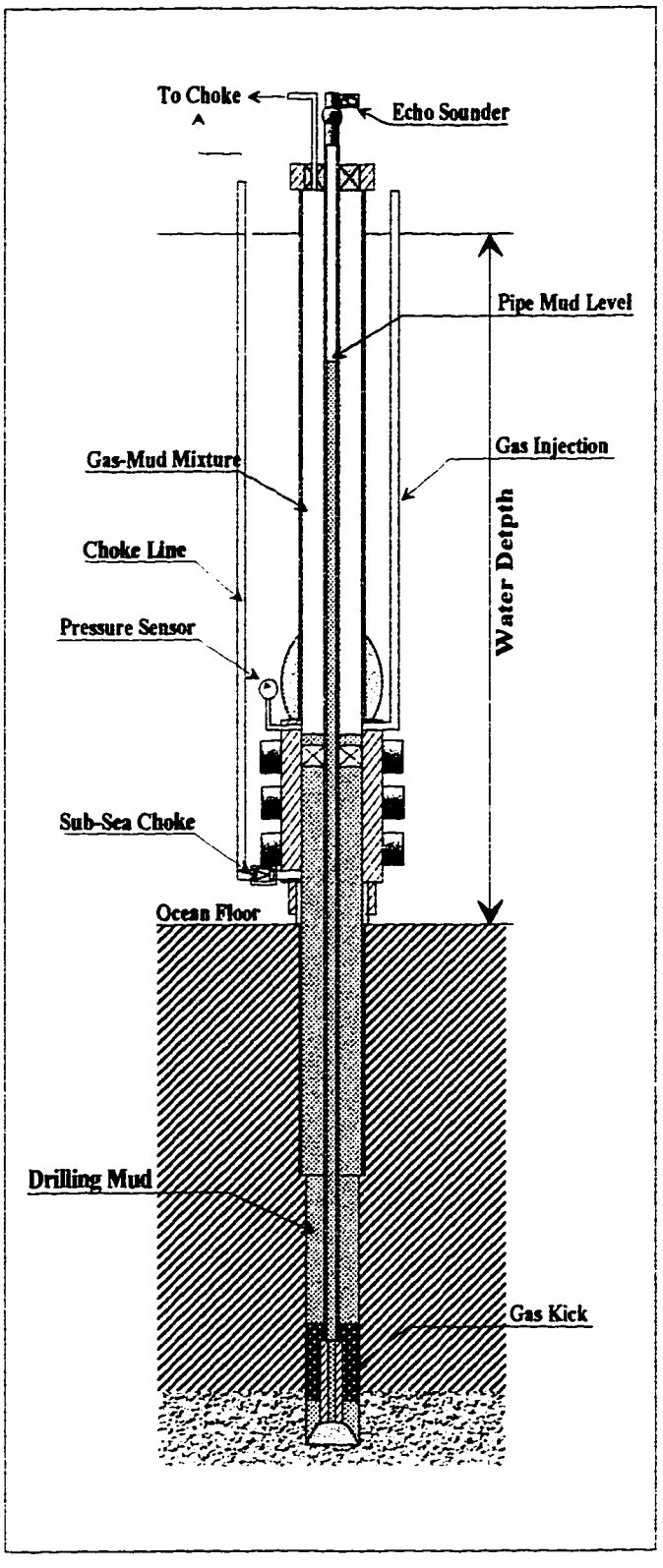

Figure 6.2 - The Dual Density Riser System With a Gas Kick

The maximum collapsing pressure of 979 psi occurs at 4,075 ft. According to Erb et al., the riser collapse is governed by elastic buckling due to its small thickness to radius ratio and a large length to diameter ratio.

The critical collapse depths for different riser diameters and thicknesses are depicted in Figure 6.4 (Erb et al., 1983). So, for 18 5/8" risers with a ½" wall, the maximum pressure differential should be around 895 psi. This value would collapse the riser in the previous example.

To increase the riser wall thickness may not be the only solution, since this would restrict the riser bore and raise the riser mass.

A possible alternative might be the adoption of a concentric riser. This is shown

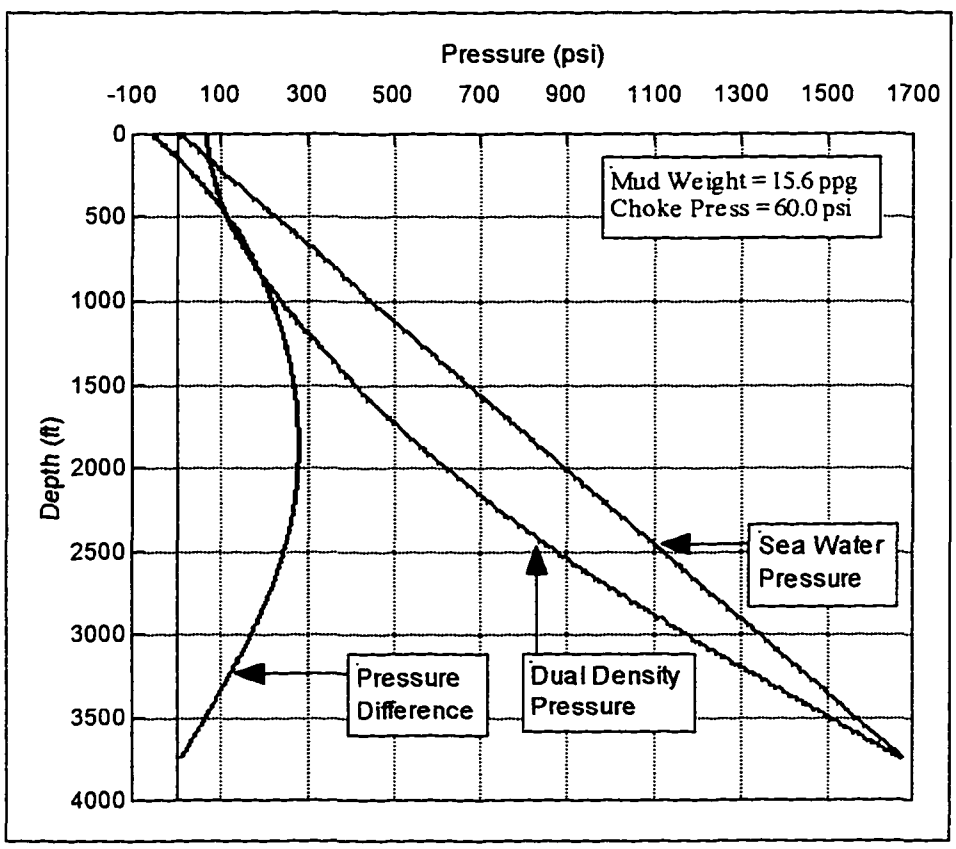

Figure 6.3 - Collapse Differential Pressure for the Dual Density System

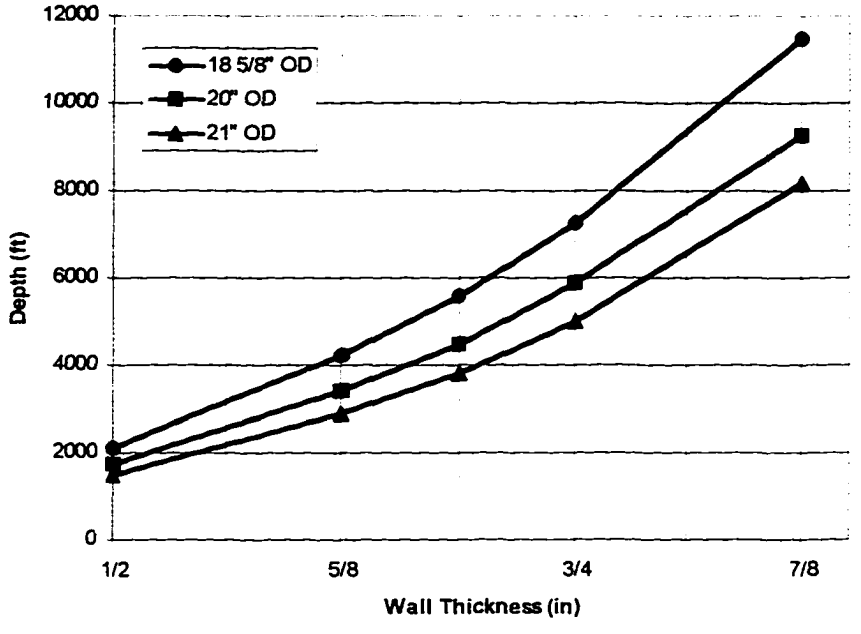

Figure 6.4 - Critical Collapse Depths for Risers

in figure 6.5, where braces between the inner and outer pipes should convey enough collapse resistance to the entire string. The increment in the riser mass, on the other hand, would be much less than if just the wall thickness was increased.

Moreover, sea water could be kept in the inner pipe while all the circulation was done through the annular space between the two pipes. This would greatly reduce the amount of injection gas needed and would provide a quick fluid changeover, for the various tasks that could use it.

6.15 - MUD FALL-BACK

In a case where all the pumps fail and the gas injection is stopped, such as in a black-out, there will be a fluid segregation in the riser annulus. The gas will separate itself from the mud and escape from the riser, in what can be called a mud fall-back. The mud level, after steady state conditions are reached, will depend largely on the liquid holdup existing before the shut-down.

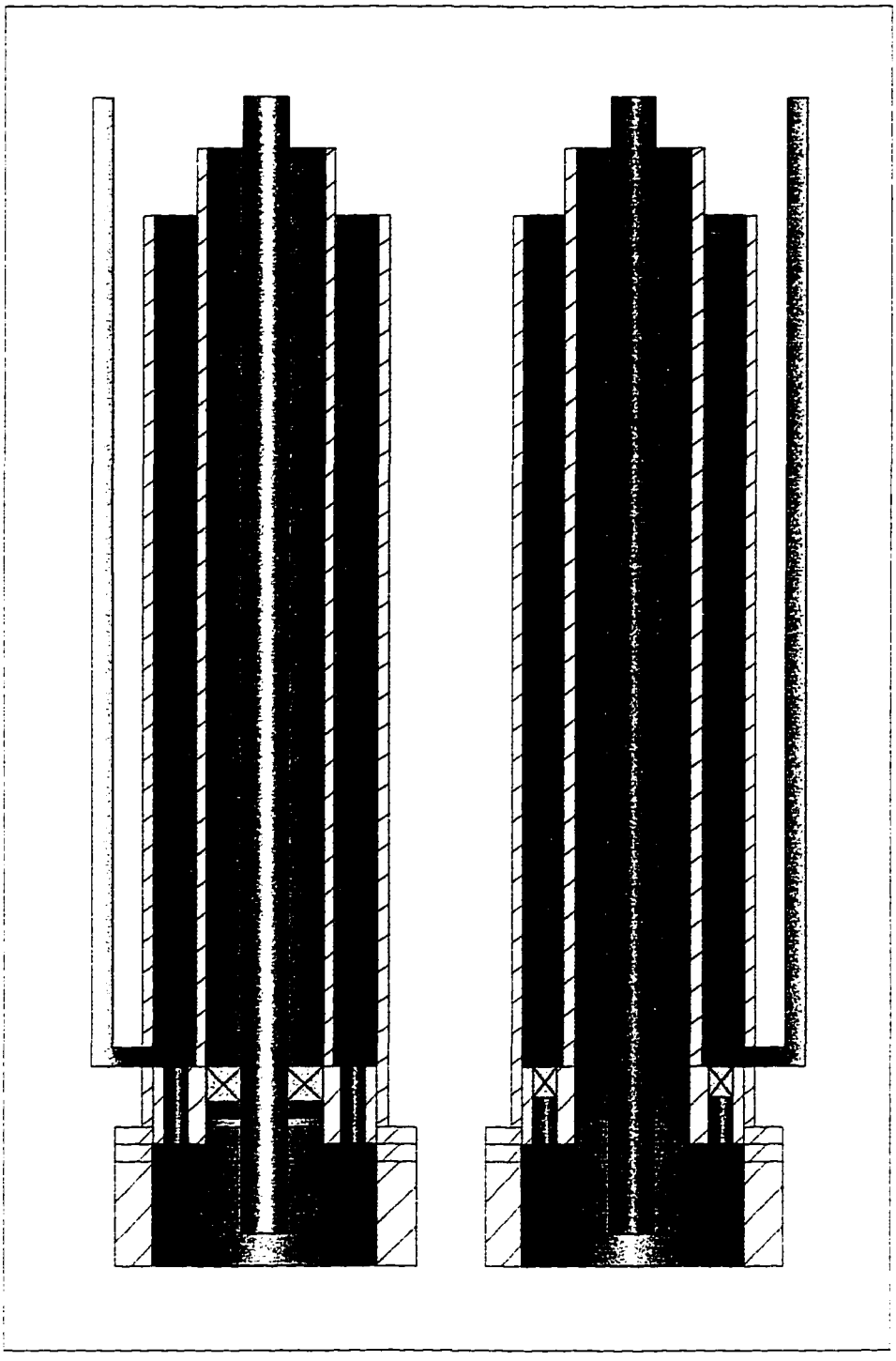

Figure 6.5 - Dual Density Concentric Riser

There will be some flow from the drill-pipe, due to the U-tube effect, but since the drill string volume is much smaller than the riser annulus volume, this contribution will be minor.

Figure 6.6 shows the liquid holdup distribution for the 10,000 ft riser, immersed in waters with temperatures typical of the Gulf of Mexico. This was obtained by simulation with a 15.6 ppg mud being aerated with nitrogen. After multiplying each data point by its cell volume and integrate over the riser length, we get that the mud volume should be 7747 cuft. This means that the mud level should be at 5,051 ft if the U-tube effect in the drill pipe should not be taken into account.

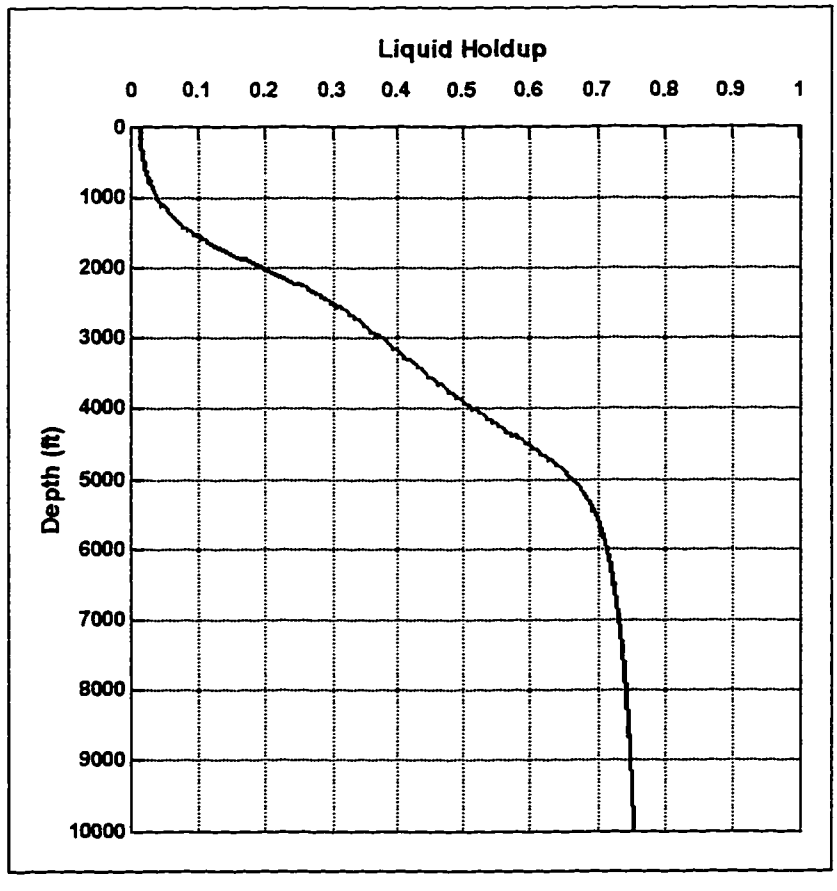

Figure 6.6 - Liquid Holdup Distribution for a 10,000 ft Riser in the Gulf of Mexico.

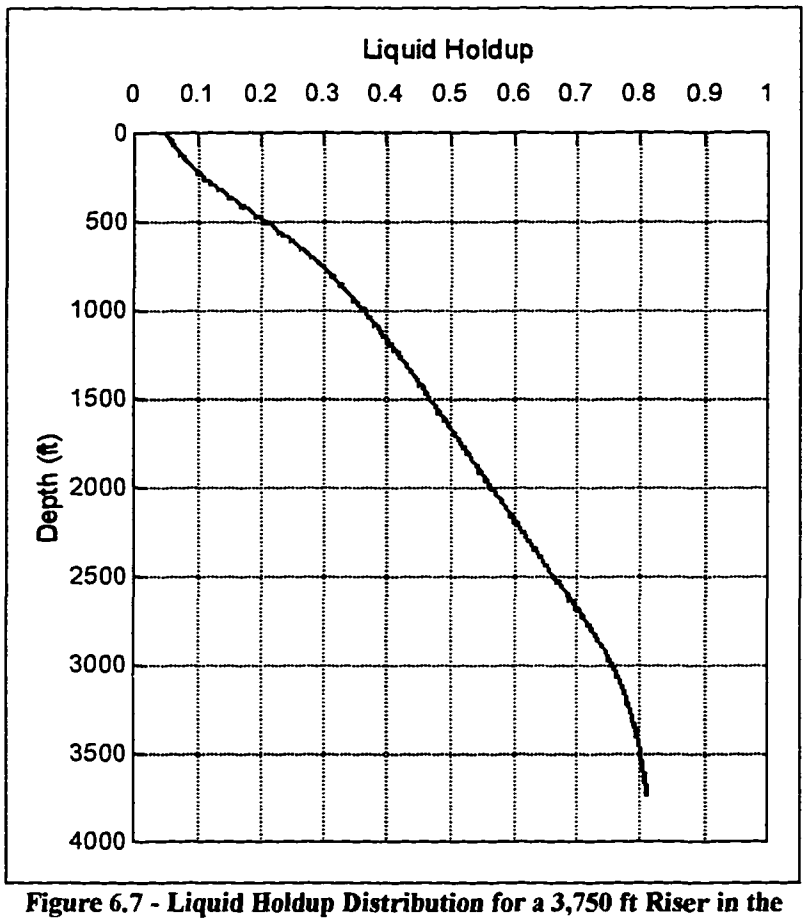

Figure 6.7 - Liquid Holdup Distribution for a 3,750 ft Riser in the Gulf of Mexico.

With it, the mud level should stabilize at 5,352 ft. The differential pressure at this point should be 2,394 psi.

Figure 6.7 shows the liquid holdup distribution for the 3,750 ft riser case. The mud level without the U-tube effect should be 1,927 ft and 2,420 ft with it. The collapse differential should be around 1,082 psi.

Power outages do occur in any offshore drilling unit. So, to account for this kind of eventuality, the riser string should incorporate a fill-up valve. The valve would open the riser annulus to take in sea water rapidly, to avoid great pressure differences that could collapse the string. These valves are used nowadays in many deep water rigs. They are placed at a chosen depth, usually 300 ft, and are equipped with a differential pressure

sensor that opens a port when a preset differential value is reached. These valves were developed for the eventuality of a formation fracture and consequent loss of circulation that would empty the riser string.

CHAPTER VII

ECONOMIC FEASIBILITY

Before the dual density riser system can be implemented, it is necessary to look into the costs involved, and see if they are favorably balanced by the savings the system can provide.

The gas to be injected would most likely be nitrogen, since air contains oxygen and its associated risks of fire and equipment corrosion. Nitrogen is abundantly generated during the extraction of oxygen from the air, so it is cheap. On the other hand, the transportation and storage costs are significant, and so are the compression or pumping costs.

Nitrogen can be generated on site (World Oil, 1995) and then compressed to the required injection pressure. Nitrogen can, also, be liquefied and stored in cryogenic tanks, then transported to the rig, where it can be pumped, heated up and then injected. The expansion process releases the energy stored in the liquid, and great pressure values can be achieved.

Each of these choices carries its advantages and penalties. In this chapter we seek to determine, based on simulations, the amount of nitrogen and the injection pressures needed to drill in different scenarios, so the costs of the two options above can be accessed.

7.1 - SCENARIOS

With the constant push towards ever increasing water depths, the industry is now contemplating drilling in 10,000 ft of water. Drillships as long as 760 ft are being built (Offshore, December 1996), in preparation for it. Thus, one of the cases in this feasibility

study includes such an ultra-deep water depth. The extra bottom hole pressure added by the riser string starts to be a problem for depths greater than 3,500 ft. So, one case was selected for 3,750 ft and another, as an intermediary, for 7,500 ft. We are referencing to them hereafter as Ultra-deep, Shallow-deep, and Medium-deep waters.

There is no formation pore pressure, nor fracture gradient data, available for water depths beyond 7,500 ft. Even for the 4,000 ft to 7,500 ft water depth range these data are hard to obtain. Being so, the research work was based on the data available for an actual well, drilled off the Louisiana Coast, in 3,750 ft waters.

The assumption of same rock matrix stress was made, to extrapolate the data to the water depths needed by the simulations. The increase in pore pressure was, essentially, due to the hydrostatic pressure from the augmented sea column (see Appendix A).

7.2 - SHALLOW-DEEP WATERS

The example chosen comes from an actual well, drilled in the Gulf of Mexico. Its casing design, pore pressure and fracture gradients have being presented in the first chapter, and are reproduced here in Figure 7.1.

It can be seen that the casing design calls for seven strings, with the need to under-ream the 26", the 20", the 17 1/2", the 9 7/8", and the 7 7/8" sections of the well. This occurs because these diameters are too big to get through the 16 3/4" BOP stack, the 20", the 16", the 9 5/8", and the 7 5/8" casings, respectively.

The 9 5/8" and the 5 1/2" casings are designed to be liners, to reduce the costs. Table 7.1 details the casing design.

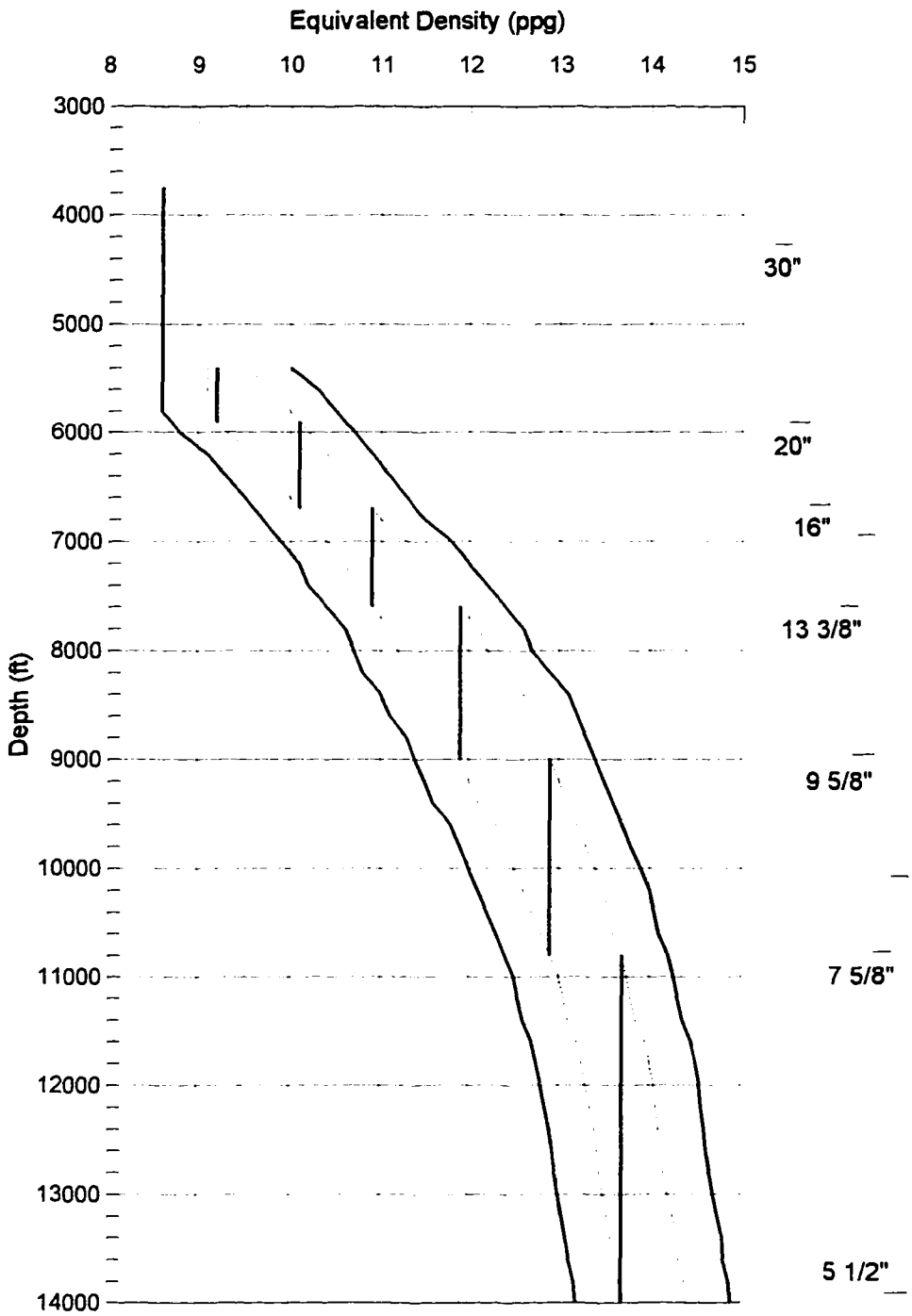

Figure 7.1 - Conventional Casing Design for 3,750 ft Case

Table 7.1 - Conventional Casing Design for the 3,750 ft Water Depth Case

Csg OD (in)	Top (ft)	Shoe (ft)	Length (ft)	Connection
20"	3750	5900	2150	-
16"	3750	6700	2950	Buttress
13 3/8"	3750	7600	3850	Buttress
9 5/8"	6950	9000	2050	Buttress
7 5/8"	3750	10800	7050	Extreme Line
5 1/2"	10150	14000	3850	Buttress

It was assumed an overlapping of 650 ft for each casing liner. The Extreme Line connection in the 7 5/8" casing is due to the small clearance between that string and the 9 5/8" casing.

Figure 7.2 shows the casing design for the dual density riser system. In this case, only five strings of casing were necessary, and the only one needing reaming is the 17 1/2" hole, assuming the use of a 16 3/4" BOP stack. Table 7.2 details the casing design. In this case, the 7" casing is set as a liner, also to cut down costs, with an overlapping section of 650 ft to anchor it on the 9 5/8" casing.

Table 7.2 - Dual Density Casing Design for the 3,750 ft Water Depth Case

Csg OD (in)	Mud Dens (ppg)	Gas Rate (SCF/min)	Bit Size (in)	Top (ft)	Shoe (ft)	Length (ft)	Connection
20"	-	-	26"	3750	5500	1750	-
13 3/8"	12.17	10323	17 1/2"	3750	6800	3050	Buttress
9 5/8"	13.55	9681	12 1/4"	3750	8150	4400	Buttress
7"	15.57	10809	8 1/2"	7500	14000	6500	Buttress

Figure 7.3 presents the gas-mud mixture and the nitrogen pressure profiles for the 3,750 ft riser simulation, taking the 8 1/2" hole as input. This is the part of the well that requires the biggest gas rate to achieve sea water density at the BOP level.

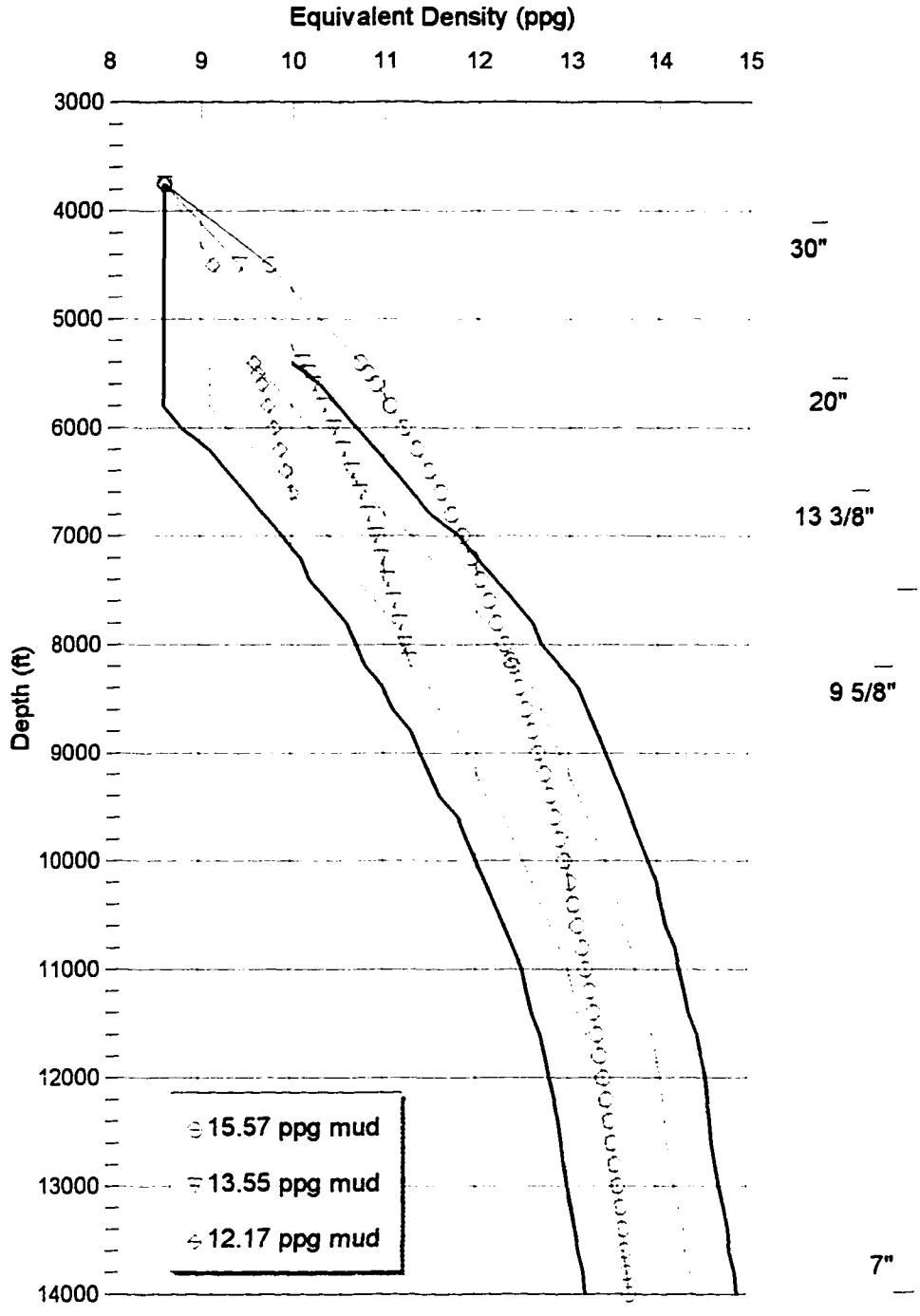

Figure 7.2 - Dual Density Casing Design for 3,750 ft Case

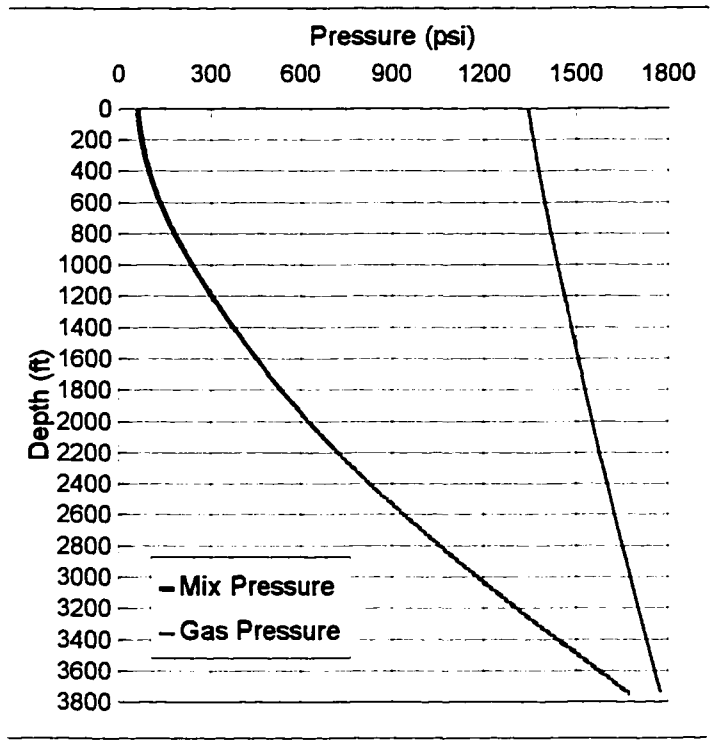

Figure 7.3 - Gas and Mixture Pressure Distribution for 3,750 ft Water Depth Simulation (8 1/2" hole)

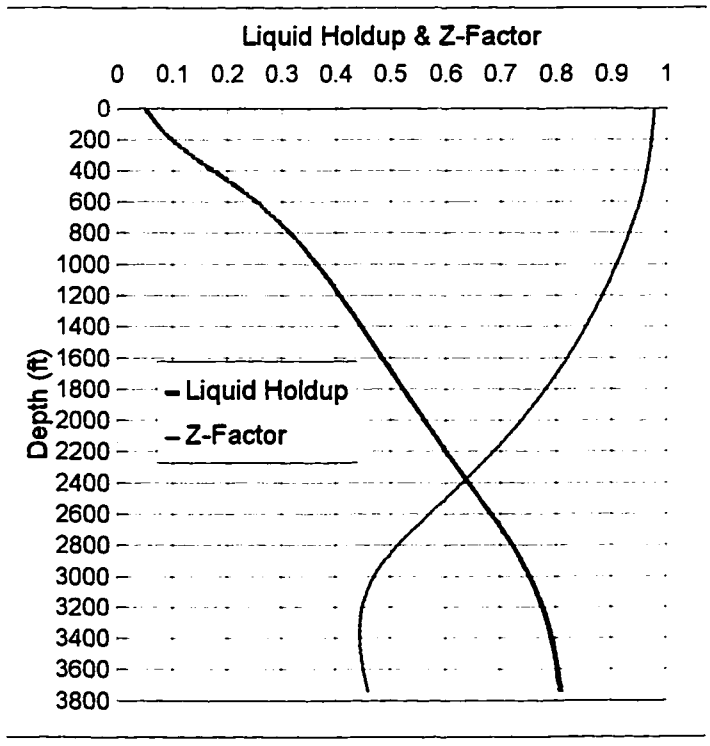

Figure 7.4 - Liquid Holdup and Gas Z-Factor for 3,750 ft Water Depth Simulation (8 1/2" hole)

To simulate a pressure drop across an injection valve at the bottom, a 100 psi pressure differential is introduced in the gas calculations.

Figure 7.4 shows the Liquid Holdup and the Gas Compressibility Factor (Z Factor) profiles for the same case. The Liquid Holdup varies from around 0.85, at the bottom, down to 0.12, at the top of the riser, maintaining a linear behavior from approximately 2800 ft up to 600 ft.

Figure 7.5 presents the Mixture Velocity and the Gas Velocity profiles for the 8 1/2" hole. The curves have similar behavior.

Figure 7.6 shows the Slip and Liquid Velocity profiles for the same case, with a linear increase on the Slip Velocity.

Figure 7.7 depicts the profiles for the Gas and Mixture Densities. It can be seen that the Mixture profile follows closely the one for the Liquid Holdup, also showing a linear section.

Figure 7.8 presents the Gas Viscosity and the Annular Friction Loss profiles. The former is read from the secondary axis on the bottom of the chart, while the latter is scaled according to the axis on the top. The behavior of the Annular Friction curve between the riser top and 300 ft is due to a discontinuity in the Beggs and Brill model that, when the value for $Y = \lambda_L/(H_L)^2$ is among 1.0 and 1.2, the ratio of the two-phase to no-slip friction factor is calculated with a separate function. In this case, Y becomes smaller than 1.0 after around 300 ft.

7.3 - GAS VOLUMES FOR SHALLOW-DEEP WATERS

To examine the costs due to the generation and injection of the nitrogen necessary to drill the simulation scenarios, some assumptions were made.

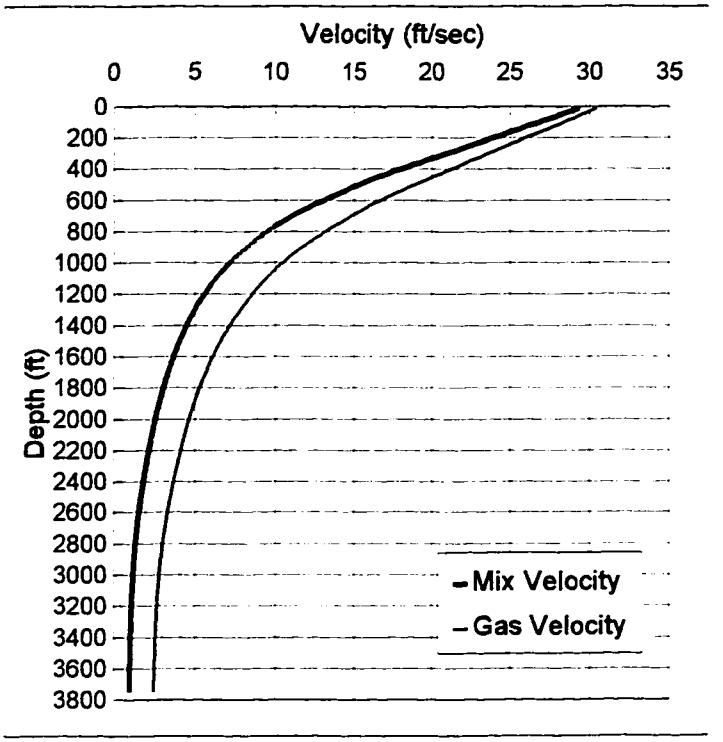

Figure 7.5 - Gas and Mixture Velocities for 3,750 ft Water Depth Simulation (8 1/2" hole)

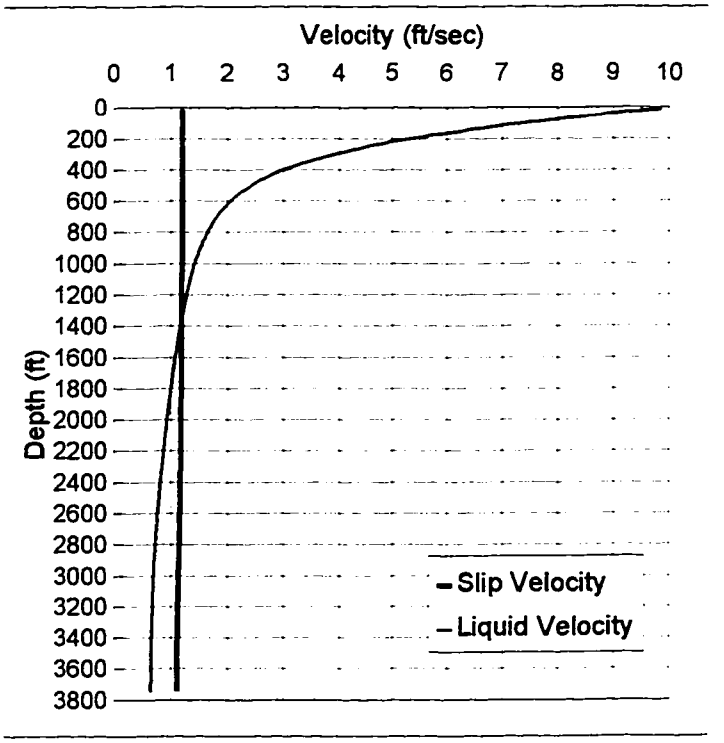

Figure 7.6 - Slip and Liquid Velocity profiles for 3,750 ft Water Depth Simulation (8 1/2" hole)

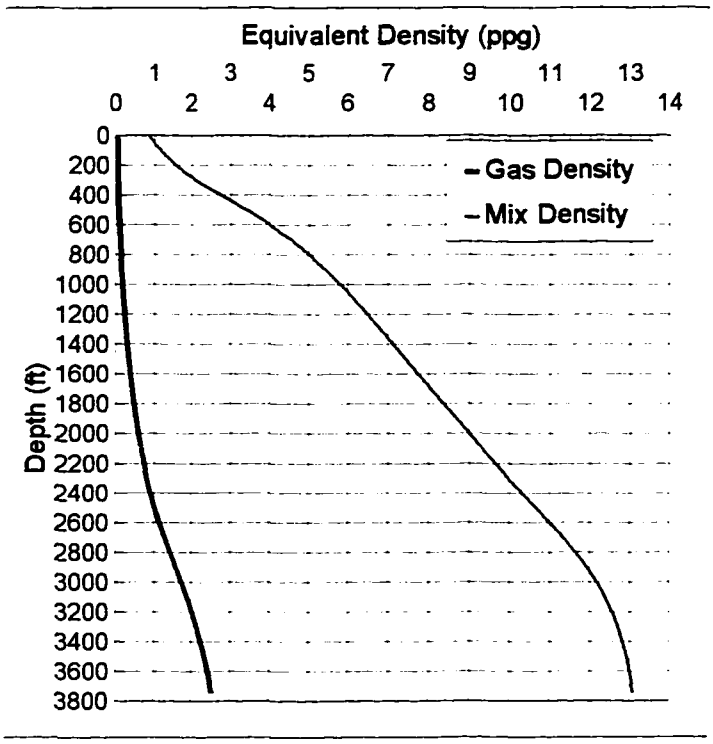

Figure 7.7 - Gas and Mixture Densities for 3,750 ft Water Depth Simulation (8 1/2" hole)

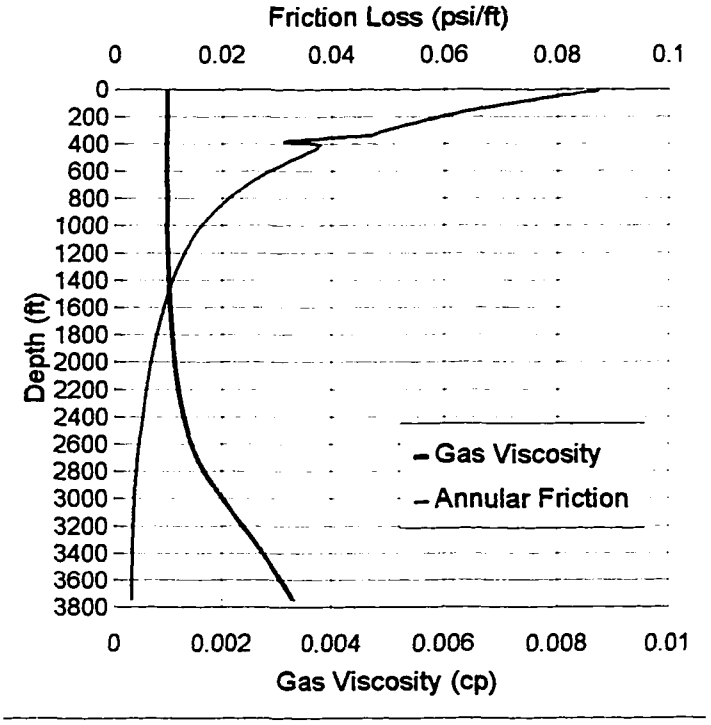

Figure 7.8 - Gas Viscosity and Annular Friction Loss for 3,750 ft Water Depth Simulation (8 1/2" hole)

Table 7.3 - Simulation Assumptions and Gas Volumes for the 3,750 ft Case

Hole (in)	MW (ppg)	Rate (gpm)	Top Pres (psi)	Gas Rate (SCF/min)	Time (days)	Circulating (%)	Gas Vol. (MMCF)
17.5	12.17	900	100	10322.72	10	40	59.4589
12.25	13.55	500	70	9680.78	10	50	69.7016
8.5	15.57	350	60	10808.56	15	60	140.079
						Total	269.239

Table 7.3 presents these assumptions and the corresponding result of the simulator runs.

The first assumption is about the values for the mud rates used to drill the different hole sizes. A full investigation on the cuttings removal capacity of the dual density system was not in the scope of this study. It was assumed mud rates equivalent to the average ones used in conventional drilling.

Small amounts of top pressure increase dramatically the necessary gas injection rate. Thus, the back pressure values under these two-phase flow rates were based on the assumption that the choke would be designed as to allow for low values.

The amount of time needed to drill each hole section is based on personal experience in deep waters in Brazil and on contacts with Petrobras representatives. The same applies to the amount of circulation time needed to achieve the casing depth of each of those sections. They represent educated estimates, at best, being used since no such data were available for the Gulf of Mexico. On the other hand, because of the smaller bottom hole pressures the rates of penetration should be greater in the new system, and drilling times smaller. So, those estimates, which are based on data from conventionally drilled wells, are probably conservative. The riser for this water depth was chosen as an 18 5/8" with a 5/8" wall thickness, and an internal diameter of 17.375".

7.4 - NITROGEN GENERATION AND COMPRESSION

The cost difference between conventional and dual density riser systems will be derived from the cost of the nitrogen itself and the cost of boosting the gas pressure to working values.

Two approaches can be readily devised: onsite generation or cryogenic injection. The first option involves the gas production onsite, and the use of compressors.

The other option is to acquire it in liquid form, store the gas onboard, and heat it up before injection.

The cryogenic injection option is attractive because of its flexibility: the gas has enough energy stored in it that no pressure boost is needed. It can also span a wide range of pressures and injection rates. The final gas pressure depends on the amount of heat transferred to the liquid nitrogen and the injection rate depends on the transfer pump capacity. On the downside there are the transportation and storage costs, along with the fact that the gas can not be economically recycled.

The onsite generation option leads to the use of large compressors, and to the use of nitrogen producing units (NPU's). The lack of pressure and flow rate flexibility will probably force designers to dimension these units for worst case scenarios. This could raise up the installation and operational costs. In the case of NPU's, although they are skid mounted and can be added as needed, the onboard space required for their use has to be allocated in the system's design phase.

7.5 - COMPRESSOR POWER FOR SHALLOW-DEEP WATERS

The type of compressor chosen for this study is the low speed (300 - 450 rpm) large integral reciprocating compressor, since it presents excellent reliability and

adaptability to change of conditions and low maintenance (Littlefield, 1982). In the designing phase the number of stages for a given compressor is dependent on the maximum compression rate. At ratios above 4 1/2 to 1, heat builds up in the gas due to molecules bumping together, and gas temperatures could exceed 300 °F (Shafer, 1993). To reduce the gas temperature in the cylinders, intercooler units can be added, which increases the compressor's efficiency.

Table 7.4 shows the initial pressures required to start the riser unloading for the different hole sizes considered, along with the respective gas rates needed.

For a single riser injection point, when the riser has only mud with densities specified in table 7.4, the unloading pressure is the initial gas injection pressure. The unloading process against a riser full of high density mud is an extreme supposition in the

Table 7.4 - Unloading and Steady-State Pressures for the 3,750 ft Riser Case

Hole (in)	Mud Weight (ppg)	Unloading Pressure (psi)	Steady-State Pressure (psi)	Gas Rate (SCF/min)
17 1/2	12.17	2044	1344	10323
12 1/4	13.55	2277	1344	9681
8 1/2	15.57	2605	1344	10809

dual density system, because this would overload the casing designed for lower hydrostatic pressures. As was pointed out in the previous chapter, unloading operations should start against a sea water column, or a mud column of equivalent pressure at the bottom of the riser. Thus, the compressor was dimensioned based on the steady-state pressure and the largest gas rate.

Table 7.5 shows the calculations for the compressor horsepower needed for the Shallow-Deep case. These calculations were done according to the method suggested by the Gas Processors Suppliers Association (GPSA, p. 13-6, 1987).

Table 7.5 - Compressor Power Requirements for the 3,750 ft Riser Case with No Intercooler

Intake (psig)	Discharge (psig)	Ratio	Stages	r	Ratio/ Stage	k	Spc. Power (Bhp/MMcf)	Gas Rate (SCF/min)
150	1344	8.960	3	2.08	2.1	1.18	40.5	10809

Stage	Tintk (F)	Pintk (psig)	Zintk	Tdisch (F)	Pdisch (psig)	Zdisch	Zavg	Spc. Pwr (Bhp/MMcf)
1	100	150	0.9559	112	315	0.916	0.93616	41.5
2	112	310	0.9177	125	651	0.842	0.87977	39.0
3	125	646	0.8430	139	1357	0.724	0.78341	34.8
							Sum	115.3
							Total Bhp	1795

In this table the subscripts "intk" and "disch" refer to the temperatures, pressures, and gas compressibility factors for the intake and discharge, respectively.

Table 7.6 presents the same calculations for the case where an intercooler system maintains the intake temperature of each stage near the initial one. As it can be seen from the two tables, there is a decrease of the total amount of horsepower needed when the intercooler system is added.

Table 7.6 - Compressor Power Requirements for the 3,750 ft Riser Case with Intercooler

Intake (psig)	Discharge (psig)	Ratio	Stages	r	Ratio/ Stage	k	Spc. Pwr (hp/MMcf)	Gas Rate (SCF/min)
150	1344	8.960	3	2.08	2.1	1.18	40.5	10809

Stage	Tintk (F)	Pintk (psig)	Zintk	Tdisch (F)	Pdisch (psig)	Zdisch	Zavg	Spc. Pwr (Bhp/MMcf)
1	100	150	0.9559	100	315	0.910	0.93310	41.4
2	100	310	0.9117	100	651	0.814	0.86268	38.3
3	100	646	0.8151	100	1357	0.635	0.72529	32.2
							Sum	111.9
							Total Bhp	1741

7.6 - CASING AND RIG COSTS FOR SHALLOW-DEEP WATERS

Table 7.7 presents the casing cost for the 3,750 ft riser case, drilled with conventional techniques (Mannesman Corporation).

Table 7.7 - Conventional Technique Casing Cost for the 3,750 ft Riser Case

Casing OD (in)	Length (ft)	Unit Cost ($/ft)	Cost ($)
20"	2150	64.00	$137,000.00
16"	2950	40.00	$118,000.00
13 3/8"	3850	20.50	$79,000.00
9 5/8"	2050	20.00	$41,000.00
7 5/8"	7050	21.00	$141,000.00
5 1/2"	3850	9.00	$81,000.00
		Total	$597,000.00

Table 7.8 shows similar data for the dual density system. The casing design for the conventional case includes the use of special couplings, such as Extreme Line, due to small clearance between some of the casing strings, with subsequent increase in casing cost.

Table 7.8 - Dual Density Casing Cost for the 3,750 ft Riser Case

Casing OD (in)	Length (ft)	Unit Cost ($/ft)	Cost ($)
20"	1750	64.00	$112,000.00
13 3/8"	3050	20.50	$63,000.00
9 5/8"	4400	15.00	$66,000.00
7"	6500	11.00	$71,000.00
		Total	$312,000.00

Table 7.9 presents the rig cost due to the time involved in under-reaming each phase of the well, and in running the casing. Hole cleaning and preparations for casing are included in the latter. The times were attributed from personal experience in such operations, since no data was available for this study. These values may be under-

Table 7.9 - Rig Time Cost for Conventional Drilling in 3,750 ft Waters

Day Rate	100,000	$/day		
OD	Operation Time (days)			
(in)	Run	Ream	BOP	Totals
20"	1.0	1.0	0.5	2.5
16"	1.0	1.0	0.5	2.5
13 3/8"	1.0	1.0	0.5	2.5
9 5/8"	1.0	0.0	0.5	1.5
7 5/8"	1.0	2.0	0.5	3.5
5 1/2"	1.0	2.0	0.5	3.5
Totals	6.0	7.0	3.0	16.0
			Cost	$1,600,000.00

estimated, since under-reaming operations are notoriously troublesome, especially because of under-reamer cone loss. Under-reamer cones are weaker than bit cones by their design, and are difficult to recover once lost, which leads many times to the side-track of part of the well. Furthermore, under-reamers can not sustain high circulation rates, again due to their design restrictions. Thus, the under-reamer arms often become "balled up", when drilling soft formations, and can not enlarge the well properly. Some other problems include the inability to maintain constant hole caliper and body "wash-outs", due to the high pressure losses needed to extend the arms. These occurrences force the crew to repeat operations and to run caliper logs (which cost is not included on this study) to verify if it is safe to attempt a casing run.

The BOP time values refer to the need to test the BOP stack every time a new casing is run in the hole. These are average times based on personal experience and do not reflect the possibility of test failure, which generally involves the recovery of the Marine Riser Package for repairs. It worth noting that the more the BOP is tested, the

greater the chances are that it will fail a test, since the seals are getting wear during each test.

Table 7.10 presents the rig cost due to under-reaming and running casing for the dual density system. Again, the data is derived from personal experience, although there is no available information on penetration rates for such an untried system. Since the bottom hole pressure is smaller, in the dual density system the penetration rates should be higher.

Table 7.10 - Rig Time Cost for the Dual Density in 3,750 ft Waters

Day Rate	100,000	$/day		
OD	Operation Time (days)			
(in)	Run	Ream	BOP	Totals
20"	1.0	1.0	0.5	2.5
13 3/8"	1.5	0.0	0.5	2.0
9 5/8"	1.5	0.0	0.5	2.0
7"	1.0	0.0	0.5	1.5
Totals	5.0	1.0	2.0	8.0
			Cost	$800,000.00

7.7 - CRYOGENIC VOLUMES FOR SHALLOW-DEEP WATERS

Table 7.11 shows the values for the liquid nitrogen needed in case the cryogenic injection option is taken. A liquid nitrogen density of 6.738 ppg was assumed in the calculations, along with a 93.11 scf/gal vapor to liquid ratio at 1 atmosphere and -320 °F.

Table 7.11 - Nitrogen Vapor and Liquid Volumes for the 3,750 ft Riser Case

Vapor				Liquid			
Total Time (days)	Total Vol (MCF)	Vol/day (MCF)	3 day Vol (MCF)	Total Vol (gal)	Vol/day (gal)	3 day Vol (gal)	Weight (tons)
35	269239.4	7692.555	23077.66	2891627	82618	247854	835.1

In these calculations it was assumed that a liquid volume sufficient for three days of work should be stored onboard. The last column of Table 7.7 shows how much liquid weight would be added to the rig in that case, without considering the tank weight.

7.8 - OPERATIONAL COSTS FOR SHALLOW-DEEP WATERS

Table 7.12 presents the estimated operational costs when using compressors and cryogenic pumps for the 3,750 ft riser case, along with the required power for each application. These costs were calculated based on a diesel engine efficiency of 23.4 % (Bourgoyne, p. 7, 1991) and a fuel cost of $1.50/gal. The information about the cryogenic pump was obtained through personal contact with L&S Cryogenics Corp.

Table 7.12 - Operational Costs for the 3,750 ft Riser Case

	Compressor		Cryogenic Pump
	No Intercooler	With Intercooler	
Power (Bhp)	1795	1741	500
Operational Cost	$92,000.00	$89,000.00	$26,000.00

The data on the compressor refer to a 3-staged compressor, low speed, reciprocating, large integral type.

7.9 - COST COMPARISON FOR SHALLOW-DEEP WATERS

Table 7.13 summarizes the costs for the conventional method and for the dual density system options: on-site nitrogen generation and cryogenic injection. It shows that the overall savings of the dual density system over the conventional technique are around $838,500.00 for the on-site generation option and $336,000.00 for the cryogenic injection.

As pointed out before, these values were obtained having in mind a rig day rate of $ 100,000.00 per day.

Table 7.13 - Dual Density Savings over the Conventional Method for the 3,750 ft Riser Case

	Dual Density		Conventional
Costs	On Site Option	Cryogenic Option	
Casing	$312,000.00	$312,000.00	$597,000.00
Rig	$800,000.00	$800,000.00	$1,600,000.00
Compressors	$89,000.00		
NPU's	$157,500.00		
Pumps		$26,000.00	
Nitrogen		$723,000.00	
Totals	$1,358,500.00	$1,861,000.00	$2,197,000.00
Savings	$838,500.00	$336,000.00	

These are current values for new deep water contracts (Petrobras, personal communication). Values as high as $ 182,000.00 per day are also cited in the literature (Offshore Magazine, February 1997). Figure 7.9 shows the behavior of the dual density system savings against the conventional method for different rig day rates. If all the considered costs were fixed for this case, the on-site option would be economically

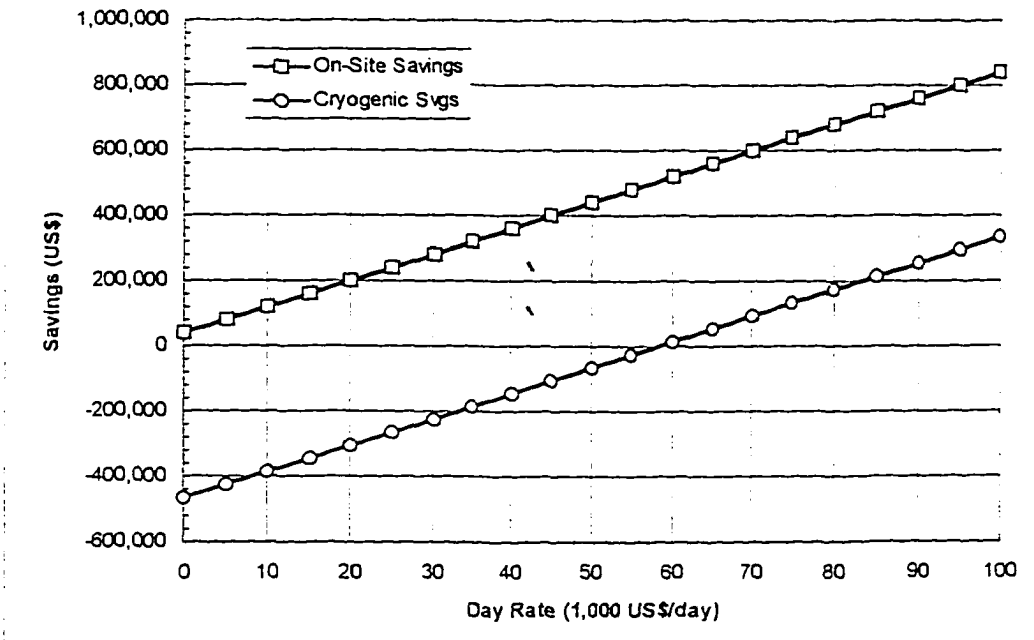

Figure 7.9 - Dual Density Savings vs. Rig Day Rate for the 3,750 ft Riser Case

better than the conventional technique even for a zero valued day rate. The cryogenic option would be feasible only for day rates greater than $ 60,000.00 per day.

7.10 - MEDIUM-DEEP WATERS

Figure 7.10 shows the casing design, pore pressure and fracture gradients for a hypothetical well drilled with conventional technology in the Gulf of Mexico. The pressure data has being extrapolated from the previous case to a water depth of 7,500 ft according to procedure described in Appendix A.

As can be seen from the chart, the interval between the values for the trip margin and the kill margin is narrower than in the case for the 3,750 ft riser. The small difference between the pore pressure and the fracture gradient reduced the range between the safety margins. A 0.35 ppg tolerance was adopted, instead of the usual 0.5 ppg, to obtain a workable casing design.

The casing design calls for nine strings, with the need to under-ream the 26", the 20", the 17 1/2", the 15", the 12 1/4", the 9 7/8", the 7 7/8", and the 6" sections of the well. These diameters are too big to get through the 16 3/4" BOP stack, the 20", the 16", the 13 3/8", the 11 3/4", the 9 5/8", the 7 5/8", and the 5 1/2" casings, respectively. Thus, a total of 8 sections would be slated for under-reaming.

The 11 3/4", 7 5/8" and the 4 1/2" casings are designed to be liners, to reduce the costs. Table 7.14 presents the casing design for the conventional method. As in the first case, it was also assumed an overlapping of 650 ft for each casing liner.

Table 7.15 details the dual density system's casing design for the medium-deep water case.

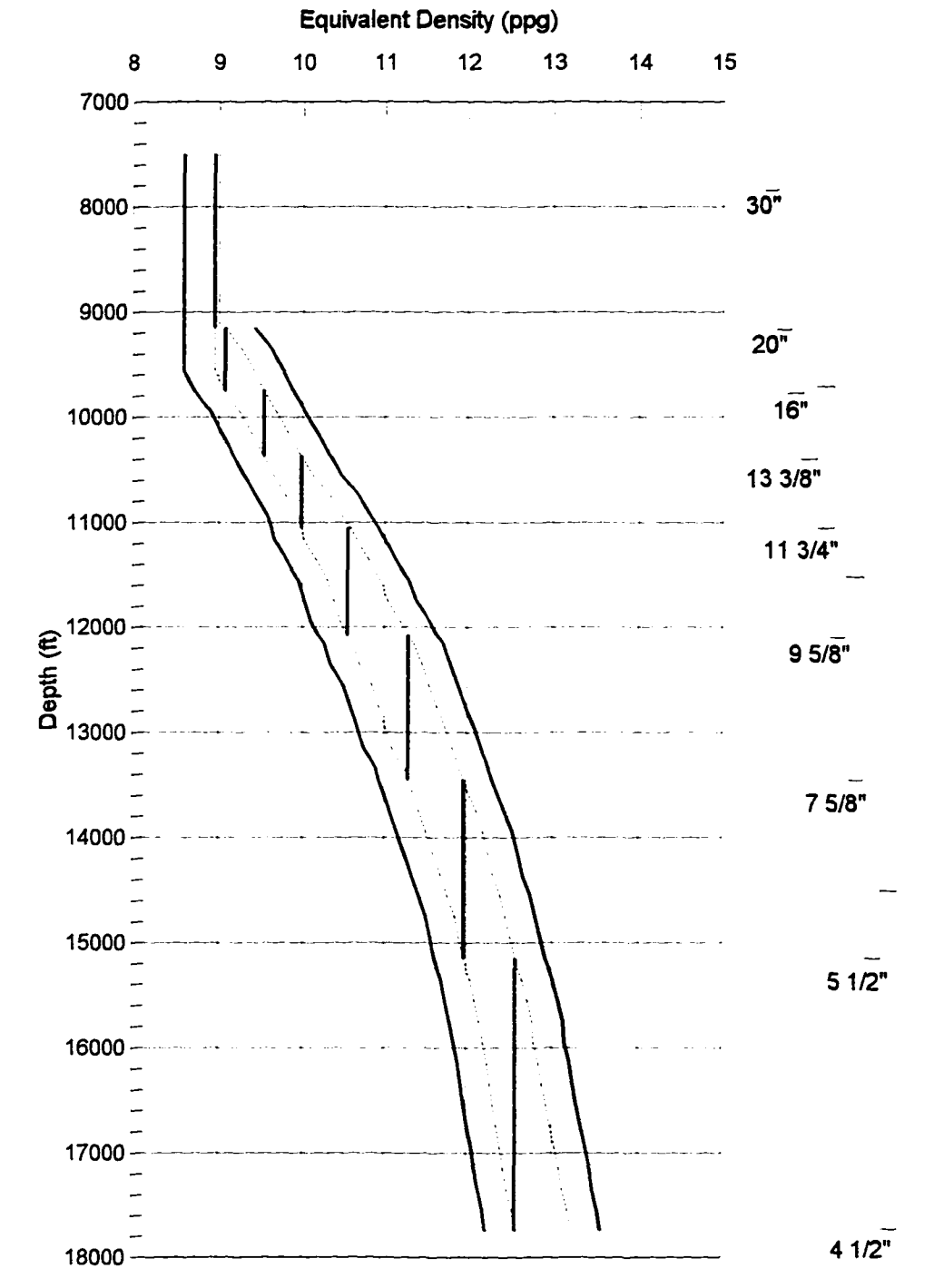

Figure 7.10 - Conventional Casing Design for the 7,500 ft Case

Table 7.14 - Conventional Casing Design for the 7,500 ft Riser Case

Casing OD (in)	Top (ft)	Shoe (ft)	Length (ft)	Connection
20"	7500	8810	1310	Buttress
16"	7500	9750	2250	Buttress
13 3/8"	7500	10350	2850	Buttress
11 3/4"	9700	11150	1450	Extreme Line
9 5/8"	7500	12150	4650	Extreme Line
7 5/8"	11500	13550	2050	Extreme Line
5 1/2"	7500	15150	7650	Buttress
4 1/2"	14500	17750	3250	Extreme Line

The 9 5/8" and for the 7" casings differ by only 50 ft, although the trip and kill margins are closer than in the shallow-deep water case. Moreover, the 20" and the 13 3/8" casing lengths differ by 100 ft and 200 ft, respectively.

Table 7.15 - Dual Density Casing Design for the 7,500 ft Riser Case

Casing OD (in)	Mud Dens (ppg)	Gas Rate (SCF/min)	Top (ft)	Shoe (ft)	Length (ft)	Connection
20"	10.37	-	7500	9350	1850	-
13 3/8"	11.96	10323	7500	10350	2850	Buttress
9 5/8"	13.59	9681	7500	11950	4450	Buttress
7"	15.49	10809	11300	17750	6450	Buttress

Figure 7.11 shows the casing design, pore pressure and fracture gradients for the medium-deep water case using the dual density system.

Figure 7.12 presents the mixture and gas pressure profiles obtained by the simulation for the 7,500 ft riser case. They have similar shapes as the ones for the previous case.

Figure 7.13 depicts the behavior of the Liquid Holdup and the Gas Compressibility Factor for the present case. The Z-Factor reaches a low value of 0.45629 at 4537.5 ft and then increases again, towards the riser bottom.

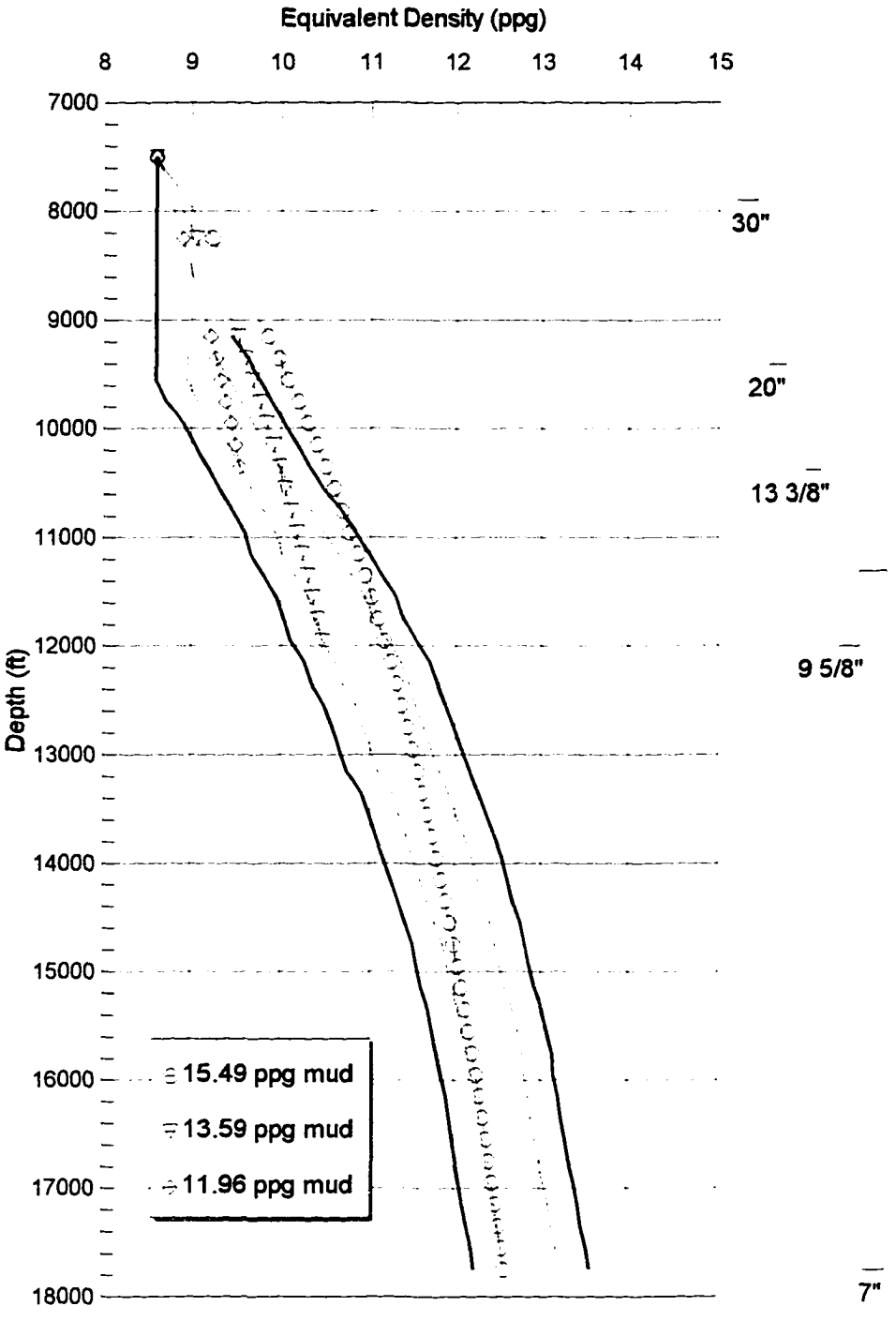

Figure 7.11 - Dual Density Casing Design for the 7,500 ft Case

Figure 7.14 presents the profiles for the Mixture and Gas Velocities, while Figure 7.15 shows the Slip Velocity and the Liquid Velocity for the case of a 7,500 ft riser.

The simulated Gas and Mixture Densities can be seen in Figure 7.16. They both show the tendency to stabilize around the values of 3.2 ppg for the gas and 12.8 ppg for the mixture, close to the bottom.

Figure 7.17 shows the behavior of the Mixture Friction Loss, with values in the top axis, and the profile for the Gas Viscosity for the 7,500 ft riser case. The latter has its values read from the bottom axis.

7.11 - GAS VOLUMES FOR MEDIUM-DEEP WATERS

Table 7.16 presents the assumptions made for the dual density drilling parameters needed to evaluate the costs for the 7,500 ft riser case. The riser OD is still 18 5/8" with

Table 7.16 - Simulation Assumptions and Gas Volumes for the 7,500 ft Riser Case

Hole (in)	MW (ppg)	Rate (gpm)	Top Pres (psi)	Gas Rate (SCF/min)	Time (days)	Circulating (%)	Gas Vol. (MMCF)
17.5	11.96	900	100	15542	10	40	89.5258
12.25	13.59	500	70	14857	10	50	106.976
8.5	15.49	350	60	16548	15	60	214.467
						Total	410.968

a 7/8" wall thickness and 17.125" riser ID. These dimensions were chosen based on the expected critical collapse water depth (Erb, 1983), so for these diameters the riser would not collapse in water depths up to 11,500 ft.

The mud weights are slightly less than in the first case, but the other assumptions remain the same. The hole diameters are identical and the casing set points are designed for approximately the same depths. The choke pressures, are the same because the mud pump rates are maintained. The gas injection volumes are much greater due to the increased riser annular volume.

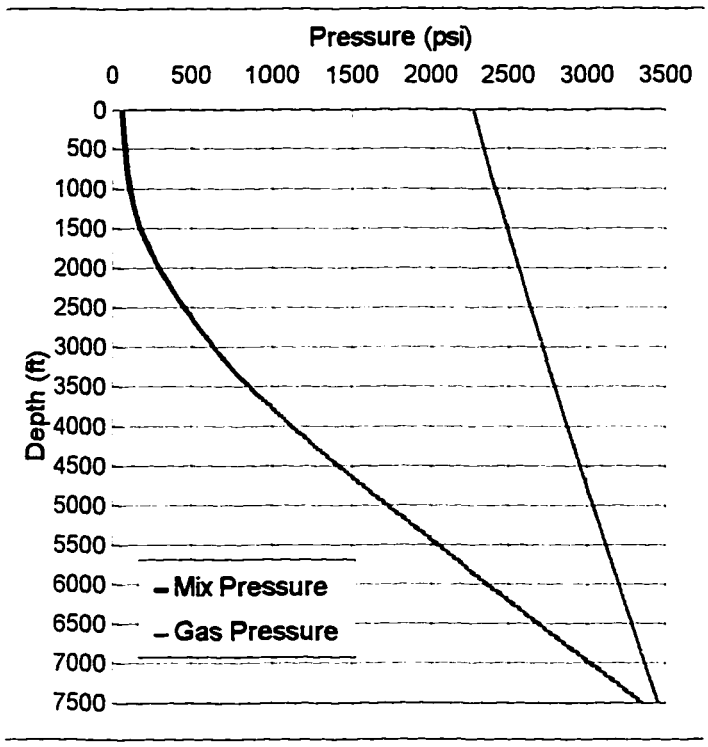

Figure 7.12 - Gas and Mixture Pressure Distribution for 7,500 ft Water Depth Simulation (8 1/2" hole)

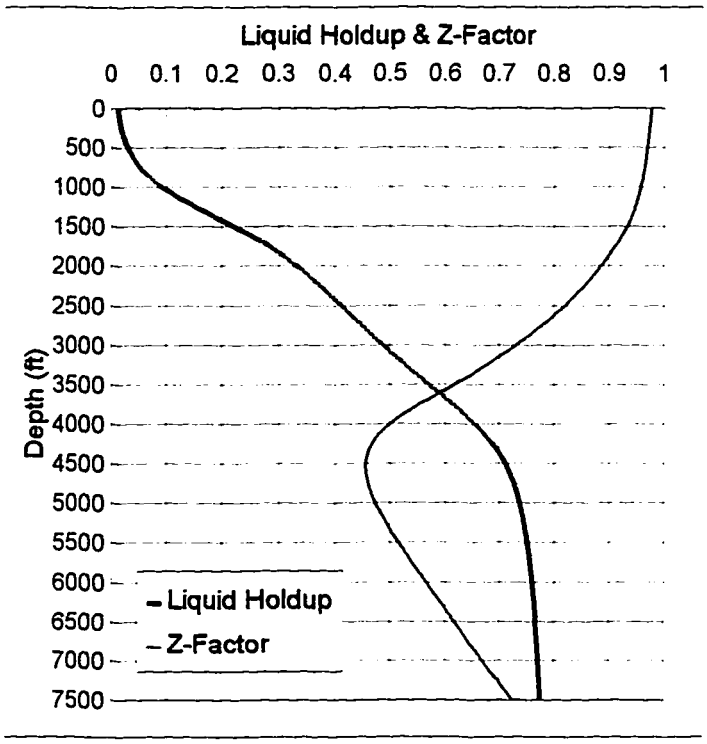

Figure 7.13 - Liquid Holdup and Gas Z-Factor for 7,500 ft Water Depth Simulation (8 1/2" hole)

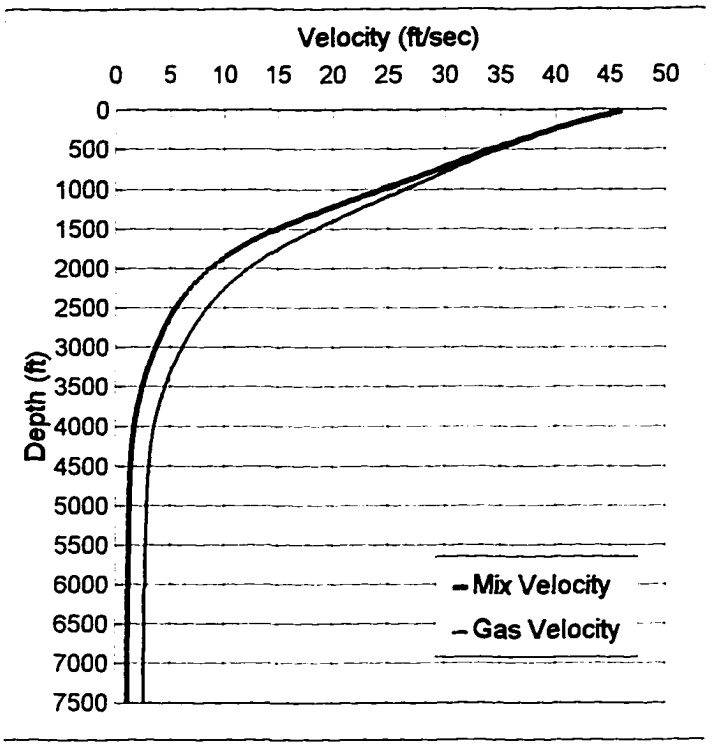

Figure 7.14 - Gas and Mixture Velocities for 7,500 ft Water Depth Simulation (8 1/2" hole)

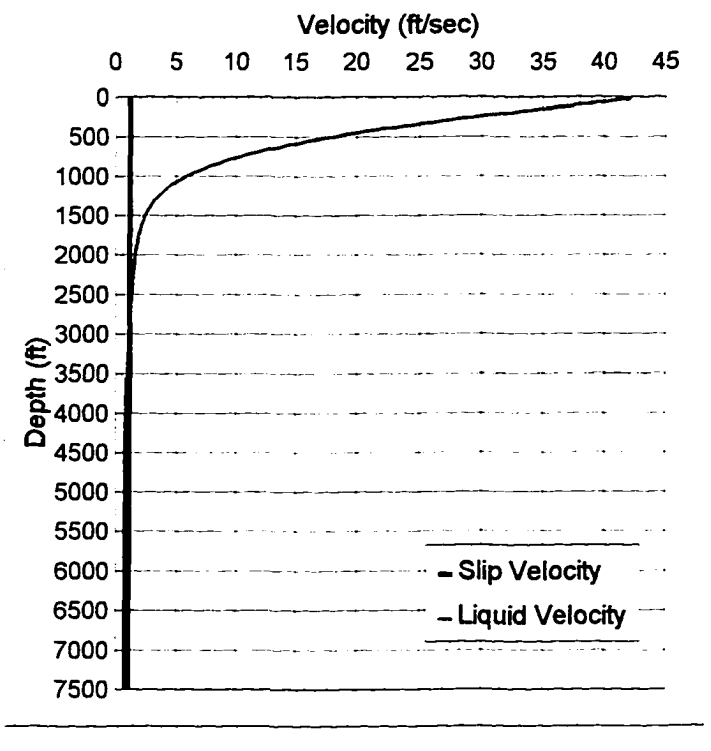

Figure 7.15 - Slip and Liquid Velocity profiles for 7,500 ft Water Depth Simulation (8 1/2" hole)

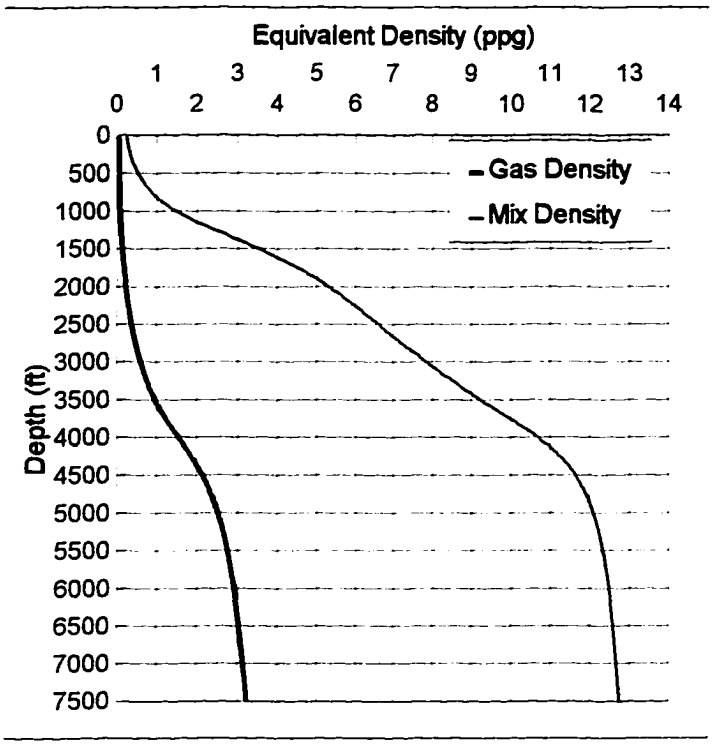

Figure 7.16 - Gas and Mixture Densities for 7,500 ft Water Depth Simulation (8 1/2" hole)

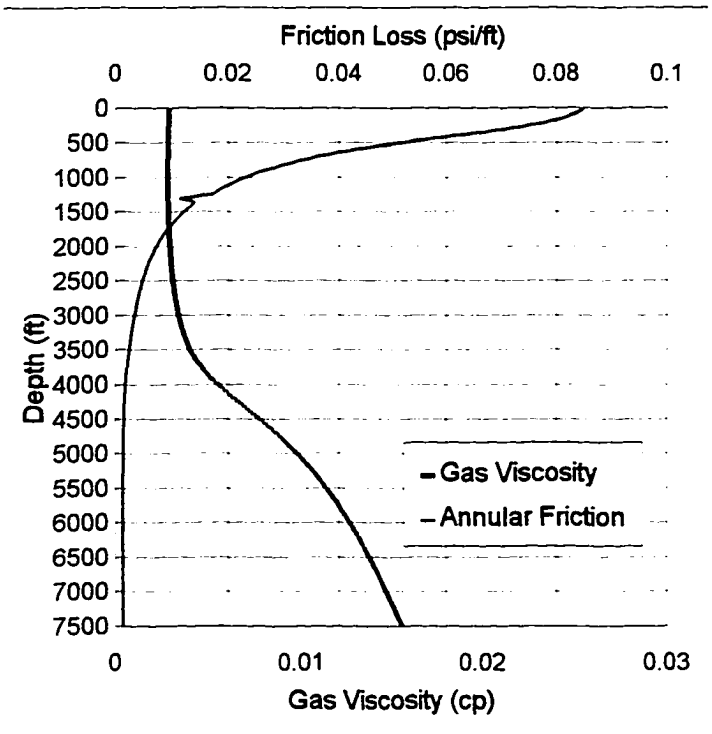

Figure 7.17 - Gas Viscosity and Annular Friction Loss for 7,500 ft Water Depth Simulation (8 1/2" hole)

7.12 - COMPRESSOR POWER FOR MEDIUM-DEEP WATERS

The steady-state gas injection pressure, at surface, for the case of a 7,500 ft riser is 2276 psig, according to the simulation run. This value, along with the highest gas injection rate, were considered as the compressor design loads for this case.

Table 7.17 tabulates the calculations for the compressor power, without any intercooler units, that would be necessary to drill the present well.

Table 7.17 - Compressor Power Requirements for the 7,500 ft Riser Case with No Intercooler

Intake (psig)	Discharge (psig)	Ratio	Stages	r	Ratio/ Stage	k	Spc. Pwr (hp/MMcf)	Gas Rate (SCF/min)
150	2276	15.173	3	2.48	2.495	1.18	52.5	16548

Stage	Tintk (F)	Pintk (psig)	Zintk	Tdisch (F)	Pdisch (psig)	Zdisch	Zavg	Spc. Pwr (Bhp/MMcf)
1	100	150	0.9559	114	374	0.903	0.92924	53.4
2	114	369	0.9039	131	921	0.787	0.84534	48.6
3	131	916	0.7879	149	2286	0.705	0.74625	42.9
							Sum	145.0
							Total Bhp	3455

Table 7.18 presents the same set of calculations for the case where intercooler units would be used.

Table 7.18 - Compressor Power Requirements for the 7,500 ft Riser Case with Intercooler

Intake (psig)	Discharge (psig)	Ratio	Stages	r	Ratio/ Stage	k	Spc. Pwr (hp/MMcf)	Gas Rate (SCF/min)
150	2276	15.173	3	2.48	2.5	1.18	52.5	10809

Stage	Tintk (F)	Pintk (psig)	Zintk	Tdisch (F)	Pdisch (psig)	Zdisch	Zavg	Spc. Pwr (Bhp/MMcf)
1	100	150	0.9559	100	375	0.893	0.92464	53.2
2	100	370	0.8948	100	925	0.735	0.81466	46.9
3	100	920	0.7359	100	2300	0.626	0.68105	39.2
							Sum	139.2
							Total Bhp	3318

7.13 - CASING AND RIG COSTS FOR MEDIUM-DEEP WATERS

Table 7.19 presents the casing cost for the 7,500 ft riser case, drilled with conventional techniques (Mannesman Corporation).

Table 7.19 - Conventional Method Casing Costs for the 7,500 ft Riser Case

Casing OD (in)	Length (ft)	Unit Cost ($/ft)	Cost ($)
20"	1310	64.00	$84,000.00
16"	2250	40.00	$90,000.00
13 3/8"	2850	20.50	$58,000.00
11 3/4"	1450	43.00	$62,000.00
9 5/8"	4650	25.00	$116,000.00
7 5/8"	2050	21.00	$43,000.00
5 1/2"	7650	9.00	$69,000.00
4 1/2"	3250	10.00	$32,000.00
		Total	$554,000.00

Table 7.20 tabulates the dual density system estimated casing cost for the 7.500 ft riser case.

Table 7.20 - Dual Density Casing Costs for the 7,500 ft Riser Case

Csg OD (in)	Length (ft)	Unit Cost ($/ft)	Cost ($)
20"	1850	64.00	$118,000.00
13 3/8"	2850	20.50	$59,000.00
9 5/8"	4450	15.00	$67,000.00
7"	6450	11.00	$71,000.00
		Total	$315,000.00

Table 7.21 presents the rig cost for the conventional drilling method due to the time involved in under-reaming each phase of the well, and in running the casing strings. The same assumptions made for the previous case were applied here, except for the rig day rate, which was estimated in US$ 120,000.00, due to the greater water depth capability required.

Table 7.21 - Conventional Drilling Rig Cost for the 7,500 ft Riser Case

Day Rate	120,000	$/day		
OD	Operation Time (days)			
(in)	Run	Ream	BOP	Totals
20"	1.0	1.0	0.5	2.5
16"	1.0	1.0	0.5	2.5
13 3/8"	1.0	1.0	0.5	2.5
11 3/4"	1.0	1.0	0.5	2.5
9 5/8"	1.0	2.0	0.5	3.5
7 5/8"	1.0	1.5	0.5	3.0
5 1/2"	1.0	3.0	0.5	4.5
4 1/2"	1.0	2.5	0.5	4.0
Totals	8.0	13.0	4.0	25.0
			Cost	$3,000,000.00

The rig cost for the same case with dual density technology is presented on Table 7.22.

Table 7.22 - Dual Density Rig Cost for the 7,500 ft Riser Case

Day Rate	120,000	$/day		
OD	Operation Time (days)			
(in)	Run	Ream	BOP	Totals
20"	1.0	1.0	0.5	2.5
13 3/8"	1.5	0.0	0.5	2.0
9 5/8"	1.5	0.0	0.5	2.0
7"	1.0	0.0	0.5	1.5
Totals	5.0	1.0	2.0	8.0
			Cost	$960,000.00

7.14 - CRYOGENIC VOLUMES FOR MEDIUM-DEEP WATERS

Table 7.23 shows the values for the liquid nitrogen needed in case the cryogenic injection option is taken for the 7,500 ft riser case. Also included are the volumes and liquid weight for 3 days of work.

Table 7.23 - Nitrogen Vapor and Liquid Volumes for the 7,500 ft Riser Case

Vapor				Liquid			
Total Time (days)	Total Vol (MCF)	Vol/day (MCF)	3 day Vol (MCF)	Total Vol (gal)	Vol/day (gal)	3 day Vol (gal)	Weight (tons)
35	410,968	11,741	35,225	4,413,793	126,108	378,325	1,274

7.15 - OPERATIONAL COSTS FOR MEDIUM-DEEP WATERS

Table 7.24 presents the estimated operational costs for the use of compressors and cryogenic pumps for the 7,500 ft riser case, along with the required power. Again, it was considered only the options for a 3 stage, reciprocal, low speed type of compressor, with and without intercooler units between the stages, and considering just the steady-state injection pressures needed.

Table 7.24 - Operational Costs for the 7,500 ft Riser Case

	Compressor		Cryogenic Pump
	No Intercooler	With Intercooler	
Power (Bhp)	3455	3318	750
Operational Cost	$177,000.00	$170,000.00	$39,000.00

7.16 - COST COMPARISON FOR MEDIUM-DEEP WATERS

Table 7.25 summarizes the costs for the conventional method and for the dual density options: on-site nitrogen generation and cryogenic injection.

Table 7.25 - Dual Density Savings over the Conventional Method for the 7,500 ft Riser Case

	Dual Density		Conventional
Costs	On Site Option	Cryogenic Option	
Casing	$315,000.00	$315,000.00	$554,000.00
Rig	$960,000.00	$960,000.00	$3,000,000.00
Compressors	$170,000.00		
NPU's	$220,500.00		
Pumps		$39,000.00	
Nitrogen		$1,103,000.00	
Totals	$1,665,000.00	$2,417,000.00	$3,554,000.00
Savings	$1,889,000.00	$1,137,000.00	

It tabulates an overall saving of US$1,889,000.00 for the On-site Nitrogen Generation option and an overall US$1,137,000.00 for the Cryogenic Injection savings.

If we vary the rig day rate, starting with the estimated value of US$ 120,000.00, the results obtained can be seen in Figure 7.18. The zero savings for the On-site Generation option happens for a rig day rate of approximately US$ 9,000.00.

The same happens to the Cryogenic Injection for a rig day rate of around US$ 52,000.00.

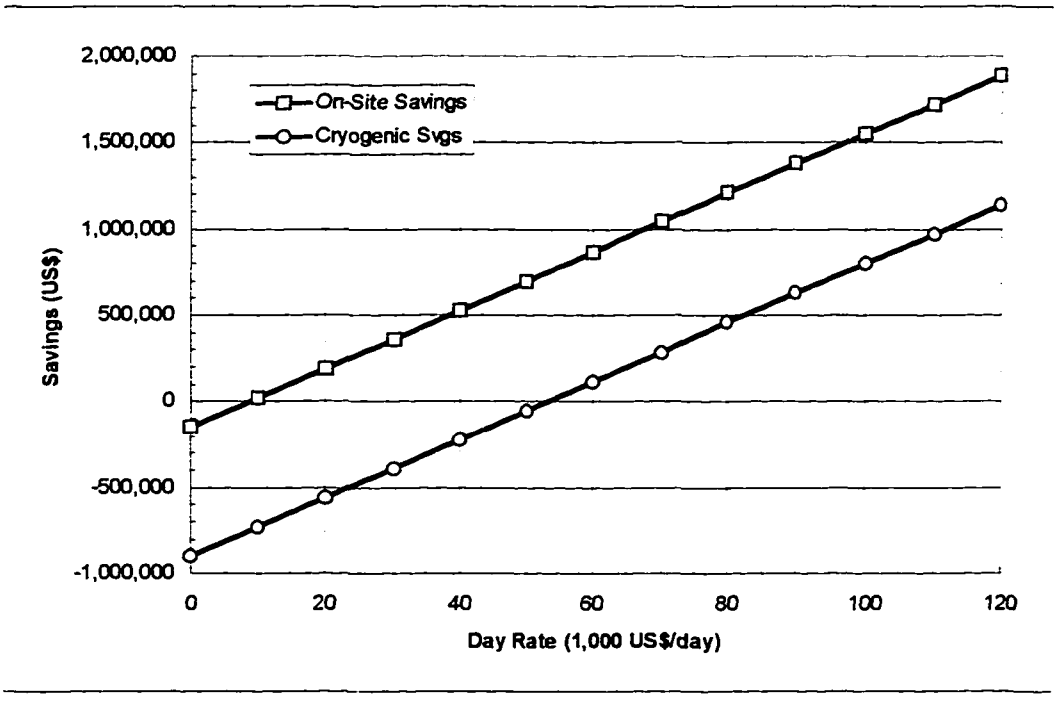

Figure 7.18 - Dual Density Savings vs. Rig Day Rate for the 7,500 ft Riser Case

7.17 - ULTRA-DEEP WATERS

Figure 7.19 shows the casing design and pressure gradients for a well drilled conventionally in the Gulf of Mexico in 10,000 ft waters. The pore pressure and fracture gradient were extrapolated from the 3,750 ft riser case. This was done following the procedure outlined in Appendix A.

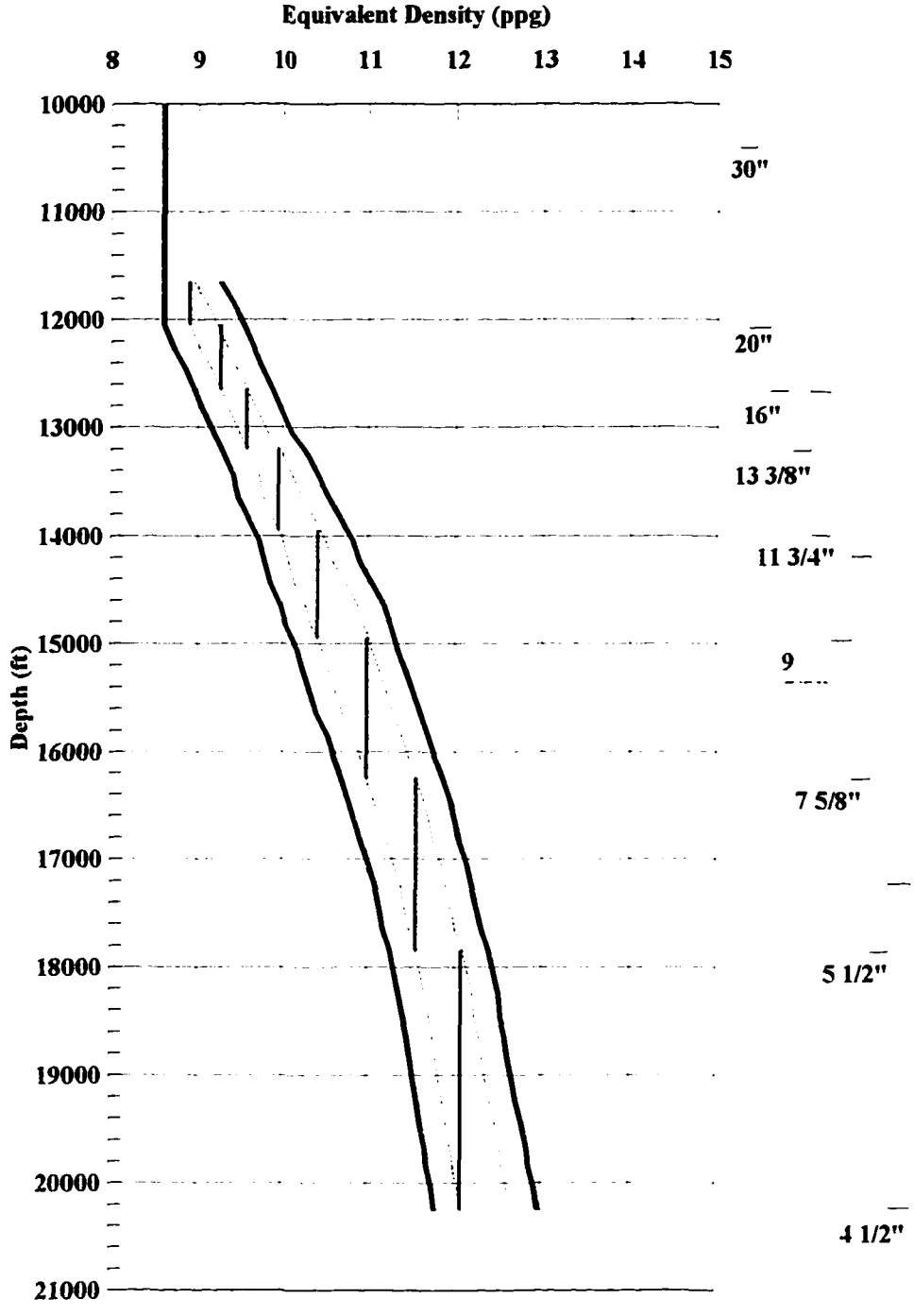

Figure 7.19 - Conventional Casing Design for 10,000 ft Case

For this case the trip and kill margins have tolerances of 0.30 ppg, instead of the usual 0.5 ppg, to obtain workable casing designs.

Table 7.26 tabulates the casing size, the top position, the shoe depth, the length, and the connections for each of the casing strings for this case.

Table 7.26 - Conventional Casing Design for the 10,000 ft Riser Case

Casing OD (in)	Top (ft)	Shoe (ft)	Length (ft)	Connection
20"	10000	12050	2050	Buttress
16"	10000	12650	2650	Buttress
13 3/8"	10000	13200	3200	Buttress
11 3/4"	12600	13950	1350	Extreme Line
9 5/8"	10000	14950	4950	Extreme Line
7 5/8"	14200	16250	2050	Extreme Line
5 1/2"	10000	17850	7850	Buttress
4 1/2"	17200	20250	3050	Extreme Line

The 11 3/4", 7 5/8" and the 4 1/2" casings are designed to be liners, to reduce costs. An overlapping of 650 ft is assumed, for anchoring each liner on the preceding casing string. Eight sections are marked for under-reaming.

Figure 7.20 shows the pore pressure and fracture gradients for the dual density system.

Table 7.27 shows the casing design for the dual density system for the ultra-deep water case. Besides the casing sizes, the top and shoe depths, casing lengths and respective connection types, the mud densities to be used and the nitrogen injection rates are included. Except for the 20" casing, which is 300 ft longer than the designed for the 3,750 ft riser case, the other casing strings are of same length, with the 9 5/8" being 50 ft longer.

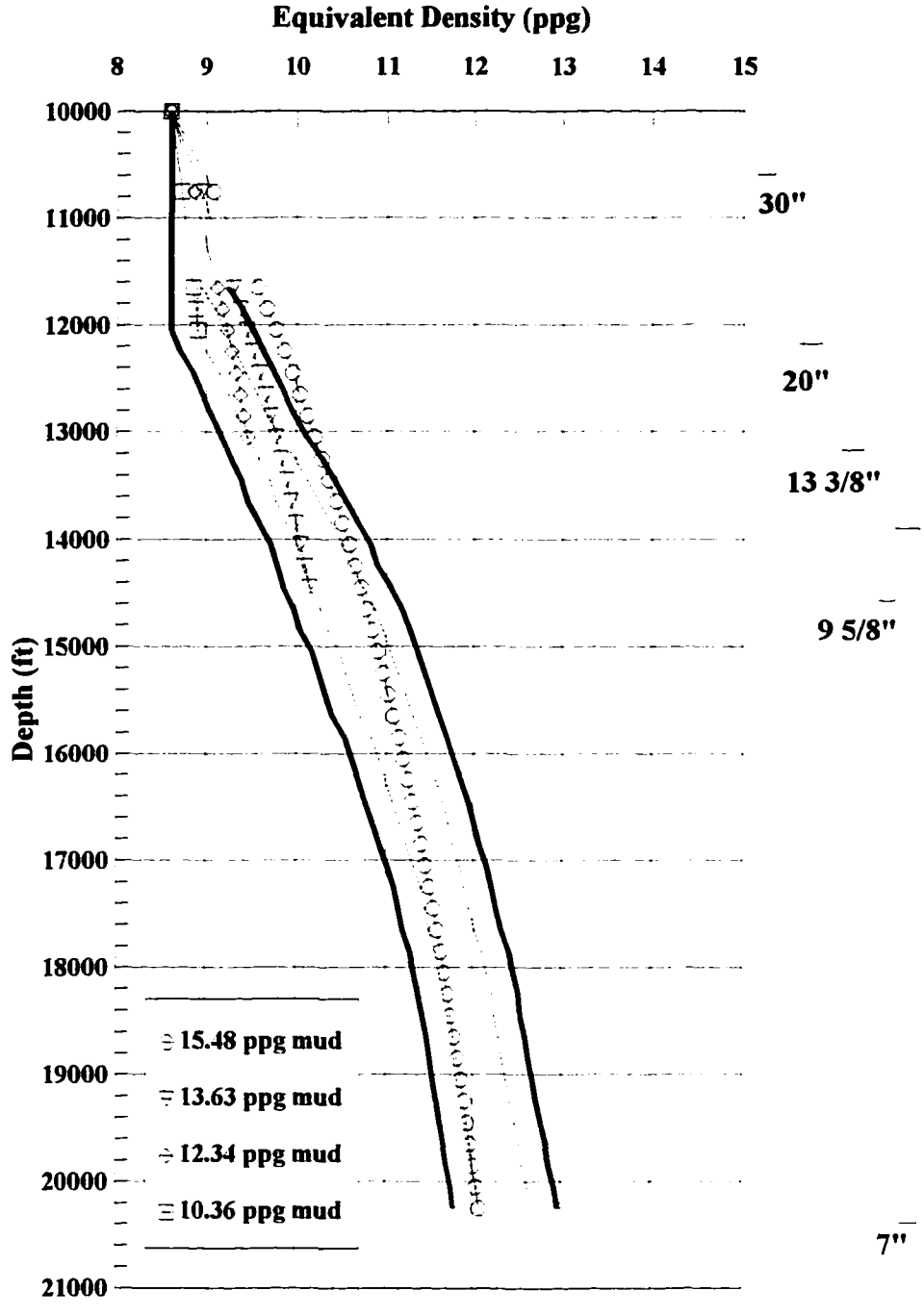

Figure 7.20 - Dual Density Casing Design for 10,000 ft Case

Table 7.27 - Dual Density Casing Design for the 10,000 ft Riser Case

Casing OD (in)	Mud Dens (ppg)	Gas Rate (SCF/min)	Top (ft)	Shoe (ft)	Length (ft)	Connection
20"	10.36	-	10000	12050	2050	-
13 3/8"	12.34	20633	10000	13050	3050	Buttress
9 5/8"	13.63	18243	10000	14450	4450	Buttress
7"	15.48	20449	13800	20250	6450	Buttress

Figure 7.21 presents the mixture and gas pressure profiles obtained by the simulation for the 10,000 ft riser case.

Figure 7.22 shows the behavior of the Liquid Holdup and the Gas Compressibility Factor for the present case.

Figure 7.23 presents the profiles for the Mixture and Gas Velocities. Figure 7.24 shows the Slip and the Liquid Velocity profiles for the case of a 10,000 ft riser.

The simulated Gas and Mixture Densities for this case can be seen in Figure 7.25. They show the tendency to stabilize around the values of 3.4 ppg for the gas and 12.5 ppg for the mixture, closer to the riser bottom.

Figure 7.26 shows the behavior of the Mixture Friction Loss, with values in the top axis, and the profile for the Gas Viscosity for the 10,000 ft riser case. The latter has its values read from the bottom axis.

7.18 - GAS VOLUMES FOR ULTRA-DEEP WATERS

Table 7.28 presents the assumptions made for the dual density drilling parameters needed to evaluate the costs for the 10,000 ft riser case. The riser OD is again 18 5/8", with wall thickness of 7/8" and an internal diameter of 17.125". The mud densities are slightly smaller than for the medium-deep case, but the pump rates were kept the same due to the identical casing design.

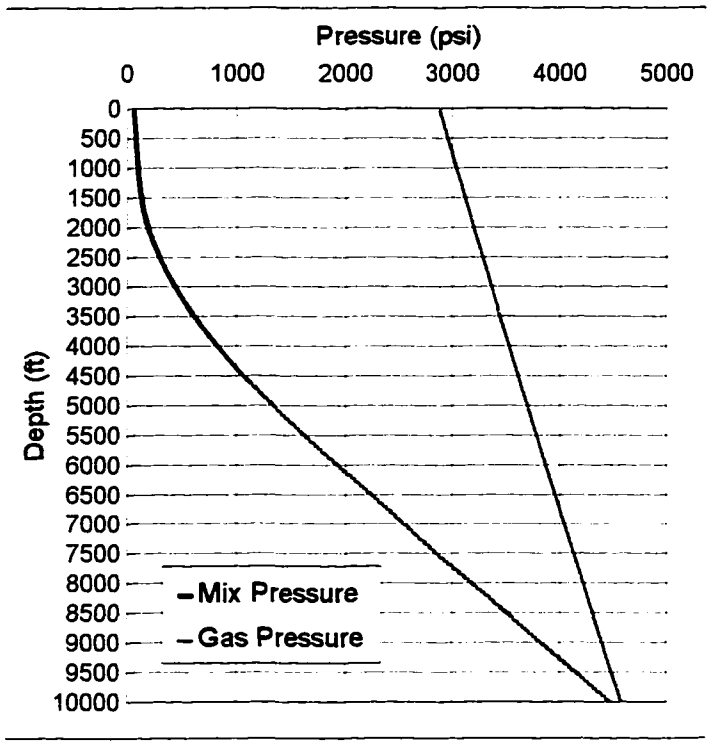

Figure 7.21 - Gas and Mixture Pressure Distribution for 10,000 ft Water Depth Simulation (8 1/2" hole)

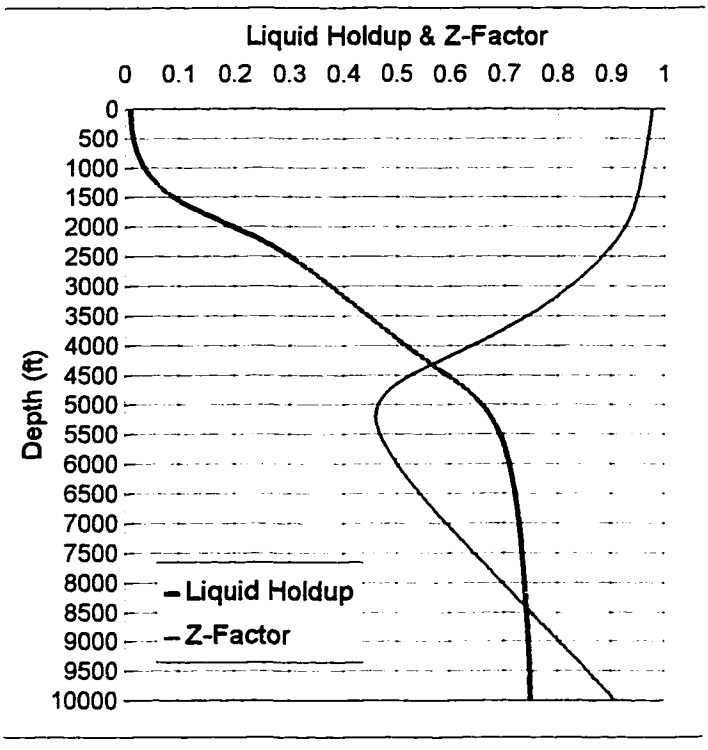

Figure 7.22 - Liquid Holdup and Gas Z-Factor for 10,000 ft Water Depth Simulation (8 1/2" hole)

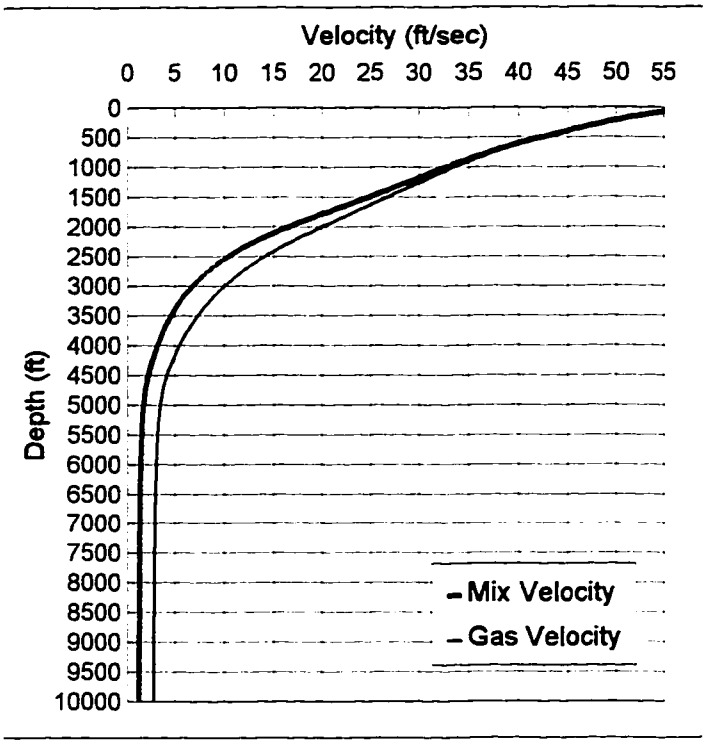

Figure 7.23 - Gas and Mixture Velocities for 10,000 ft Water Depth Simulation (8 1/2" hole)

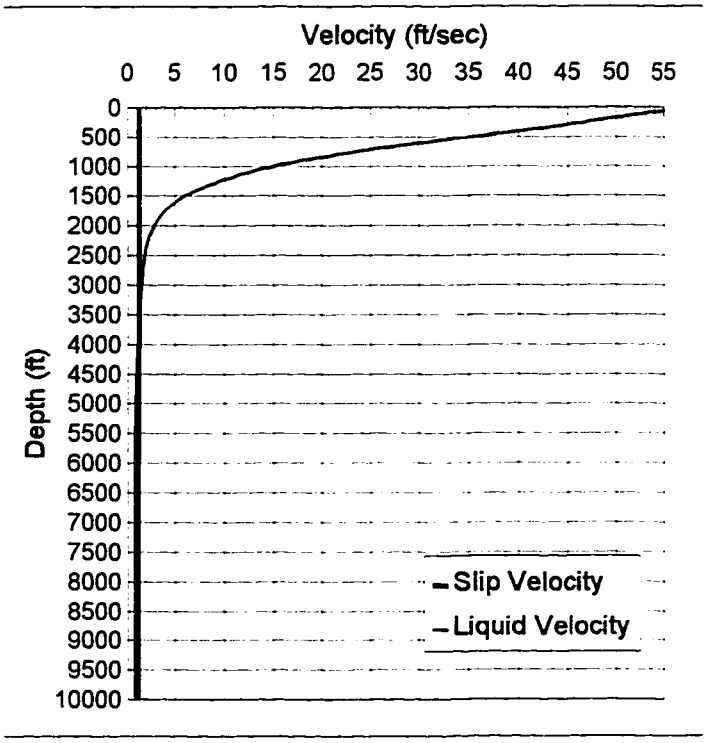

Figure 7.24 - Slip and Liquid Velocity profiles for 10,000 ft Water Depth Simulation (8 1/2" hole)

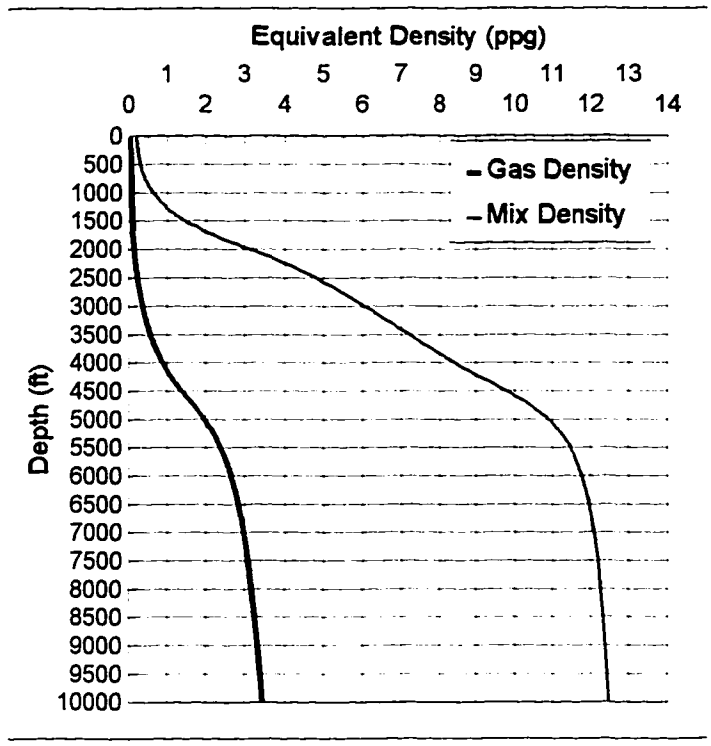

Figure 7.25 - Gas and Mixture Densities for 10,000 ft Water Depth Simulation (8 1/2" hole)

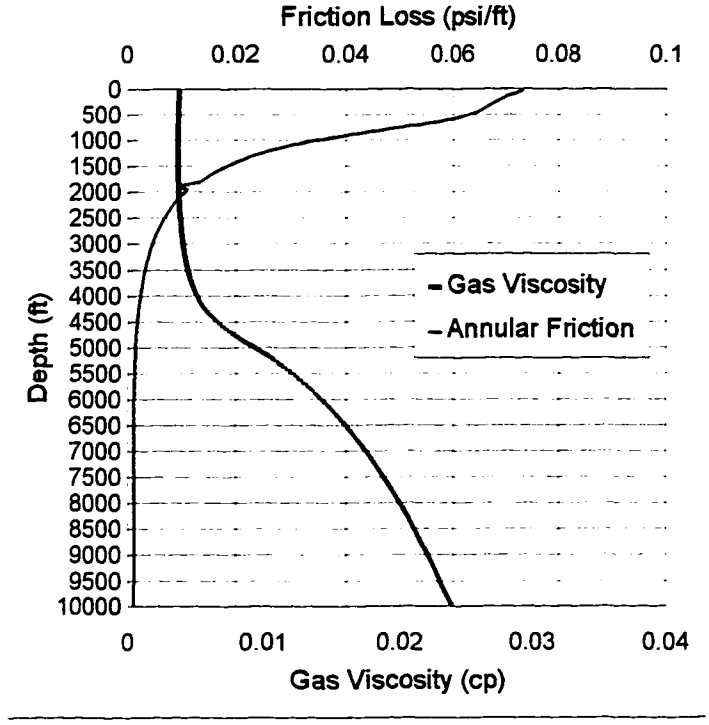

Figure 7.26 - Gas Viscosity and Annular Friction Loss for 10,000 ft Water Depth Simulation (8 1/2" hole)

Table 7.28 - Simulation Assumptions and Gas Volumes for the 10,000 ft Riser Case

Hole (in)	MW (ppg)	Rate (gpm)	Top Pres (psi)	Gas Rate (SCF/min)	Time (days)	Circulating (%)	Gas Vol. (MMCF)
17.5	12.34	900	100	20633	10	40	118.845
12.25	13.63	500	70	18243	10	50	131.348
8.5	15.48	350	60	20449	15	60	265.015
						Total =	515.208

This allowed maintaining the same times required to complete each phase, and the circulation percentages.

7.19 - COMPRESSOR POWER FOR ULTRA-DEEP WATERS

For the case of a 10,000 ft riser, the gas injection pressure at surface, during the steady-state simulation, was 2886 psig. This value, plus the highest gas injection rate (8 1/2" hole), was considered as the compressor design load for this case.

Table 7.29 presents the calculations done for the required compressor power, without the use of intercooler units between stages, for this case.

Table 7.29 - Required Compressor Power for the 10,000 ft Riser Case without Intercooler units

Intake (psig)	Discharge (psig)	Ratio	Stages	r	Ratio/ Stage	k	Spc. Pwr (hp/MMcf)	Gas Rate (SCF/min)
150	2886	19.240	3	2.68	2.7	1.18	57	20449

Stage	Tintk (F)	Pintk (psig)	Zintk	Tdisch (F)	Pdisch (psig)	Zdisch	Zavg	Spc. Pwr (Bhp/MMcf)
1	100	150	0.9559	115	405	0.895	0.9257	57.8
2	115	400	0.8967	133	1080	0.759	0.8277	51.7
3	133	1075	0.7597	154	2903	0.749	0.7544	47.1
							Sum	156.6
							Total Bhp	4612

Table 7.30 tabulates similar data for the case when intercooler units are used to maintain the suction temperature between stages close to the intake temperature.

Table 7.30 - Required Compressor Power for the 10,000 ft Riser Case with Intercooler units

Intake (psig)	Discharge (psig)	Ratio	Stages	r	Ratio/ Stage	k	Spc. Pwr (hp/MMcf)	Gas Rate (SCF/min)
150	2886	19.240	3	2.68	2.7	1.18	57	10809

Stage	Tintk (F)	Pintk (psig)	Zintk	Tdisch (F)	Pdisch (psig)	Zdisch	Zavg	Spc. Pwr (Bhp/MMcf)
1	100	150	0.9559	100	405	0.885	0.92038	57.5
2	100	400	0.8848	100	1080	0.693	0.78899	49.3
3	100	1075	0.6944	100	2903	0.691	0.69251	43.2
							Sum	150.0
							Total Bhp	4417

7.20 - CASING AND RIG COSTS FOR ULTRA-DEEP WATERS

Table 7.31 presents the casing cost for the 10,000 ft riser case, drilled with the conventional method, while Table 7.32 shows comparative values for the case when the dual density system is employed.

Table 7.31 - Casing Costs for the 10,000 ft Riser Case with the Conventional Method

Casing OD (in)	Length (ft)	Unit Cost ($/ft)	Cost ($)
20"	2050	64.00	$130,000.00
16"	2650	40.00	$105,000.00
13 3/8"	3200	20.50	$65,000.00
11 ¾"	1350	43.00	$60,000.00
9 5/8"	4950	20.00	$100,000.00
7 5/8"	2050	21.00	$45,000.00
5 1/2"	7850	9.50	$75,000.00
4 1/2"	3050	10.00	$30,000.00
		Total	$610,000.00

Table 7.33 presents the rig time costs, for the Conventional Method, involved in under-reaming, preparing and running the casing strings, and the time required to test the BOP stack, after each casing.

Table 7.32 - Dual Density Casing Costs for the 10,000 ft Riser Case

Csg OD (in)	Length (ft)	Unit Cost ($/ft)	Cost ($)
20"	2050	64.00	$131,000.00
13 3/8"	3050	20.50	$62,000.00
9 5/8"	4450	15.00	$67,000.00
7"	6450	11.00	$71,000.00
		Total	$331,000.00

The rig day rate, in this case, was estimated in US$ 150,000.00. This was based on the assumption that a rig capable of drilling in such water depths would cost more than the ones in the previous cases.

Table 7.33 - Conventional Method Rig Time Costs for the 10,000 ft Riser Case

Day Rate	150,000	$/day		
OD	Operation Time (days)			
(in)	Run	Ream	BOP	Totals
20"	1.0	1.0	0.5	2.5
16"	1.0	1.0	0.5	2.5
13 3/8"	1.0	2.0	0.5	3.5
11 3/4"	1.0	1.0	0.5	2.5
9 5/8"	1.0	1.5	0.5	3.0
7 5/8"	1.0	1.0	0.5	2.5
5 1/2"	1.0	3.5	0.5	5.0
4 1/2"	1.0	4.0	0.5	5.5
Totals	8.0	15.0	4.0	27.0
			Cost	$4,050,000.00

Table 7.34 shows the equivalent data for the dual density system, where the same rig day rate was used in the calculations.

7.21 - CRYOGENIC VOLUMES FOR ULTRA-DEEP WATERS

Table 7.35 shows the values for the liquid nitrogen needed in case the Cryogenic Injection option is chosen. Also tabulated are the estimated volumes, in MCF and in gallons, for 3 days of normal work, and the liquid nitrogen weight for this volume.

Table 7.34 - Dual Density Rig Time Costs for the 10,000 ft Riser Case

Day Rate	150,000	$/day		
OD	Operation Time (days)			
(in)	Run	Ream	BOP	Totals
20"	1.0	1.0	0.5	2.5
13 3/8"	1.5	0.0	0.5	2.0
9 5/8"	1.5	0.0	0.5	2.0
7"	1.0	0.0	0.5	1.5
Totals	5.0	1.0	2.0	8.0
			Cost	$1,200,000.00

Table 7.35 - Nitrogen Vapor and Liquid Volumes for the 10,000 ft Riser Case

Vapor				Liquid			
Total Time (days)	Total Vol (MCF)	Vol/day (MCF)	3 day Vol (MCF)	Total Vol (gal)	Vol/day (gal)	3 day Vol (gal)	Weight (tons)
35	515,208	14,720	44,161	5,533,327	158,095	474,285	1,598

7.22 - OPERATIONAL COSTS FOR ULTRA-DEEP WATERS

Table 7.36 presents the estimated operational costs for the use of compressors and cryogenic pumps for the 10,000 ft riser case, along with the required power.

Again, it was considered only the options for a 3 stage, reciprocal, low speed type of compressor, with and without intercooler units between the stages, and considering just the steady-state injection pressures needed.

7.23 - COST COMPARISON FOR ULTRA-DEEP WATERS

Table 7.37 summarizes the operational and rig costs for the conventional and the dual density systems. It shows the totals and the differences between the total cost of the

Table 7.36 - Operational Costs for the 10,000 ft Riser Case

	Compressor		Cryogenic Pump
	No Intercooler	With Intercooler	
Power (Bhp)	4612	4417	950
Operational Cost	$237,000.00	$227,000.00	$49,000.00

Table 7.37 - Dual Density Savings over the Conventional Method for the 10,000 ft Riser Case

	Dual Density		Conventional
Costs	On Site Option	Cryogenic Option	
Casing	$331,000.00	$331,000.00	$610,000.00
Rig Time	$1,200,000.00	$1,200,000.00	$4,050,000.00
Compressors	$227,000.00		
NPU's	$252,000.00		
Pumps		$49,000.00	
Nitrogen		$1,385,000.00	
Totals	$2,010,000.00	$2,965,000.00	$4,660,000.00
Savings	$2,650,000.00	$1,695,000.00	

dual density options, on-site generation and cryogenic injection, and the equivalent cost for the conventional method.

When varying the rig day rate, from the starting value of US$ 150,000.00 down to zero, we obtain the results shown in Figure 7.27. The on-site generation crosses the zero savings line at a day rate of around US$ 8,000.00. The cryogenic injection crosses zero savings at a day rate of approximately US$ 52,000.00.

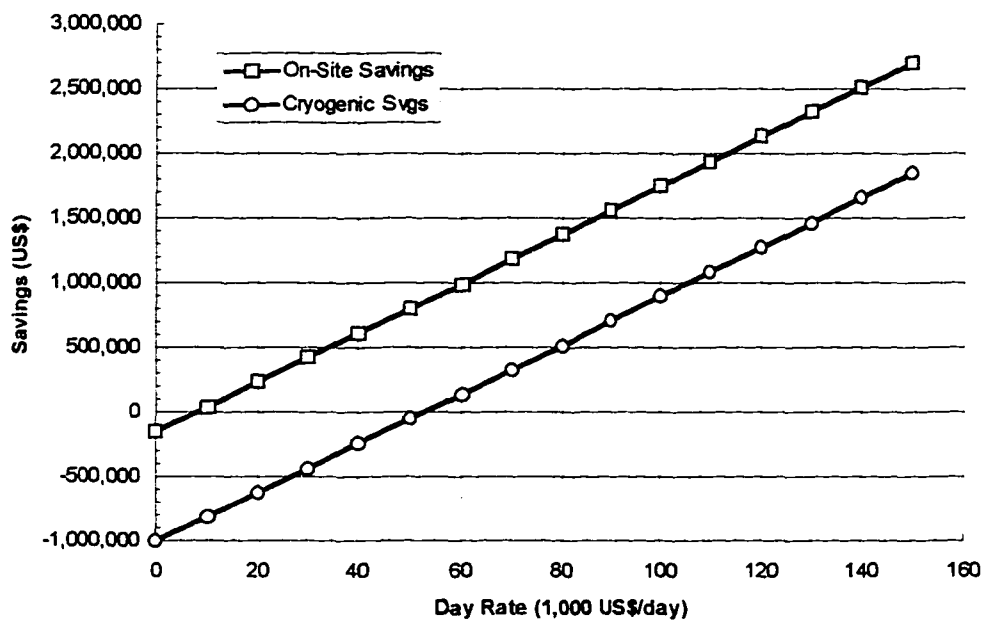

Figure 7.27 - Dual Density Savings vs. Rig Day Rate for the 10,000 ft Riser Case

7.24 - SMALL RISER DIAMETERS

The riser size has a profound influence on the costs of deep water drilling. The greater the riser is, the greater is its mass, the slower it is handled, and the greater space on board it requires. The external diameter of a riser string is also responsible for the amount of drag the marine currents impose on it. This drag force has to be absorbed by the wellhead and by the rig itself, when the riser is connect to the well.

In case of a disconnection, all the drag force is transmitted to the riser point of contact with the rig. When the riser diameter is increased, the mud volume required to fill it is increased, requiring increases in the annular mud velocity, to maintain the riser clean of cuttings. With the increased mud volume the riser overpull has to increase, too, to prevent buckling and failure of the riser string.

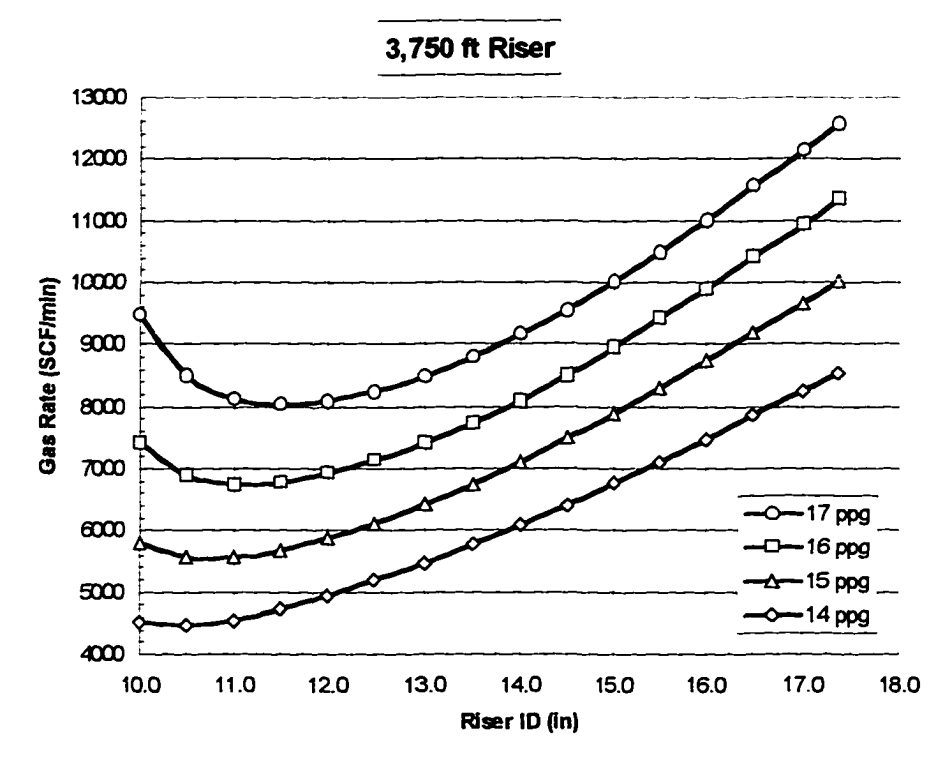

Figure 7.28 - Riser ID versus Gas Injection Rate for the 3,750 ft Riser Case

The dual density system requires less gas if the riser mud volume decreases, but requires more nitrogen if the annular pressure losses increase. Figure 7.28 shows this behavior when we consider the shallow-deep water case.

The simulations consider the 8 1/2" hole, for four different mud densities and a pump rate of 400 gal/min. The optimal riser internal diameter found for the case examined, with a 15.57 ppg mud, was 11".

Figure 7.29 presents equivalent curve for the 7,500 ft riser case. Again, the simulations took in account the 8 1/2" hole, for the same mud densities and a pump rate of 400 gal/min. The optimal riser internal diameter for the case studied was 12.5".

Finally, for the 10,000 ft riser case, the data is presented on Figure 7.30. The same simulation parameters were used and the optimal riser ID determined was 13.25".

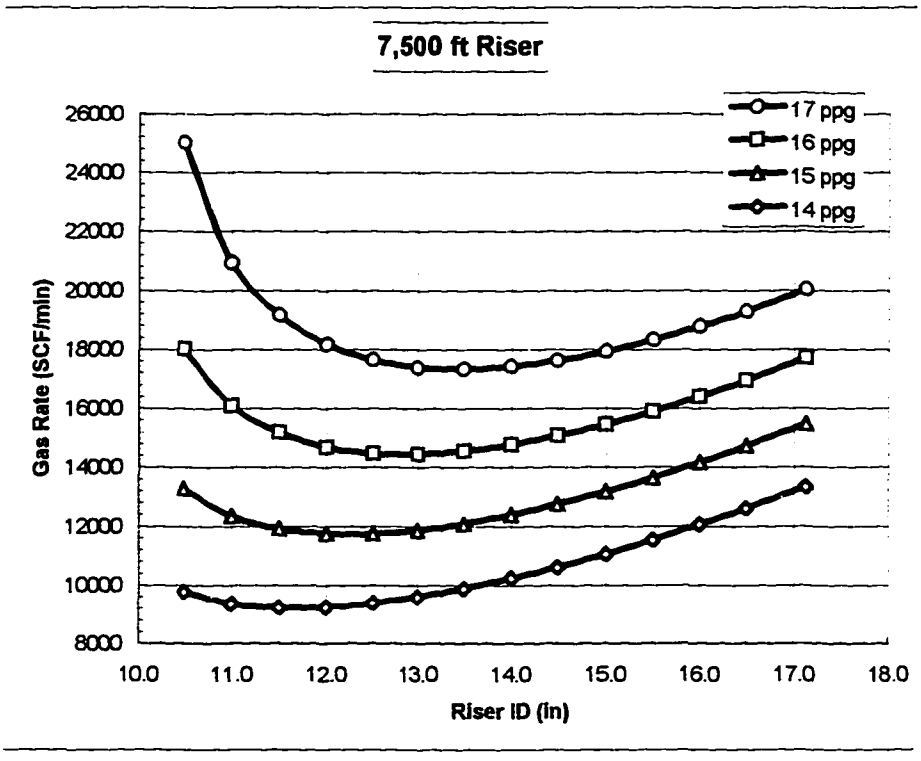

Figure 7.29 - Riser ID versus Gas Injection Rate for the 7,500 ft Riser Case

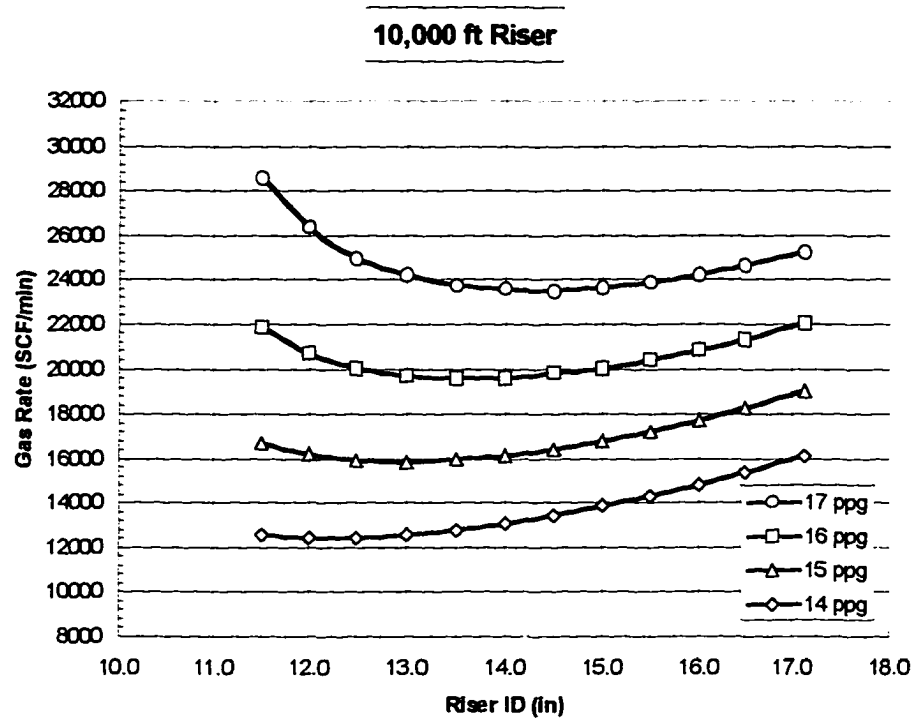

Figure 7.30 - Riser ID versus Gas Injection Rate for the 10,000 ft Riser Case

CHAPTER VIII

CONCLUSIONS AND RECOMMENDATIONS

This chapter summarizes the results discussed in this dissertation and tries to recommend ways that would possibly improve the research on this subject.

8.1 - INTRODUCTION

With the present rapid expansion in the world's demand for oil and gas, the industry is being pushed towards ever increasing water depths, in search for new reservoirs. But, there are practical limits to the present deep water drilling technology, and one of them is represented by the added bottom hole hydrostatic pressure introduced by the riser system in use today.

Deep waters tend to narrow the range between the pore pressure and fracture gradients, and this fact sometimes places operators facing an emergency disconnection without a safe riser margin added to the mud density.

Beside the safety concern associated with drilling without a riser safety margin, the pressure overbalances when using it often leads to excessive number of casing strings, and small production diameters.

The Dual Density Riser System might be an alternative to the present riser technology, with the development of new concepts for riser pressure monitoring, kick detection and circulation, gas injection automation and drilling procedures. The work done in this research may represent the initial tentative steps towards the achievement of those goals.

8.2 - SUMMARY

The ultimate objective of this research work was to conclude on the feasibility of the proposed Dual Density Riser System. To accomplish this, the following steps were taken:

8.2.1 - Computer Simulator

A computer program was developed that is capable to accurately estimate the gas injection rates needed to obtain sea water hydrostatic pressure at the riser bottom. The simulator takes as input parameters the riser geometric parameters, the mud rate, the estimated choke pressure, and the mud properties. It calculates either the necessary gas injection rate to achieve sea water density, at the BOP level, or to estimate the riser bottom pressure for a given set of those input parameters.

This research went further and tried to develop an unloading computer simulator, as a basis for a gas injection controller. The objective, then, was to investigate how fast the riser bottom pressure would react to readjustments in the gas injection rate due to any perturbations. These perturbations could come from changes in the mud rate, choke pressure, or mud properties.

This objective was not achieved since it was not possible to validate the unsteady-state simulator with experimental data. Nonetheless, it was concluded that this simulator lacked an algorithm that would account for different gas rising velocities within the gas mass. Furthermore, the unloading simulator replicated the results obtained with the validated steady-state algorithm. Thus is believable that, with a better unloading algorithm, the simulator could be the basis for an automatic gas injection controller.

8.2.2 - Experiments

The computer simulator needed to be tested against experimental data, to be validated, before drilling scenarios could be built and the Dual Density Riser System's feasibility could be accessed.

Only two experiments, out of the six originally planned, were conducted, due to delays in the availability of funds. These tests were done in an actual well, with a depth similar in length to a deep water riser, and an annular space that generated compatible frictional losses.

The result of the experimental work was to validate the steady-state simulator module and to point out problems with the mathematical model used in the development of the unloading simulator module.

8.2.3 - Simulation Scenarios

Once the computer simulator was validated, simulation scenarios were built for the Gulf of Mexico region, due to its increasing economical importance and high pore pressure environment.

Studies on the approximation of pore pressure and fracture gradients as a function of depth were taken and three cases were built. The scenarios included a shallow-deep water (3,750 ft), for which real data was available, a medium-deep water case (7,500 ft), and an ultra-deep water (10,000 ft).

Casing sizes and set points were then designed for each case scenario, for the conventional and the dual density riser systems. The conclusions were that the latter system is capable of significantly reducing the number of casing strings needed to drill in

those conditions. This should result in larger production diameters and cost reductions in rig time and casing expenditures, without the requirement of riser safety margins.

8.2.4 - Drilling Procedures

The dual density system would represent a major change in the way drilling operations are conducted. So, it was necessary to investigate the drilling sequence of events and procedures, to find out if there was any intrinsic incompatibility between the new technology and drilling operations.

The drilling of a well was divided in a chain of tasks. After the descent of the riser column, operations like bit runs, pipe connections, and others were examined. The task list included the case of a kick occurrence.

It was concluded that the biggest hurdles for the implementation of a dual density riser system would be imposed by kick detection and kick circulation. Although ways to circumvent the difficulties during these operations are suggested, further analysis must be devoted to the subject, to develop new sensors and kick control techniques tailored to the dual density system.

8.2.5 - Economic Feasibility

After investigating the potential savings provided by the proposed riser system in casing expenditures and rig time, it was mandatory to fathom the involved operational costs associated with the new technology.

The option for air utilization was discarded in the early research stages, due to the potential problems related with equipment corrosion and the possibility of down-hole fires. Thus, the problem of nitrogen supply to a remote off-shore rig became a matter of

concern. Two basic approaches were investigated: the in-situ nitrogen generation and the cryogenic transportation.

The first option requires the lease of multiple Nitrogen Producing Units (NPU's) and the use of high capacity, high pressure compressors to adequately meet the gas needs of a rig. The drawback of this option is the lack of flexibility represented by having a fixed amount of compressor power and capacity installed, imposing limits to the rig's drilling range.

The cryogenic option was considered since it would not require the use of compressors, adding flexibility to the system. On the other hand, it would demand a reliable and sophisticated fleet of boats, equipped with cryogenic tanks, pumps and special hoses to supply liquid nitrogen to an off-shore rig. Moreover, the rig itself would have to be equipped to hold enough liquid nitrogen to keep the rig operative during the periods when bad weather would prevent the docking of a supply boat.

After analyzing the costs imposed by both options, against the savings provided by the dual density riser system, the conclusion was that the in-situ generation represents, by far, the most cost effective choice. But, depending on the rig day-rate, the cryogenic method can also be economical. Since nowadays the demand for a deep water capable rig is so great, such a supply and injection method should not be readily put aside.

Thus, the research work concluded that the dual density riser system is potentially feasible economically, independent of which choice is taken regarding the supply of nitrogen to the rig.

8.3 - RECOMMENDATIONS

8.3.1 - Gas Injection Controller

The maintenance of a nearly constant riser bottom pressure at sea water hydrostatic levels will require the use of an automated, computer controlled, gas injection system. The complexity of computing the combined effect of mud and gas densities on the pressure at the BOP forcibly involves the use of a computer program. The simulator developed in this research work can be used for scheduled changes in the gas injection rate, but is inadequate for constant readjustments. Furthermore, a well-tuned gas injection controller might give the operator the freedom to concentrate on drilling operations, reducing the chances for costly mistakes.

Investigation on the feasibility of such a device will demand the refinement of the present unsteady-state flow simulator and its validation with experimental data. The present mathematical model assumes that all the gas bubbles inside each unit volume of gas pumped into the riser will homogeneously change their velocity along their way up to the surface. This is the same as assuming only one bubble size for all the injected gas. It is reasonable to assume that, even if the gas bubbles start out with the same size at the injection point, they will coalesce along the way, changing their velocity profile.

Thus, a more thorough study of these velocity distributions and the development of an algorithm to keep track of their evolution in the riser annular space is suggested here. This algorithm could, then, be used for the coding of a gas injection controller. Also, more experiments should be conducted to investigate how fast the bottom pressure would respond to changes in the gas injection rates.

8.3.2 - Kick Detection and Circulation

Since the first well drilled, the possibility of a blow-out has being an intrinsic part of the drilling process. Either triggered by human error or by unpredictable factors, kicks do occur and have to be planned for. The modifications introduced by a technology such as the dual density riser system demand new approaches to that task, and so can not be taken lightly.

More research, backed by experimental work, has to be done on this subject, especially on the development of sensors to detect the presence of influx and techniques to provide its safe disposal.

REFERENCES

1. Allan, P. D. *"Nitrogen Drilling System for Gas Drilling Applications."* SPE 28320. SPE 69th Annual Technical Conference and Exhibition, New Orleans, LA, September 25-28, 1994.

2. Ansari, A. M., Sylvester, N. D., Sarica, C., Shoham, O., Brill, J. P., *"A Comprehensive Mechanistic Model for Upward Two-Phase Flow in Wellbores."* SPE 20630. 65th Annual Technical Conference and Exhibition of the Society of Petroleum Engineers, New Orleans, September 23-26, 1990.

3. Aziz, K., Petals, N. *"New PC-Based Software for Multiphase Flow Calculations."* SPE 28249. SPE Petroleum Computer Conference, Dallas, Texas, July 31-August 3, 1994.

4. Bang, J., Svein, M., Solstad, A., Hendriks, P., Jensen, L. K. *"Acoustic Gas Kick Detection With Wellhead Sonar."* SPE 28317. 69th Annual Technical Conference and Exhibition, New Orleans, Louisiana, September 25-28, 1994.

5. Beggs, H. D. *"Production Optimization."* Oil and Gas Consultants International Inc. Publications, 1991.

6. Beggs, H. D., Brill, J. P. *"A Study of Two-Phase Flow in Inclined Pipes."* SPE 4007. AIME/SPE 47th Annual Fall Meeting, San Antonio, Texas, October 8-11, 1972.

7. Benabdelkarim, M., Galiana, C. *"Nonradioactive Densitometer for Continuous Monitoring of Cement Mixing Process."* SPE 23262. First International Conference on Health, Safety and Environment, The Hague, The Netherlands, November 10-14, 1991.

8. Bourgoyne Jr., A. T., Milheim, K. K., Chenevert, M. E., Young, F. S. *"Applied Drilling Engineering."* Society of Petroleum Engineers, 1991.

9. Bryant, T. M., Grosso, D. S., Wallace, S. N. *"Gas-Influx Detection With MWD Technology."* SPE 19973. IADC/SPE Drilling Conference, Houston, Texas, February 27 - March 2, 1990.

10. Cappuci, E. C., Serra, K. V. *"Transient Aspects of Unloading Oil Wells Through Gas-Lift Valves."* SPE 22791. 66th Annual Technical Conference and Exhibition of the Society of Petroleum Engineers, Dallas, Texas, October 6-9, 1991.

11. Casariego, V., Bourgoyne, A. T., *"Generation, Migration, and Transportation of Gas-Contaminated Regions of Drilling Fluid."* SPE 18020. 63rd Annual Technical

Conference and Exhibition of the Society of Petroleum Engineers, Houston, Texas, October 2-5, 1988.

12. Cobbet, J. S. *"Application of an Air-Drilling Package in Oman."* SPE 9600. Middle East Oil Technical Conference of the Society of Petroleum Engineers, Manama, Bahrain, March 9-12, 1981.

13. Cooksey, A., Pool, M. *"Production Automation System For Gas Lift Wells."* SPE 29453. Production Operations Symposium, Oklahoma City, OK, April 2-4, 1995.

14. Craft, B. C., Holden, W. R., and Graves, E. D. *"Well Design: Drilling and Production."* Prentice-Hall, Inc., 1962.

15. Craytor, B., Manning, K. J. *"Drilling a Medium-Radius Horizontal Well With Aerated Drilling Fluid: a Case Study."* SPE 21988. SPE/IADC Drilling Conference, Amsterdam, The Netherlands, March 11-14, 1991.

16. Crittendon, B. C. *"The Mechanics of Design and Interpretation of Hydraulic Fracture Treatments."* SPE 1106-G. 88th Annual Fall Meeting of the Society of Petroleum Engineers, Houston, Texas, October 5-8, 1958.

17. Energy Technology Services Corp. - Personal Communication.

18. Erb, P. R., Ma, Tien-Chi, Stockinger, M. P., *"Riser Collapse - A Unique Problem in Deep-Water Drilling."* SPE 11394. IADC/SPE Drilling Conference, New Orleans, Louisiana, February 20-23, 1983.

19. Fisher, W., Ludwig, M. *"Design of Floating Vessel Drilling Riser."* SPE 1220. SPE Annual Meeting, Denver, CO, October 3-6, 1965.

20. Gas Processors Suppliers Association *"Engineering Data Book."* Published by GPSA, 1987.

21. Gault, A. *"Riserless drilling: circumventing the size/cost cycle in deepwater."* Offshore Magazine. Drilling Technology Section. May, 1996.

22. George, D. *"Boom!"* . Offshore Magazine. International Focus Secion. February, 1997.

23. Guo, B., Hareland, G., Rajtar, J. *"Computer Simulation Predicts Unfavorable Mud Rate and Optimum Air Injection Rate for Aerated Mud Drilling."* SPE 26892. Eastern Regional Conference & Exhibition, Pittsburgh, PA, November 2-4, 1993.

24. Guo, B., Hareland, G., Rajtar, J. *"Volume Requirements for Aerated Mud Drilling."* SPE 26956. SPE Latin American/Caribbean Petroleum Engineering Conference, Buenos Aires, Argentina, April 27-29, 1995.

25. Hall, J. E., Roche, J. R., Boulet, C. G. *"Means for Handling Gas Influx in a Marine Riser."* SPE 14739. IADC/SPE Drilling Conference, Dallas, Texas, February 10-12, 1986.

26. Hagedorn, A. R., Brown, K. E. *"Experimental Study of Pressure Gradients Occurring During Continuous Two-Phase Flow in Small-Diameter Vertical Conduits."* SPE 940. 89th Annual Fall Meeting of the Society of Petroleum Engineers, Houston, Texas, October 11-14, 1964.

27. Heuze, L. R., Chaussumier, D., Guesnon, J., Simondon, D. *"A 4,000-Foot Riser."* SPE 5483. Seventh Annual Offshore Technology Conference, Houston, TX, May 5-8, 1975.

28. Hovland, F., Rommetveit, R. *"Analysis of Gas-Rise Velocities From Full-Scale Kick Experiments."* SPE 24580. 67th Annual Technical Conference and Exhibition of the Society of Petroleum Engineers, Washington, DC, October 4-7, 1992.

29. Ikoku, C. U., Azar, J. J., Williams, C. R. *"Practical Approach to Volume Requirements for Air and Gas Drilling."* SPE 9445. 55th Annual Fall Technical Conference and Exhibition of the Society of Petroleum Engineers of AIME, Dallas, TX, September 21-24, 1980.

30. Johnson, A. B., White, D. B. *"Gas-Rise Velocities During Kicks."* SPE 20431. 65th Annual Technical Conference and Exhibition of Society of Petroleum Engineers, New Orleans, Louisiana, September 23-26, 1990.

31. Kitsios, E., Kamphuis, H., Quaresma, V., Rovig, J. W., Reynolds, E. *"Underbalanced Drilling Through Oil Production Zones With Stable Foam in Oman."* SPE 27525. IADC/SPE Drilling Conference, Dallas, TX, February 15-18, 1994.

32. Lai, D. T., Dzialowski, A. K. *"Investigation of Natural Gas Hydrates in Various Drilling Fluids."* SPE 18637. SPE/IADC Drilling Conference, New Orleans, LA, February 28-March 3, 1989.

33. Langlinais, J. P., Bourgoyne Jr., A. T., Holden, H. R. *"Frictional Pressure Losses for the Flow of Drilling Mud and Mud/Gas Mixtures."* SPE 11993. 58th Annual Technical Conference and Exhibition of Society of Petroleum Engineers, San Francisco, California, October 5-8, 1983.

34. Littlefield, R. G., *"Gas Compressor Design & Operation."* SPE 9996. International Petroleum Exhibition and Technical Symposium of the Society of Petroleum Engineers, Beijing, China, March 18-26, 1982.

35. L&S Cryogenics Corp. - Personal Communication

36. McCoy, J. N., Podio, A. L., Becker, D. *"Pressure Transient Digital Data Acquisition and Analysis From Acoustic Echometric Surveys in Pumping Wells."* SPE 23980. SPE Permian Basin Oil and Gas Recovery Conference, Midland, TX, March 18-20, 1992.

37. McLeod, W. R. *"A review of Riserless Drilling Alternatives."* SPE 5768. European Spring Meeting 1976 of the Society of Petroleum Engineers of AIME, Amsterdam, The Netherlands, April 8-9, 1976.

38. Nakagawa, E. Y. *"Gas Kick Behavior During Well Control Operations in Vertical and Slanted Wells."* Ph.D. Dissertation, Louisiana State University, December 1990.

39. Nickens, H. V. *"A Dynamic Computer Model of a Kicking Well."* SPE 14183. SPE Annual Technical Conference and Exhibition, Las Vegas, Nevada, September 22-25, 1985.

40. Ohara, S. *"Improved Method for Selecting Kick Tolerance During Deepwater Drilling Operations."* Ph.D. Dissertation, Louisiana State University, December 1995.

41. Petrobras/EP - personnal communication.

42. Press, W. H., Flannery, B. P., Teukolsky, S. A., Vetterling, W. T., *"Numerical Recepies - The Art of Scientific Computing."* Cambridge University Press. 1986.

43. Rader, D. W., Bourgoyne Jr., A. T., Ward, R. H., *"Factors Affecting Bubble-Rise Velocity of Gas Kicks."* SPE 4647, 48th Annual Fall Meeting, Las Vegas, Nevada, September 30 - October 3, 1973.

44. Rizo, T. M., Cuenca, A. P. *"Aerated Fluid Drilling Observations in Geothermal Operation in Luzon, Philippines."* SPE 12455. 5th Offshore South East Asia Conference and Exhibition, Singapore, Philippines, February 21-24, 1984.

45. RSV Gusto Engineering b. v. *"Dynamically Positioned Drillships."* Technical Specifications. 1979.

46. Santos, O. L. A. *"A Dynamic Model of Diverter Operations for Handling Shallow Gas Hazards in Oil and Gas Exploratory Drilling."* Ph.D. dissertation, Louisiana State University, May 1989.

47. Schnatzmeyer, M. A., Yonker, J. H., Pool, C. M., Golffon, J. J. *"Development of a Surface-Controlled Electric Gas-Lift Valve."* SPE 26553. SPE Annual Technical Conference and Exhibition, Houston, TX, October 3-6, 1993.

48. Shafer, J. L. *"Basic Approach to the Application of Field Gas Compressors for Production Engineers."* SPE 25486. Production Operations Symposium, Oklahoma City, OK, March 21-23, 1993.

49. Vestavik, O. M., Aas, B., Podio, A. L. *"Downhole Gas Detection Method in Drilling Fluids."* SPE 19971. IADC/SPE Drilling Conference, Houston, Texas, February 27 - March 2, 1990.

50. Wallace, L. H., Walker, J. A. *"Evaluation of Aerated Drilling Fluids Used at the Nevada Test Site."* SPE 8222. 54th Annual Fall Technical Conference and Exhibition of the Society of Petroleum Engineers of AIME, Las Vegas, Nevada, September 23-26, 1979.

51. Westermark, R. V. *"Drilling With a Parasite Aerating String in the Disturbed Belt, Gallatin County, Montana."* SPE 14734. IADC/SPE Drilling Conference, Dallas, TX, February 10-12, 1986.

52. World Oil, August 1995. *"Onsite-generated Nitrogen for Oil and Gas Well Drilling."* Technology at Work, pp. 146-147.

53. World Oil, December 1995. Pp. 127-154.

NOMENCLATURE

Greek Letters

ϕ_o = surface porosity, assumed as 0.45;

γ_g = specific gravity of gas, 1.0 for air

λ = no-slip liquid holdup

μ = Poisson's ratio;

μ_p = mud plastic viscosity (cp)

ρ_c = cuttings density, lb/ft^3 [kg/m^3]

ρ_f = fluid (mixture) density, lb/ft^3 [kg/m^3]

ρ_{fi} = interstitial fluid density, assumed as 1.074 g/ cm^3;

ρ_g = gas density (ppg)

ρ_{gr} = grain density, assumed as 2.60 g/cm^3;

ρ_m = mud density, lb/ft^3 [kg/m^3]

ρ_{ns} = two-phase no-slip density

ρ_w = sea water density (ppg), assumed as 8.60 ppg

σ_{ob} = vertical overburden stress, psig;

σ_h = horizontal matrix stress, psig;

σ_z = vertical matrix stress, psig.

Roman Letters

B = the buoyant force

C_r = riser capacity per foot

d = internal diameter of pipe (inches)

D = total depth (well + riser), (ft)

D_e = equivalent circular diameter of conduit, ft [m]

D_s = sediment depth, ft;

D_w = water depth, ft;

f = friction factor, dimensionles

f_F = no-slip friction factor (dimensionless)

f_{Fan} = Fanning friction factor (dimensionless)

f_{tp} = two-phase flow friction factor (dimensionless)

g = gravitational constant;

g_c = Newton's law conversion factor, ft-lbm/lb

h = riser length

H = riser length (ft)

H_{tot} = total depth, ft [m]

Id_r = riser inside diameter

K = porosity decline constant, assumed as 0.000085.

M_w = gas molecular weight

N_{re} = Reynolds Number (dimensionless)

O = the riser tensioner overpull

OD_r = riser outside diameter

P = pressure, psia [Pa]

P_1 = pressure due to mud column alone, psig [Pa]

P_2 = pressure due to the combined columns of mud and sea water, psig [Pa]

P_d = downstream pressure, psia [Pa]

P_p = equivalent pore pressure (ppg)

P_{sc} = standard condition pressure, psia [Pa]

P_u = upstream pressure, psia [Pa]

Q_c = volumetric flow rate of cuttings, ft^3/min [m^3/min]

Q_{gsc} = gas flow rate under standard conditions, ft^3/min [m^3/min]

Q_m = mud flow rate, gpm [m^3/min]

R_w = riser string weight in air

RM = riser margin (ppg)

s = non-slip friction

SM = safety margin equivalent density (ppg)

T = temperature (°R)

T_{avg} = average temperature, °R [°K]

T_{sc} = standard condition temperature, °R [°K]

v_m = mixture velocity

V_g = gas velocity (ft/sec)

V_m = mixture velocity (ft/sec)

W_1 = equivalent density for P_1, ppg;

W_2 = equivalent density for P_2, ppg.

W_{mud} = weight of the mud inside the riser

V_s = slip velocity (ft/sec)

z = gas compressibility factor, dimensionless

APPENDIX A

EXTRAPOLATION OF PORE AND FRACTURE GRADIENTS

Since it is very difficult to obtain data on pore pressure and fracture gradient for wells with water depths beyond 3,000 ft, an algorithm for extrapolating available data was used to establish the examples to be used for the simulations in this study.

A.1 - ASSUMPTIONS

For a given set of data, the objective is to transport the sediments, for which the data is available, from the relatively shallow water depth given to a deeper one. In order to do this, the following assumptions were made:

1. The rock vertical matrix stress remains the same. This assumption is based on the idea that the matrix stress is dependent on the depth of the sediments, and would not change would there be an increase of the hydrostatic provided by the column of sea water.
2. The horizontal stresses σ_x and σ_y are approximately equal and the sediments behave elastically.
3. The horizontal strain ε_x is essentially zero.
4. The rock horizontal matrix stress stays unchanged. Again, this is based on the same idea that the matrix stress is dependent on the depth of the sediments.

A.2 - EQUATIONS

The procedure begins by calculating the vertical overburden stress, σ_{ob}, using the following relationship:

$$\sigma_{ob} = \rho_w g D_w + \rho_{gr} g D_s - \frac{(\rho_{gr} - \rho_{fi}) g \phi_o}{K}(1 - e^{-KD_s}) \qquad (A.1)$$

The vertical grain-to-grain, or matrix stress, σ_z is the difference between the overburden stress and the pore pressure, which is given by:

$$\sigma_z = \sigma_{ob} - P_p \qquad (A.2)$$

Next, the Poisson's ratio that reproduces the fracture gradient given is found. A starting point can be the data provided by Eaton (Bourgoyne et al., p. 290, 1991). The Poisson's ratio is used to calculate the horizontal matrix stress:

$$\sigma_h = \left(\frac{\mu}{1-\mu}\right)\sigma_z \qquad (A.3)$$

The pore pressure for the new water depth is obtained by adding the difference in hydrostatic pressure due to the two different water depths, the initial and the new one, to the pore pressure data available.

$$P_{p2} = P_{p1} + (D_{w2} - D_{w1}) g \rho_w \qquad (A.4)$$

The fracture gradient for the new water depth is calculated by adding the horizontal matrix stress, obtained for the initial water depth, to the new values of pore pressure:

$$P_{f2} = \sigma_h + P_{p2} \qquad (A.5)$$

A.3 - ALGORITHM

The calculations used can be carried out in an electronic spreadsheet. The procedure is as following:

1. For the initial water depth, calculate the overburden stress - σ_{ob} , using equation (A.1);
2. Calculate the vertical matrix stress - σ_z , using equation (A.2) and the available pore pressure data for the initial water depth;
3. Compute the horizontal matrix stress - σ_h , using equation (A.3) and finding the necessary Poisson's ratios that reproduce the available fracture gradient data for the initial water depth;
4. Find the pore pressure for the new water depth - P_{p2} , using equation (A.4);
5. Determine the fracture gradient for the new water depth - P_{f2} , using equation (A.5).

APPENDIX B

RISER SAFETY MARGIN

Let us consider two fluid columns: the first consisting of mud, from surface down to the bottom of the hole, and the second made up of sea water, from the sea surface down to the wellhead, and mud from there on to the bottom of the well. If we express the two different bottom hole pressures in equation form, we must have:

$$P_1 = 0.052\rho_m \cdot D \tag{B.1}$$

$$P_2 = 0.052\rho_m \cdot (D - H) + 0.052\rho_w H = 0.052\rho_m \cdot D - 0.052H(\rho_m - \rho_w) \tag{B.2}$$

Expressing these pressures in their equivalent density form, we obtain:

$$W_1 = \frac{P_1}{0.052D} = \rho_m \tag{B.3}$$

$$W_2 = \frac{P_2}{0.052D} = W_1 - \frac{H}{D}(\rho_m - \rho_w) \tag{B.4}$$

Usually, when working with pore pressure values, the drilling fluid designer adds in a safety factor, to account for pressure fluctuations caused mainly when tripping the drill string out of the hole. This is normally called trip margin or simply safety margin.

We can now define the riser safety margin as the difference between the pore pressure equivalent density, plus the trip margin, and the equivalent density provided by the combined hydrostatic columns of mud and sea water. In equation form, this is given by:

$$RM = W_2 - (P_p + SM) = W_1 - \frac{H}{D}(\rho_m - \rho_w) - P_p - SM \tag{B.5}$$

or:

$$RM = \frac{\rho_m (D - H)}{D} + \frac{\rho_w \cdot H}{D} - (P_p + SM) \qquad (B.6)$$

VITA

Clovis Lopes, born in Lages, Brazil, received a Bachelor Science degree in Civil Engineering from Universidade Federal do Rio Grande do Sul, Rio Grande do Sul, Brazil, in 1978. After graduation, he joined Petroleo Brasileiro S.A. (Petrobras) where he took two years of graduate courses in petroleum engineering at Petrobras Training Center in Bahia, Brazil. After this course, he was transferred to Petrobras Drilling District in Macae, Rio de Janeiro. There he worked for six years as a company's representative and rig manager for deep water rigs. In August 1987, he entered Universidade Estadual de Campinas where he earned his Master of Science degree in petroleum engineering in May 1990. Following his graduation, he returned to Macae to resume work as company representative and internal consultant for deep water drilling operations. In 1993 he was sent to Louisiana State University, where he entered the doctoral program in petroleum engineering. He is married to Angela Lopes and they have three children: Bruna (11 years old), Luiza (10 years old), and Clowis (4 years old).

DOCTORAL EXAMINATION AND DISSERTATION REPORT

Candidate: Clovis Antonio Lopes

Major Field: Petroleum Engineering

Title of Dissertation: Feasibility Study on the Reduction of Hydrostatic Pressure in a Deep Water Riser Using a Gas-Lift Method

Approved:

Adam T. Bourgoyne Jr.
Major Professor and Chairman

Dan M. Larkin
Dean of the Graduate School

EXAMINING COMMITTEE:

A. Wojtanowicz

J. Langlinais

Gary Byrd

Date of Examination:

April 3/97